A ZIGBEE-BASED WIRELESS BIOMEDICAL SENSOR NETWORK AS A PRECURSOR TO AN IN-SUIT SYSTEM FOR MONITORING ASTRONAUT STATE OF HEALTH

by

XIONGJIE DONG

B.S., Kansas State University, 2011

A THESIS

submitted in partial fulfillment of the

requirements for the degree

MASTER OF SCIENCE

Department of Electrical & Computer Engineering

College of Engineering

Kansas State University

Manhattan, Kansas

2014

Approved by

Major Professor

Steve Warren

ABSTRACT

Networks of low-power, in-suit, wired and wireless health sensors offer the potential to track and predict the health of astronauts engaged in extra-vehicular and in-station activities in zero- or reduced- gravity environments. Fundamental research questions exist regarding (a) types and form factors of biomedical sensors best suited for these applications, (b) optimal ways to render wired/wireless on-body networks with the objective to draw little-to-no power, and (c) means to address the wireless transmission challenges offered by a spacesuit constructed from layers of aluminized mylar.

This thesis addresses elements of these research questions through the implementation of a collection of ZigBee-based wireless health monitoring devices that can potentially be integrated into a spacesuit, thereby providing continuous information regarding astronaut fatigue and state of health. Wearable biomedical devices investigated for this effort include electrocardiographs, electromyographs, pulse oximeters, inductive plethysmographs, and accelerometers/gyrometers. These ZigBee-enabled sensors will form the nodes of an in-suit ZigBee Pro network that will be used to (1) establish throughput requirements for a functional in-suit network and (2) serve as a performance baseline for future devices that employ ultra-low-power field-programmable gate arrays and micro-transceivers. Sensor devices will upload data to a ZigBee network coordinator that has the form of a pluggable USB connector. Data are currently visualized using MATLAB and LabVIEW.

TABLE OF CONTENTS

LIST OF FIGURES

LIST OF TABLES

ACKNOWLEDGMENTS

I would like to express my appreciation for the support and assistance of my major professor, Dr. Steve Warren, and the other members of my graduate committee: Dr. Dwight Day, Dr. Bill Kuhn, and Mr. Tim Sobering. I am thankful for these great project opportunities and the kind instruction along the way. Through these lessons and many more, I have grown as an individual and become a better, more productive member of society. Finally, I thank my parents and my good friends for supporting me wholeheartedly throughout this project.

This work was supported under NASA/EPSCoR Grant/Cooperative Agreement NNX11AM05A. Any opinions, findings and conclusions, or recommendations in this material are those of the author(s) and do not necessarily reflect the views of NASA.

CHAPTER 1: INTRODUCTION

1.1 Project Overview

The primary goal of the parent project for this work (supported under NASA/EPSCoR Grant/Cooperative Agreement NNX11AM05A) is to evaluate the feasibility of low-power wireless sensor networks for in-suit health monitoring in reduced or zero-gravity environments. The project is divided into five tasks. Task 1 seeks to identify a sensible biomedical sensor set to monitor physiological parameters of interest inside a spacesuit. Task 2 focuses on radio propagation inside the suit, and Task 3 targets the design of a custom, ultra-low-power wireless network that can support biomedical sensors. Task 4 addresses radio hardware for short- and long-range links, and Task 5 focuses on outreach and diversity enhancement. This thesis work primarily relates to Task 1 [Hodges2013, KSU-NASA1, Song2013a].

The objective of the work described here was to design and implement a collection of biomedical sensors whose data can be uploaded to a computer for display. The designs emphasize high-quality data, small size, low power consumption, and enhanced subject mobility. More specifically, this work addresses the creation of a ZigBee wireless network of medical sensors that can be used to test new sensor prototypes and can serve as a comparison baseline for low-power custom networks that will be built into spacesuits [Dong2013].

In prior KSU work, three-axis accelerometers were used to assess acceleration at various body locations/joints during activities intended to emulate tasks on the moon or Mars. These types of accelerometers can potentially be placed in locations such as the chest, leg, or wrist to track or predict activity intensity and fatigue [Song2013,]. A similar ZigBee-enabled unit was designed at KSU for a project that sought to track gait instability that might then indicate the potential for slips and falls [Krenzel2012] In other work, a wireless reflectance pulse oximeter was designed that could potentially function effectively in a helmet (e.g., for forehead measurements) or a glove (e.g., for wrist and

finger measurements) [Li2012a]. Efforts for this thesis focused on the design of additional low-power biomedical devices that employed a ZigBee platform consistent with previous work. These devices include an inductive plethysmograph to determine respiration rate, one/two-channel electrocardiographs (ECGs), an electromyograph, and a modified board layout for an accelerometer/gyrometer. The inductance plethysmograph obtains respiration rate by using a belt (typically worn around the chest) which may be sewn into the upper portion of a cooling garment worn under a spacesuit [Dong2013]. The two-channel electrocardiograph (ECG) was intentionally designed as a filter-free unit whose data can potentially provide parameters other than heart rate, such as respiration rate and a metric related to ambient environmental noise.

1.2 Background – Biomedical Sensing in Reduced Gravity Environments

One inevitable risk associated with space missions is threats posed to the physical and mental health of astronauts because of these harsh, isolated environments. Exposure to such environments for long periods of time negatively impacts all physiological subsystems. ECGs can provide crucial information about an astronaut's cardiopulmonary system, thereby lowering the possibility of mission failure. Respiration rate is another indicator of physiological viability during long-term extravehicular activities (EVAs). Studies have shown that respiratory rate is one of the earliest indicators of health instability [Akbulut2011]. Accelerometers and gyrometers can be used to quantify activity and identify activity type. In addition, they may offer the potential to track or predict fatigue during EVAs as an alternative to electromyograms, which are the current standard for fatigue assessment [Ade2011].

To evaluate the sensibility of using wearable sensor data to monitor an astronaut's state of health, the KSU Kinesiology Department worked with the KSU ECE Department to develop and utilize a collection of field tests in the form of an obstacle course in which individual tests mimic typical EVAs. Tasks include lifting weighted boxes, climbing ladders and stairs, and transporting weighted objects in a wheelbarrow (lifting weighted boxes and transporting weighted objects are shown in Figure 1). Commercial sensors

provided physiological monitoring for these tasks [Ade2011, Ade2012,Broxterman2012, Broxterman2013].

Figure 1. Representative field tests performed by subjects wearing inspiration/ expiration masks, electromyographs, and chest-worn electrocardiographs/ accelerometers

For this work, a portable commercial gas exchange system measured whole body metabolic rate with sufficient breath-by-breath temporal resolution to track metabolism changes during various tasks. Electromyograph (EMG) and three-axis accelerometer data (Delsys Trigno [Delsys]) were acquired by placing wireless sensors over 16 muscles/sites (Figure 2, upper). A Zephyr BioHarness (Figure 2, lower) provided heart rate and acceleration data from the chest.

This collective information from off-the-shelf sensors allowed the ability to track or predict muscle fatigue and task failure. To date, 87 subjects have completed the obstacle course under fatiguing and non-fatiguing conditions while wearing sensors. The team is currently analyzing these acquired data. Early results from these fatigue assessments were presented at recent NASA Human Research Program Investigators Workshops [Ade2011, Ade2012, Broxterman2012, Broxterman2013, KSU-NASA1, Dong2014, Kuehl2014].

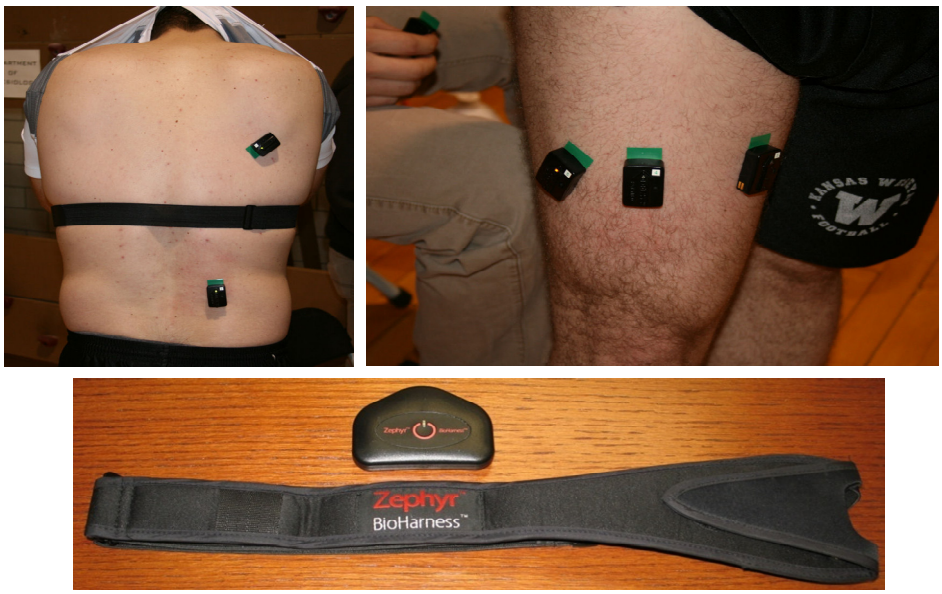

Figure 2. EMG sensors on various muscle groups (upper). Zephyr Bioharness for heart rate and activity monitoring (lower).

Acceleration data acquired during the experiments were also analyzed for their ability to indicate activity type, with the hope that these data may also provide a surrogate indicator for fatigue that does not require skin-contact electrodes (EMG sensors require electrodes). A representative confusion matrix from this work is depicted in Figure 3, indicating that simple accelerometer data may be a sensible resource for automatic task identification functions [Song2013a].

More focused assessments of changes in forearm EMG signals (and corresponding spectra) due to fatigue were performed with the assistance of a custom hand-forearm ergometer, depicted in Figure 4. Preliminary results suggest that changes in mean firing frequency assessed through short-time FFT analysis are well correlated with fatigue [Gude2013a, Gude2013b].

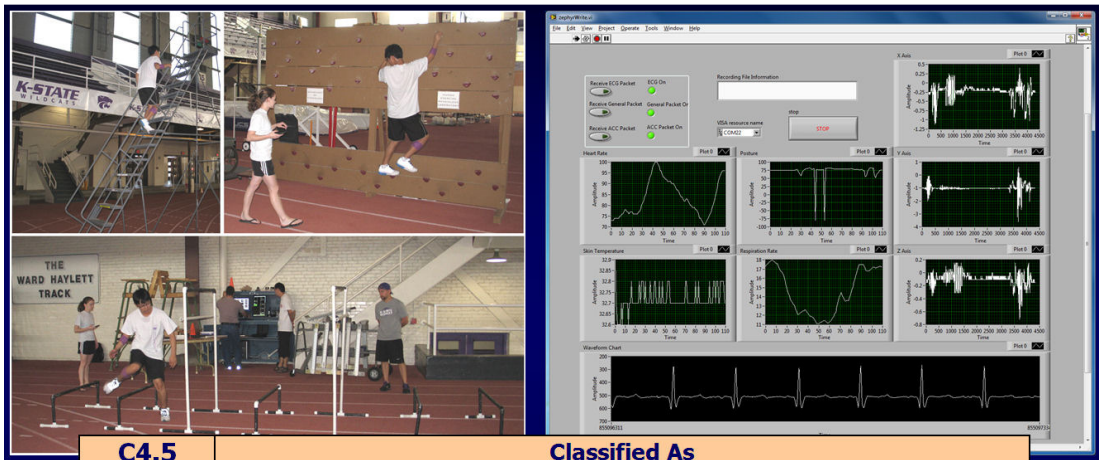

C4.5	Classified As					
Activity	Cones	Ladder	Lift	Step	Stair	Wall
Cones	52	2	0	0	0	0
Ladder	0	82	10	1	3	8
Lift	0	9	138	2	11	8
Step	1	0	0	142	0	1
Stair	0	7	4	0	171	0
Wall	0	11	6	0	0	73

Figure 3. Confusion matrix: accelerometer-based activity identification [Song2013a].

Figure 4. Automated hand-forearm ergometer to assess forearm EMG data as a function of fatigue [Gude2013a, Gude2013b].

Based on these field tests and ergometer studies, the team affirmed the importance of [Song2013, Ade2011]:

- EMGs from targeted muscle groups to assess/predict fatigue,
- inspiration/expiration masks to measure whole body oxygen uptake, carbon dioxide production, and ventilation, and
- chest-worn accelerometers to quantify activity and identify activity type.

Additional types of sensors (e.g., the respiration belt, accelerometer, and pulse oximeter noted earlier) could be integrated into a spacesuit to potentially provide a supplement and/or alternative to electrode-based sensors such as ECGs and EMGs that currently gather state-of-health information. Examples of such sensors are noted in the next section.

1.3 Sensor Selection

For customized sensors, existing ZigBee-enabled pulse oximeters and accelerometer/ gyrometer sensors were supplemented with a respiration rate sensor, ECGs, and EMGs. Illustrated in Figure 5, the filter-free ZigBee-based pulse oximeter can be used to measure heart rate and blood oxygen saturation, plus potentially estimate metabolic rate using the difference between SpO_2 and SvO_2 values. The design employs a JN5139 ZigBee-integrated microprocessor module from Jennic. Jennic more recently released a new ultra-low-power ZigBee-Pro-based wireless microcontroller, the JN148. Unfortunately, the JN5148 is not backward compatible with the JN5139 since they utilize different integrated development environments (IDEs) and software development kit (SDK) libraries. However, they share identical pin configurations, so if the printed circuit board (PCB) layout design could be maintained and the JN5139 on the board could be replaced with a JN5148 module, firmware could then be modified to update the system.

As illustrated in Figures 6 through 8, circuitry that provides EMGs and ECGs was previously implemented in *ECE 772/773 –Biomedical Instrumentation* [Warren2011]. Board-level upgrades to these designs utilized the same ZigBee Pro template present in Devon Krenzel's accelerometer board [Krenzel2012] and the respiration rate belt [Dong2013, Dong2014]. Figure 6 depicts the basic data acquisition system that employs

an AD620 instrumentation amplifier to acquire ECG or EMG signals due to the amplifier's high common mode rejection ratio. The combination of filters and amplifiers was achieved by cascading operational-amplifier-based stages with appropriate components and feedback (refer to Figure 7). ECG signals acquired in ECE 772/773 were sampled by myDAQ units from National Instruments and displayed in LabVIEW virtual instruments (VIs) (see Figure 8).

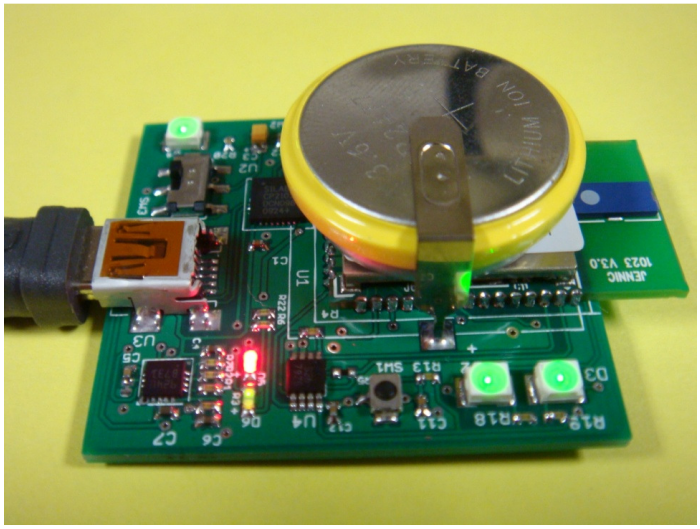

Figure 5. Pulse oximeter designed by Kejia Li [Li2012a,Li2012b].

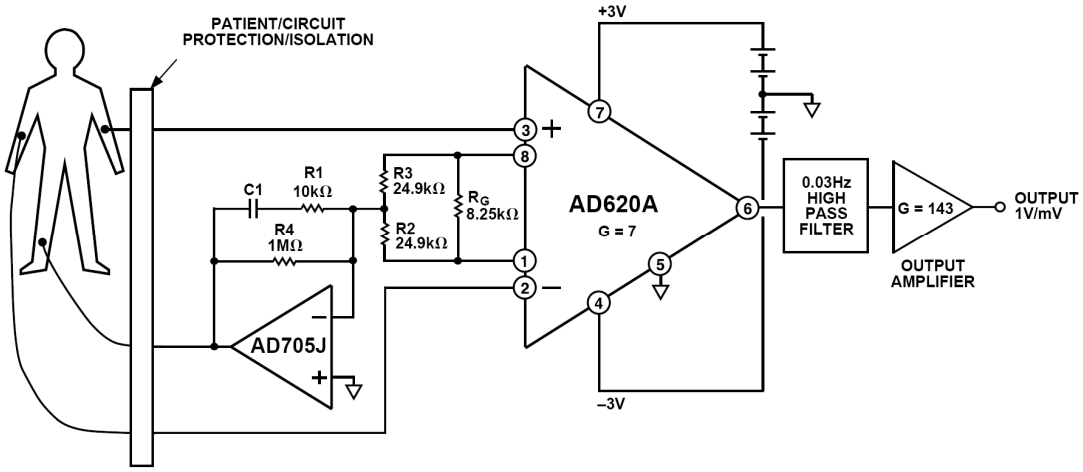

Figure 6. AD620-based electrocardiogram sensing circuit [Analog1999].

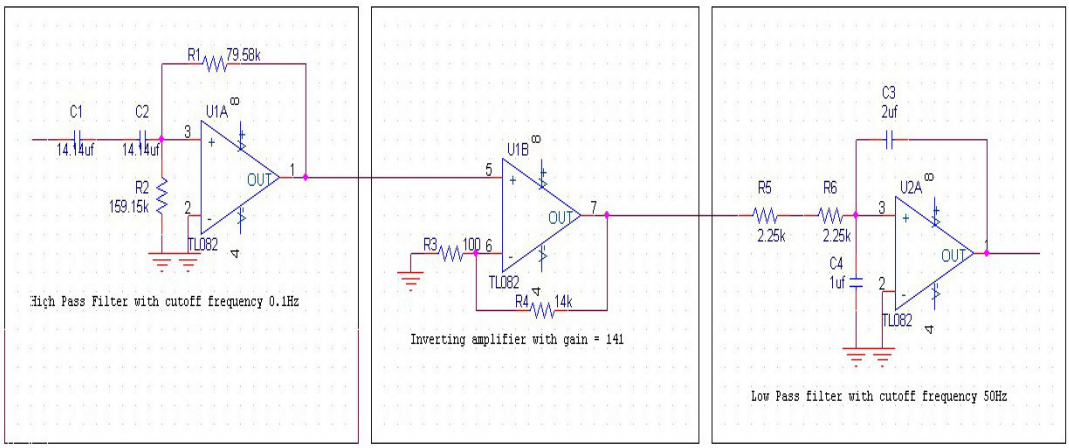

Figure 7. ECG filter cascade.

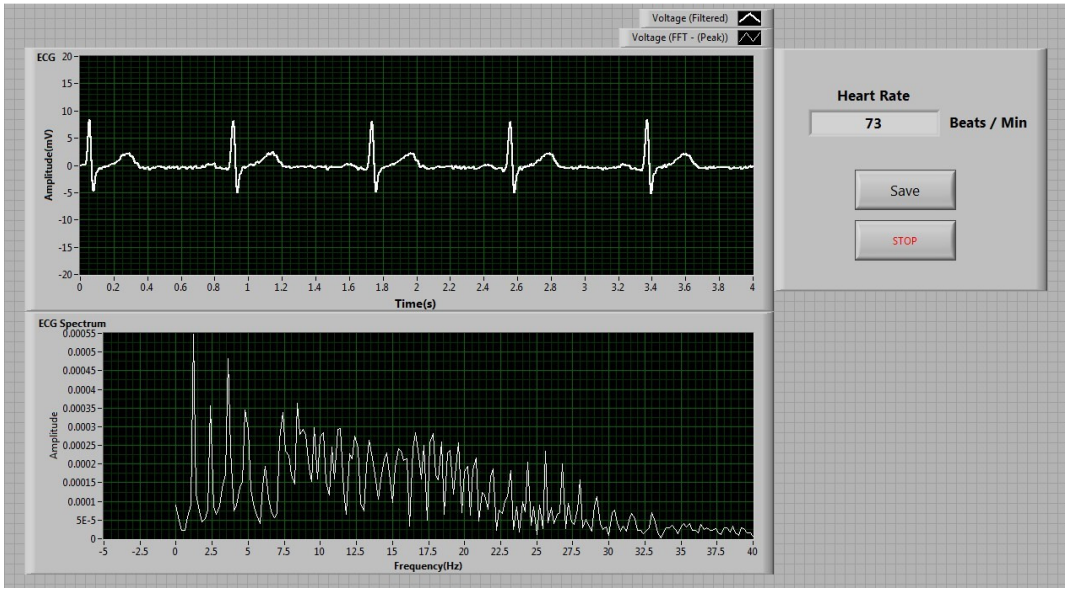

Figure 8. ECG acquisition and analysis VI [Warren2011].

1.4 Wireless Transmission Protocol Selection

ZigBee is a wireless communication standard based on the IEEE 802.15.4 specification, natively designed for sensor networks. Each ZigBee node offers a transmission range of tens of meters, and adding routing nodes increases coverage. Data traffic is not substantial for most biomedical sensing networks, since sample rates are typically only a few hundred Hz per signal at most, so ZigBee's transfer rate of 250 kbps is able to meet physiological parameter transmission requirements [Liu2009]. In addition, ZigBee power

consumption is low when compared to common wireless protocols such as Bluetooth and Wi-Fi, potentially allowing for continuous long-term health monitoring powered only by a battery. Table 1 compares the core ZigBee specifications with the corresponding Wi-Fi and Bluetooth specifications.

Table 1. Comparison of various wireless technology specifications.

	ZigBee	Wi-Fi	Bluetooth	Bluetooth LE
Frequency Band	868/915 MHz, 2.4 GHz	2.4/5.8 GHz	2.4 GHz	2.4 GHz
Data Rate	250 kbits/s	11 to 105 Mbits/s	1-3 Mbits/s	1 Mbits/s
Battery Life	Years	Hours	Hours to Days	Years
RF Range	10 to 300 m	10 to 100 m	10 m	5-10 m
Topology	Mesh, Star, Tree	Star	Star	Star
Max Nodes Per Receiver	65524	32	7	8

Wi-Fi is typically used for high-throughput data communication such as local cell phone use because it offers a wide bandwidth (300 MHz) and operates in the license-free 2.4 GHz band. Wi-Fi's primary drawbacks for use with biomedical sensor networks are its relative expense and power consumption when used in continuous or frequent medical health monitoring [Kim2013, Trasvina2014].

Like ZigBee and Wi-Fi, Bluetooth also operates in the 2.4 GHz frequency band. The data rates that Bluetooth supports are also more than sufficient for biomedical sensor networks. Bluetooth's transmission range is up to 10 m. “Classic” Bluetooth has been utilized in medical products such as wireless blood glucose meters. Although a Bluetooth transceiver board can be powered by one single coin cell battery, Bluetooth's high power consumption relative to ZigBee limits its battery life to only a few hours of continuous transmission, thereby limiting the biomedical sensor network applications that may benefit from the standard. A new version of the protocol, known as Bluetooth Low Energy (BLE), was developed for short range, low-power control and application monitoring. The primary difference between classic Bluetooth and BLE is that BLE is

designed for transmission of occasional data parameters instead of data streaming. Like Bluetooth, BLE employs a frequency-hopping spread spectrum method which prevents interference from other radio sources. [Liu2013 ,Zhou2013].

Note that BLE could also be a good match for a suit-based biomedical sensor network due to its low power consumption, high data rate, and interference immunity [Liu2013,Zhou2013]. ZigBee was employed for this effort primarily as a means to take advantage of legacy designs that were created at a time when BLE was not yet available.

1.5 System Features

One objective of this overall NASA project (and a primary objective of Tasks 1 and 3) is to create an in-suit sensor network that provides high-quality physiological data while requiring little power input. The sensor designs and supporting ZigBee wireless network presented in this thesis are intended to act as a comparison baseline for field programmable gate array (FPGA) based low-power sensors, textile-based devices/antennas, custom low-power wireless links, and network protocols. The sensors and sensing network in this study were pursued with the following features in mind:

- small-size, low-power sensors powered by a coin cell battery or with energy harvesting to support continuous health monitoring,
- ZigBee-based low-power wireless body sensor network,
- sensors operated in filter-free mode (e.g., ECG, pulse oximeter, or respiration belt) so that data streams incorporate all signal elements, and
- a small-sized, pluggable USB-connector network coordinator for data recording.

As illustrated in Figure 9, the target biomedical sensor network incorporates a one/two channel ECG, a respiratory belt, a pulse oximeter, one or more accelerometer/gyrometer sensors, one or more EMG sensors, and a USB pluggabe wireless receiver. The ZigBee wireless network will support both JN5139 and JN5148 modules from Jennic.

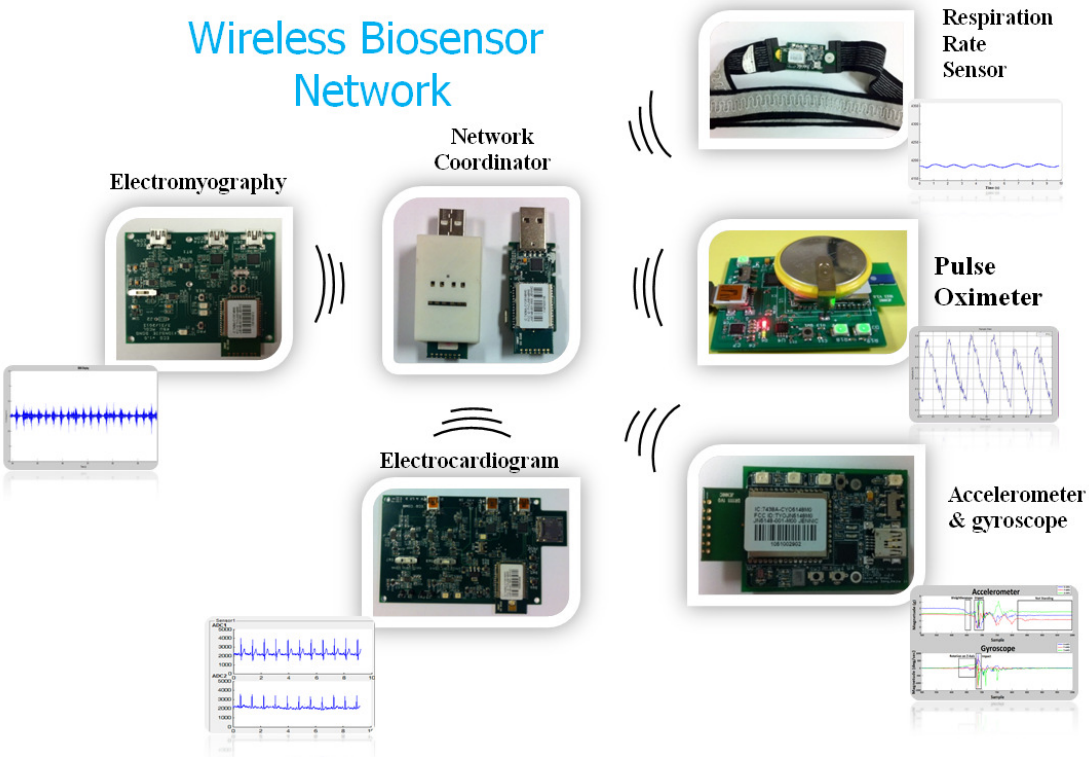

Figure 9. Target ZigBee-based wireless biosensor network.

CHAPTER 2: WIRELESS SENSOR AND NETWORK DESIGN

2.1 Sensor Design and Implementation

2.1.1 Inductive Plethysmograph

Respiration rate is an important parameter for establishing state of health in environments with potential oxygen constraints. Respiratory information can be (a) extracted from signals such as ECGs or pulse plethysmograms or (b) measured directly with capacitive respiration sensors [Merritt2009], impedance plethysmography [Ansa2011], piezosensors [Nan2007, Bu2007], thermistors, or other sensors that track movement, temperature, acoustic noise ,etc.

Impedance plethysmography senses impedance changes as a cross section of the human body expands and contracts, allowing qualitative measurement of chest movement during breathing. This technique requires two electrodes attached to the skin and a weak alternating current that passes through these electrodes, allowing impedance to be measured directly as a function of time [Ansa2011]. However, impedance plethysmography yields a non-linear signal, and electrical current must be passed through the subject, generating both safety and battery power issues, especially inside an oxygenated, pressurized spacesuit where electrical current should be avoided and battery power should be minimized.

In some piezosensing techniques, a piezo-crystal-based respiration sensor is located on a short section of a belt. However, when the subject lies on top of the piezo crystal, breathing effort may not be detected, and incorrect readings or unexplained changes in polarity can be produced [Nan2007, Bu2007].

For long-term EVAs, a technique such as respiratory inductive plethysmography (RIP) is appealing if it can be implemented in a manner that is comfortable for the wearer. RIP relies on the principle that alternating electric current passed through a loop of wire generates a magnetic field perpendicular to the loop. In such a situation, the wire loop

("belt") exhibits self-inductance, *L*. The act of breathing changes the cross area of the chest, thus changing the magnetic field and the self-inductance of the loop. If the self-inductance is made to be part of a resonant circuit (e.g., an *LC* oscillator), then changes in chest cross-sectional area will correlate to changes in resonant frequency, which can then be demodulated to create a respiration voltage waveform. No electrical current passes through the body with RIP, and the weak magnetic field does not affect the human subject. The resulting signal is a linear, accurate representation of the change in the cross-sectional area [Lee2008, Dong2013].

The process is illustrated in Figure 10, where the respiration rate sensor includes three electronic components: an *LC* Colpitts oscillator, a comparator, and a pulse counter with time windowing. When the coil is expanded or compressed (meaning a change in belt length and shape), a series inductance ΔL is added, thereby changing the frequency of the *LC* oscillator. A comparator follower then converts the sine waveform into a square wave which can be digitally sensed by a microcontroller.

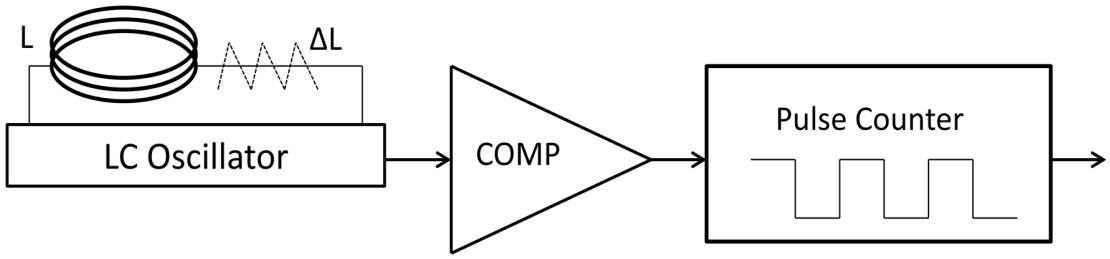

Figure 10. Block diagram of the respiration sensing system.

Colpitts Oscillator

A Colpitts circuit, similar to other *LC* oscillators, consists of a gain element (e.g., a BJT, MOSFET, or amplifier) and an output that is connected to its input in a positive feedback loop that contains a parallel *LC*-tuned circuit which functions as a bandpass filter to set the oscillating frequency. This positive feedback configuration results in a 0^o or 360^o overall phase shift. A Colpitts oscillator is typically configured as a common emitter amplifier with an output signal 180^o out of phase with respect to the input signal. The additional 180^o phase shift required for oscillation is achieved because two capacitors are

connected together in series, and the pair is in parallel with an inductor, resulting in an overall circuit phase shift of 0° or 360°.

As illustrated by the BJT Colpitts oscillator in Figure 11, the oscillator utilizes a capacitor voltage divider as its feedback element because resistors are not pure resistors at high frequencies – they would load the output. The amount of feedback is determined by the ratio of *C*1 and *C*2, and the oscillation frequency of a Colpitts oscillator is determined by the resonant frequency of the *LC* tank circuit, given as

$$f = \frac{1}{2\pi\sqrt{LC}} \text{ Where } C = \frac{C1*C2}{C1+C2} \quad (1)$$

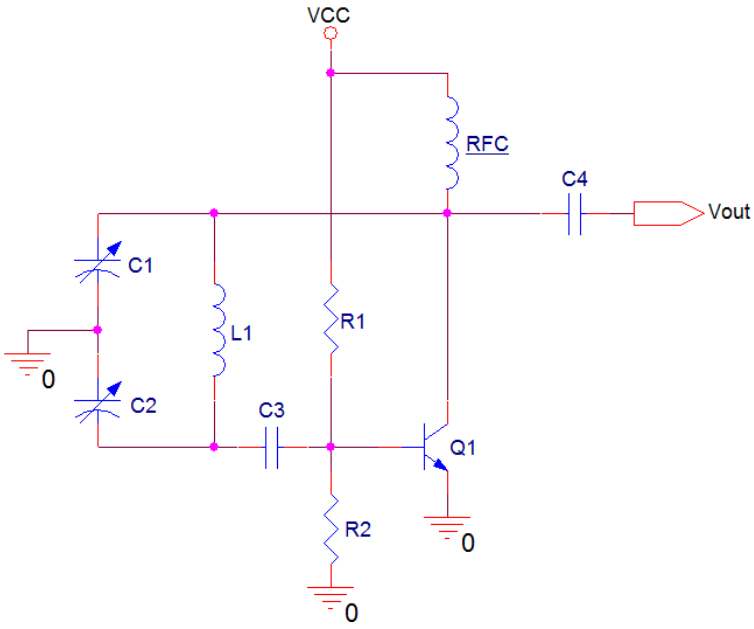

Figure 11. BJT *LC* Colpitts oscillator.

Rather than using a BJT, an op amp can be used as an active component with feedback – see Figure 12. The operation of an op-amp Colpitts oscillator is similar to the BJT version, and the resonant frequency is calculated in a similar manner.

Changes in the magnetic field result in changes in self-inductance, which can be tracked by variations in the oscillator resonant frequency. A Colpitts oscillator produces a relatively pure sinusoidal waveform due to the low-impedance paths provided by the

capacitors at high frequencies. The oscillator experiences relatively small changes in frequency compared to its base resonant frequency.

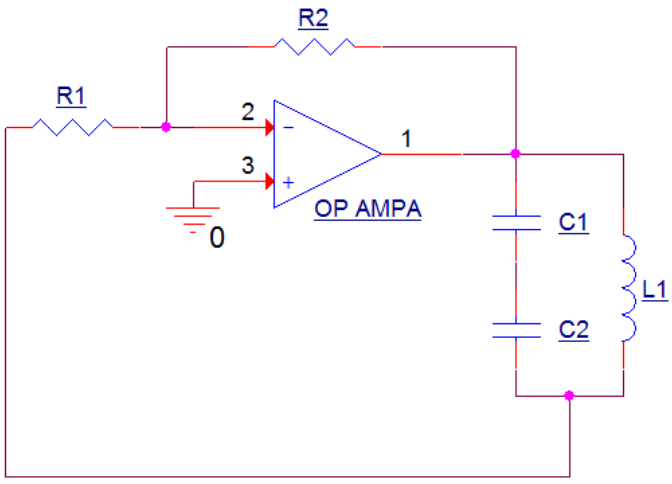

Figure 12. Op amp Colpitts oscillator.

A circuit must be designed that converts changes in resonant frequency to a respiration signal. The conversion can be achieved in two ways: analog or digital. With an analog solution, a frequency-to-voltage converter is applied that converts frequency variations into voltage variations that can be transduced by the microprocessor analog-to-digital converter ADC. Table 2 lists existing frequency-to-voltage converters on the market and their corresponding specifications.

Table 2. Specifications for existing frequency-to-voltage converters.

	Supply Voltage	Power Dissipation	Non-Linearity	Conversion Scale	Size(inches)
LM2907	0 – 28V	1200mW (Max)	±0.3%	f_{in}*VCC*R*C	0.4 X 0.26
LM331	5 – 40V	20mW (+5V)	±0.3%	1kHz/V	0.4 X 0.26
TC9400	8 to 15V (Single Supply)	470mW	0.05%	$V_{out} = v_{ref}*c_{ref} *R_{int}*F_{in}$	0.74 X 0.29
AD650	±5 - ±15V (Dual Supply)	144mW	0.005% typ at 100 kHz	f_{in}*VCC*R*C	0.765 X 0.32
VFC32	±11 - ±20V (Dual Supply)	82.5mW	±0.05% max at 100kHz	2kHz/V	0.375 X 0.255

These limited options specify (a) a minimum power supply of 5 V for the converter, which requires an extra voltage regulator to convert 3.3V to 5V, (b) additional power

dissipation during conversion, (c) a dual power supply (required by some), (d) extra space for extra components, and (e) non-linear frequency-to-voltage modules. These factors drove the decision to seek a digital solution, as noted in Figure 10, consequently saving space, reducing power consumption, and improving signal accuracy. Figures 13 through 15 contain top, bottom, and overall views of the respiration sensor prototype.

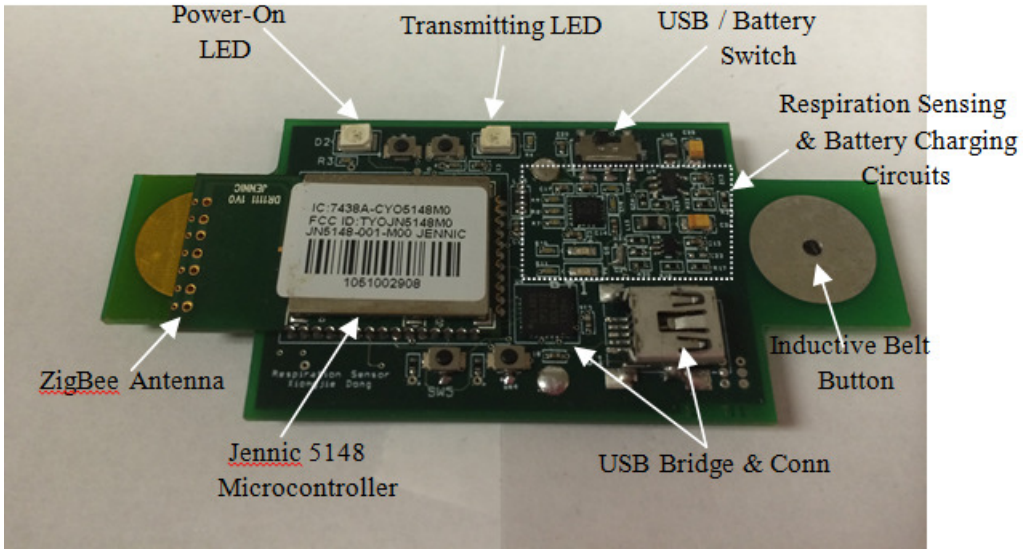

Figure 13. Top view of the respiration sensor board.

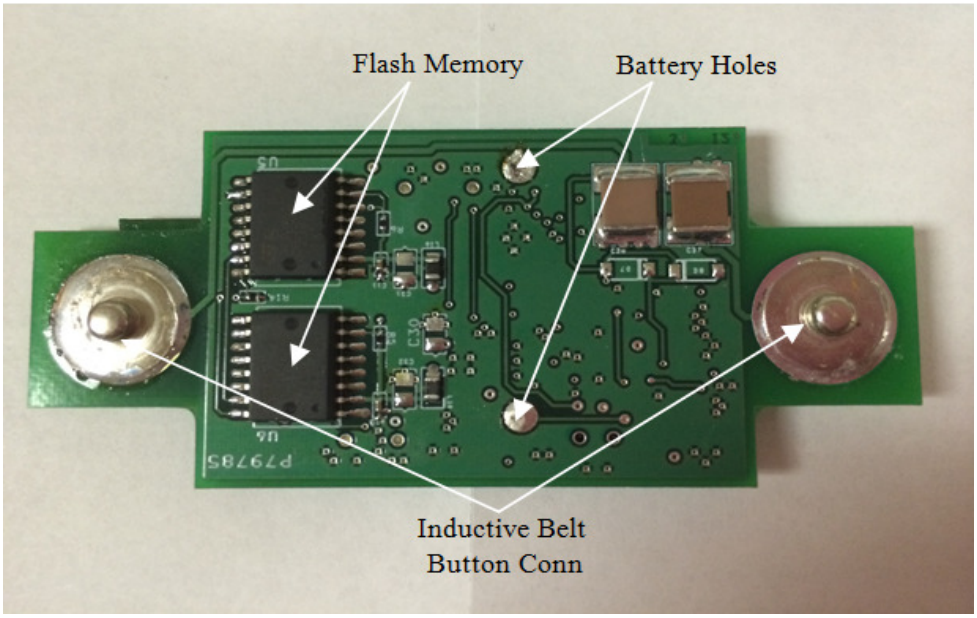

Figure 14. Bottom view of the respiration sensor board.

Figure 15. View of the entire respiration sensor belt.

The respiration sensor hardware is divided into five modules: a microprocessor module, an *LC* Colpitts oscillator, a signal sampling module, a power management module, and other auxiliary circuitry (including a USB bridge). The microprocessor module is a Jennic JN5148 module, designed specifically for robust and secure low-power wireless applications. This sensor unit and its receiver employ Jennic microcontrollers that support an integrated ZigBee wireless protocol.

The main sensor module is the *LC* Colpitts oscillator depicted in Figure 16. An *LC* tank circuit is formed by components *L*1, *C*27, and *C*28, and the sampling frequency is configured to be about 400 kHz by Equation 1. An LM8261op amp was chosen for the active feedback component due to its rail-to-rail common mode voltage range, unlimited capacitive load drive capability, large slew rate, and high bandwidth. The LMV7219 is a low-power, high-speed comparator with internal hysteresis which ensures clean output transitions. The LMV7219 comparator was used to convert the sinusoidal output signal from the Colpitts oscillator into pulses which can be sensed by the microprocessor. Since the respiratory belt is powered by either a cell battery or USB, *R*17, *R*18, *R*22, and *R*23 were used for a DC bias. *R*24 and *R*25 were applied for the loop gain.

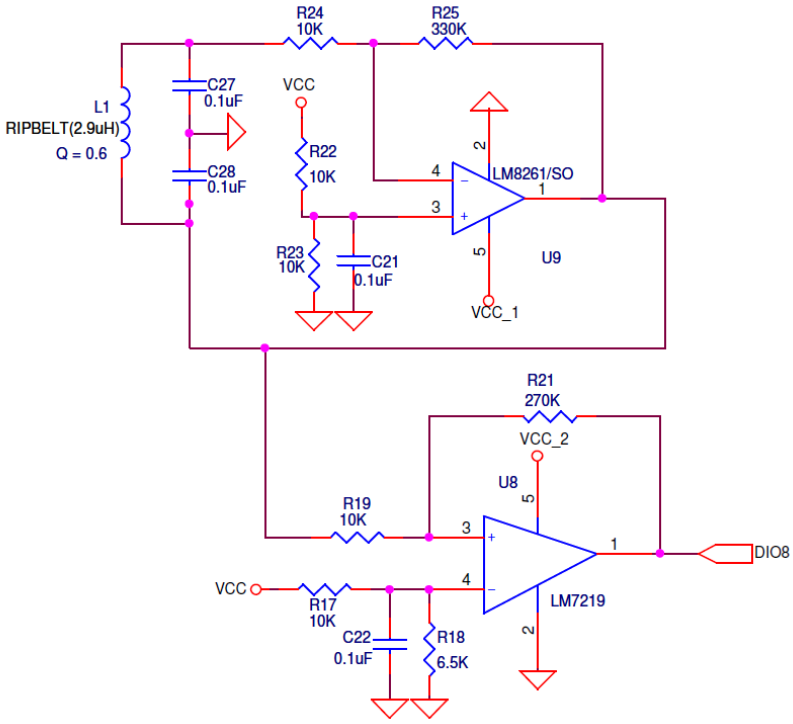

Figure 16. LC Colpitts oscillator employed for respiration sensing.

The remainder of the circuit-level functionality is illustrated in Figure 17. As noted earlier, the respiration sensing circuit employs a digital solution. The respiration belt typically uses a wireless link to communicate with a receiver on a PC, and data storage on the PC is managed through a graphical MATLAB interface. A mini-USB connection can provide a wired interface to the PC while the battery recharges. If neither the wireless link nor the USB connection are available, sampled data are temporarily stored on flash memory.

Extensive bench testing was conducted to verify the correct operation of the respiration sensor hardware. The ZigBee wireless link proved to be stable and reliable. Using a CR2032 Maxell lithium cell battery, the system can operate up to 3 hours with continuous wireless transmission. Table 3 contains specifications for the respiration sensor unit.

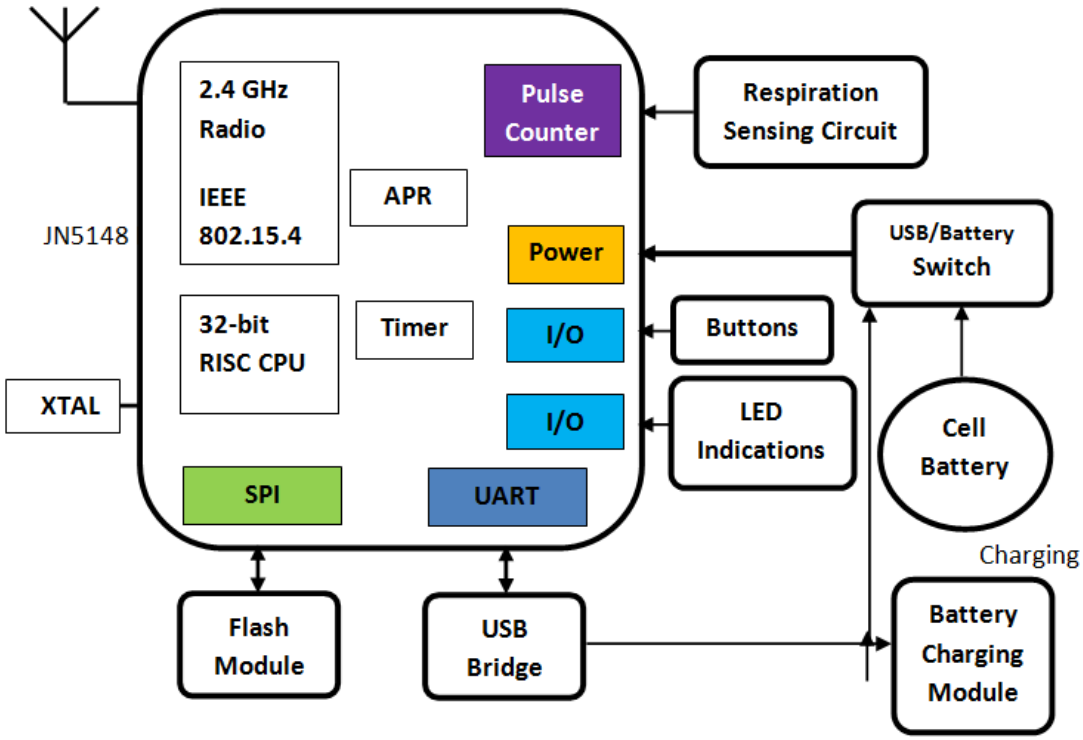

Figure 17. Respiration sensor circuit-level system layout.

Table 3. Specifications for the respiration hardware module.

ITEM	PARAMETER
Peak Power Consumption	60mW
Power Supply Voltage	3.3V
Supply Current	18mA
Resonant Frequency	400KHz
Belt Inductance Without Deformation	2.9uH
Resistance of the Sensor Belt	0.9Ohm

Respiration tests were conducted on female and male subjects (see Figures 18 and 19). Figures 20 and 21 display respiratory signals for both subjects, respectively, with the *y* axis representing pulse counts in a 10 ms time window and the *x* axis representing time in seconds, The waveform in Figure 20 is biased at approximately 9100, and the waveform in Figure 21 is biased at approximately 4250 because the pulse counter was initially

configured to count only rising edges. The belt was wrapped tighter on the female subject's chest and looser on the male subject's chest. Tighter belt placement results in a larger variation in pulse counts (i.e., a larger signal amplitude), but a belt that is too tight also results in discomfort.

Figure 18. Respiration rate measurement on a male subject.

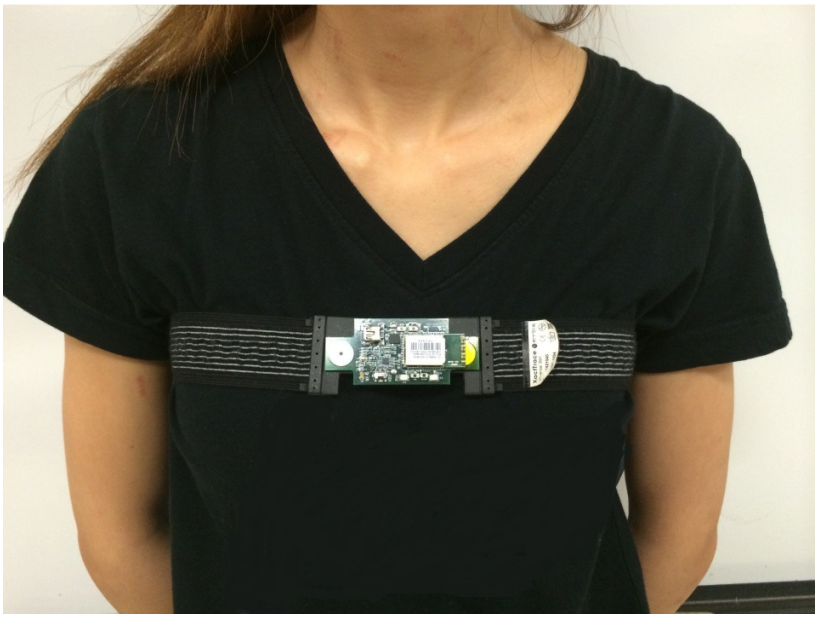

Figure 19. Respiration rate measurement on a female subject.

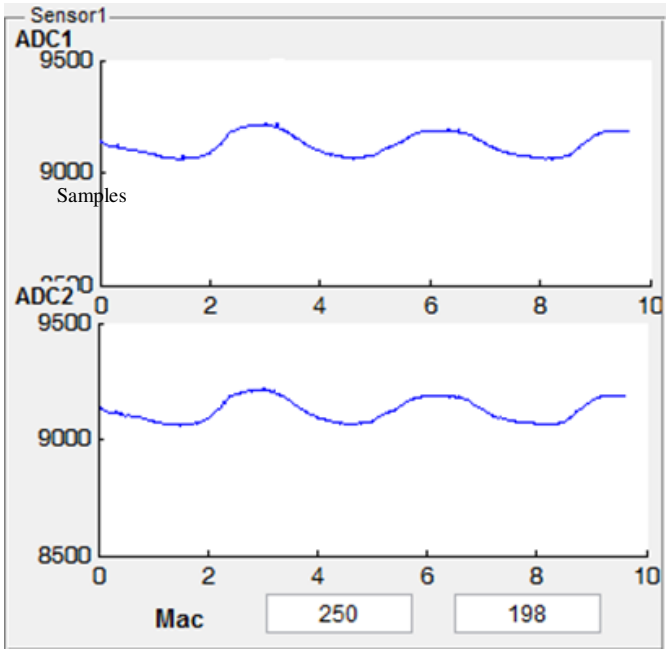

Figure 20. Typical respiration signal obtained with the belt (male subject).

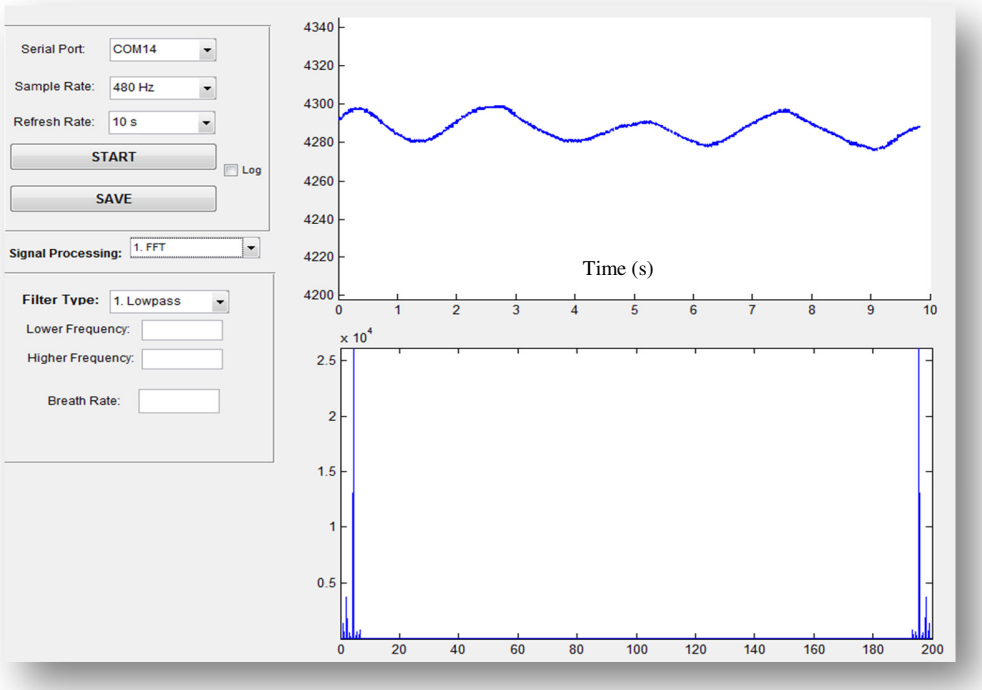

Figure 21. Respiration signal and spectrum (female subject)..

2.1.2 Electrocardiograph

Long-term space missions affect all physiological systems, including the cardiopulmonary system. An ECG can provide crucial information for the rapid diagnosis of medical conditions in astronauts and prevent mission failure due to poor health. The ECG device designed in this study utilizes electrodes to convert ionic signals from the body into electrical signals [Gao 2012].

Circuit Design

An ECG circuit needs to both amplify small signals measured from the heart and filter internal/external noise or interference. Amplification is primarily implemented through a differential amplifier, and a right leg drive circuit can be used to help cancel noise and other common mode signals.

Due to the small amplitude of the signal (typically 1 mV or less), the circuit gain should be large. A gain of over 1000 is typically implemented in ECG circuits. In addition, amplifiers should have a high common mode rejection ratio to eliminate large offset signals or noise. These factors drive the need for an instrumentation amplifier with the characteristics of very low DC offset, low drift, low noise, very high open loop gain, very high common-mode rejection ratio, and very high input impedance. Figure 22 illustrates the circuit schematic for the ECG sensor utilized in this effort.

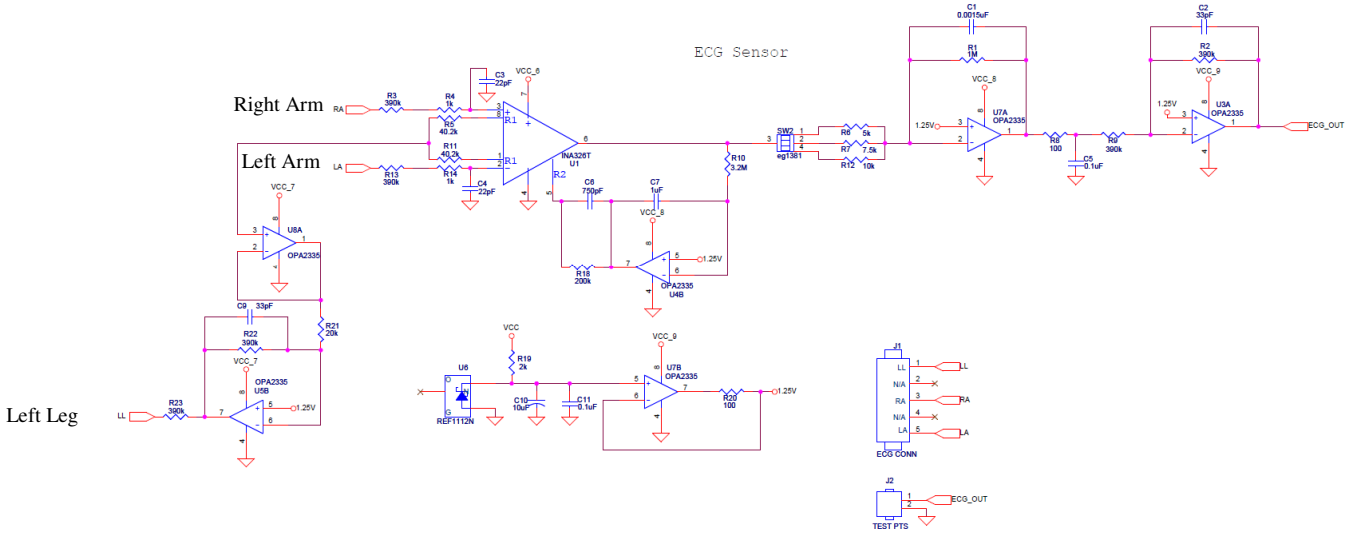

Figure 22. Circuit schematic for the ECG sensor.

As noted in the schematic in Figure 22, an INA326 instrumentation amplifier is used due to its low voltage offset (100 µV), low offset drift (0.4 µV/°C max), and high common-mode rejection (100 dB). The INA326 input gain is set to 5 since G1 = 2(*R*18/ (*R*5+*R*11)) = 2(200k/80k) = 5. To cancel resistor noise (i.e., reduce noise bandwidth), a 22 pF capacitor is placed parallel to *R*14 and *R*4. The output stage provides an adjustable gain ranging from 100 to 200 V/V, so the overall gain of the ECG sensing circuit ranges from 500 to 1000 V/V. The input common-mode voltage was fed back via the amplifier U8A and U5B to the right leg to further reduce 50/60 Hz noise.

Figures 23 and 24 contain top and side views of the ECG prototype and the ABS housing designed in Solidworks.

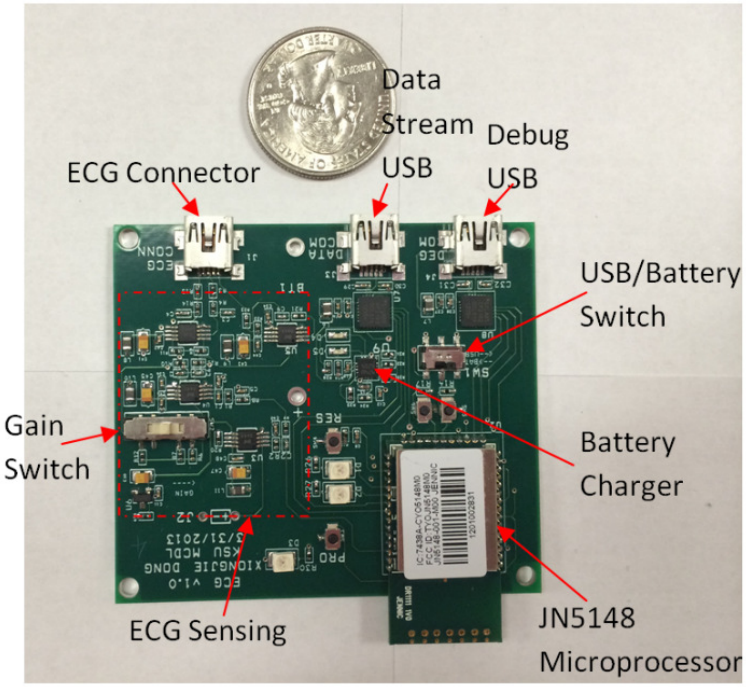

Figure 23. ECG circuit prototype (top view).

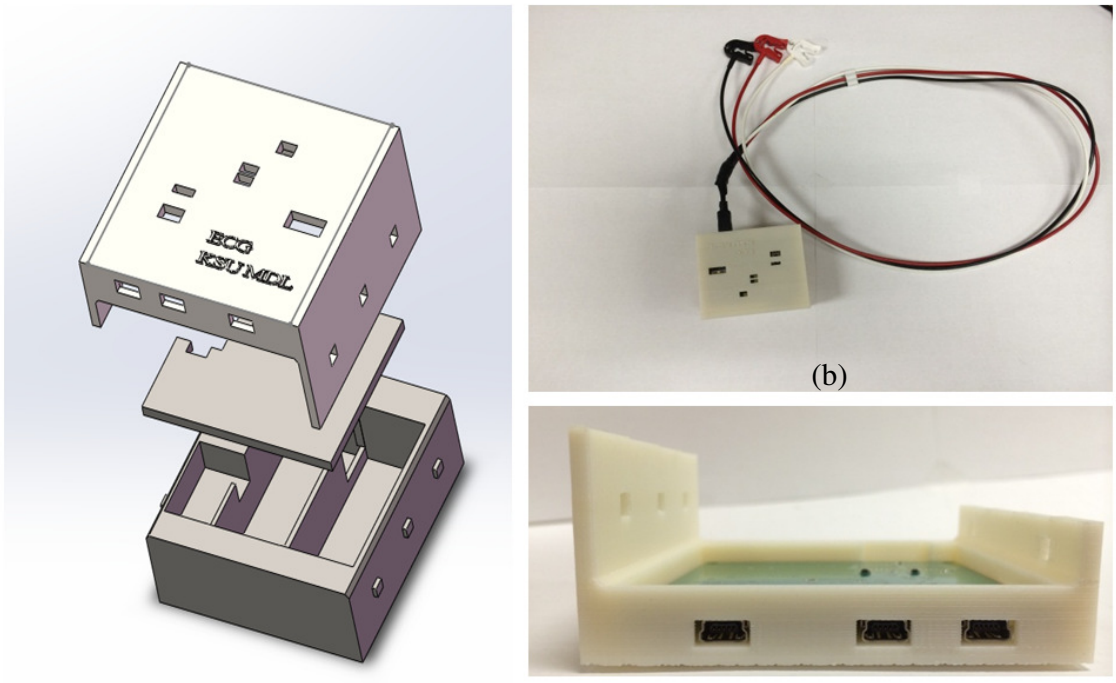

(a) (b) (c)

Figure 24. Solidworks design for the ECG case.

The three-lead ECG system can be easily modified to acquire an EMG signal. EMG spectral contents fall in the range of 0 to 500 Hz, and the amplitude of an EMG signal can range from 0 to 1.5 mV, similar to an ECG signal amplitude. Since the filter is optional on the ECG board, cutoff frequencies can be modified, or the analog filter can be bypassed and the digital filter can be applied.

A 2-channel ECG system was also designed as a filter-free unit whose data can potentially provide respiration rate and a metric related to ambient environmental noise. This ECG board is depicted in Figure 25. The two-channel ECG system can either provide two lead arrangements or serve as a redundant system. ECG experiments were conducted on a male subject, as depicted in Figure 26. Figure 27 displays a representative set of ECG waveforms acquired with this unit.

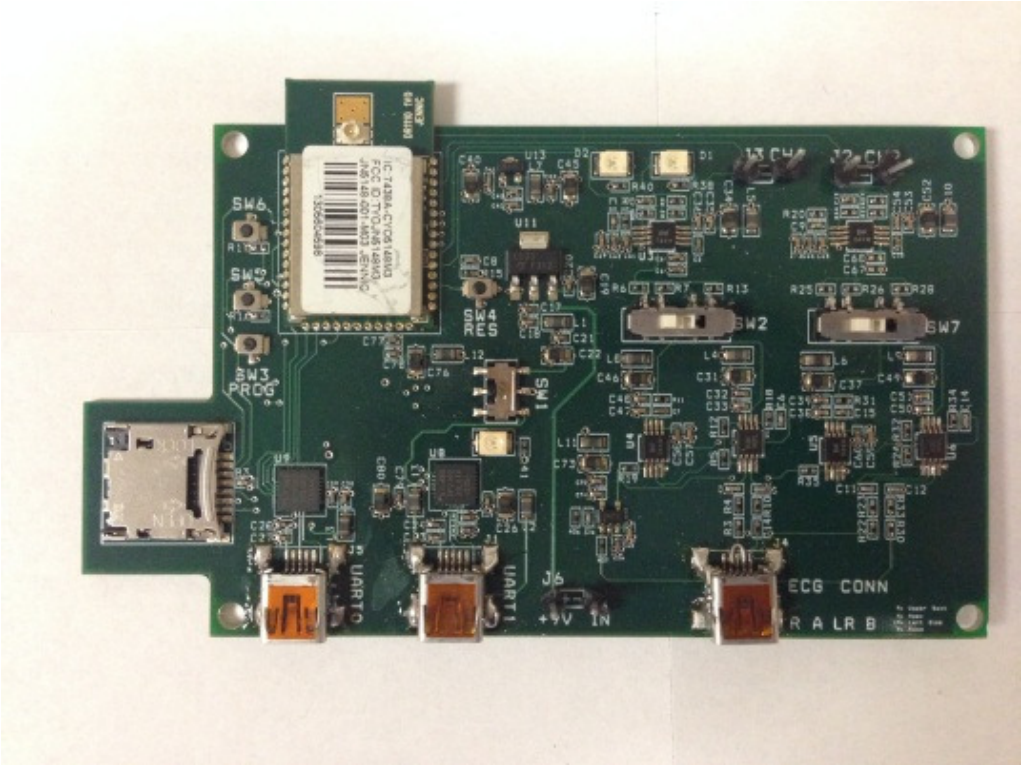

Figure 25. Two-channel ECG board.

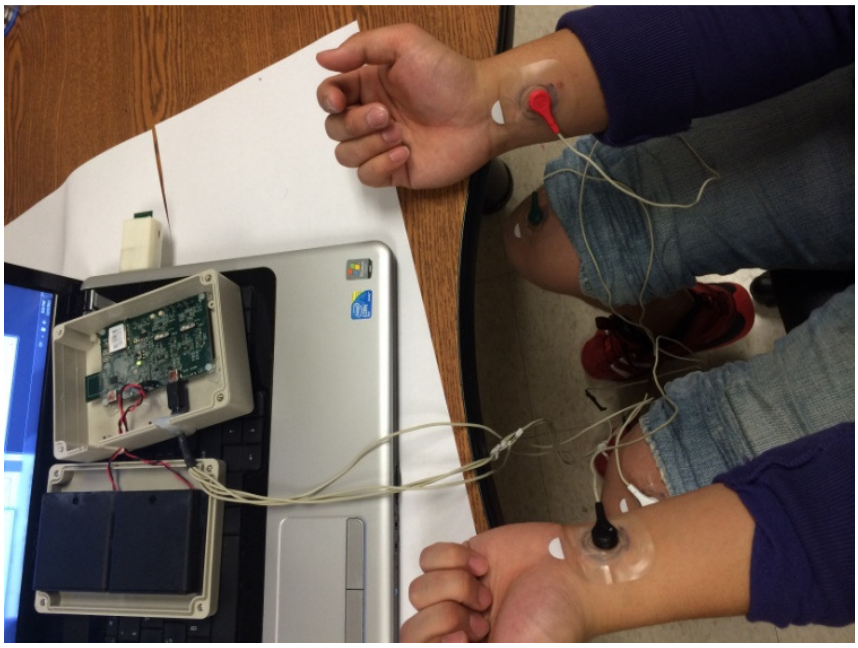

Figure 26. ECG measurement setup.

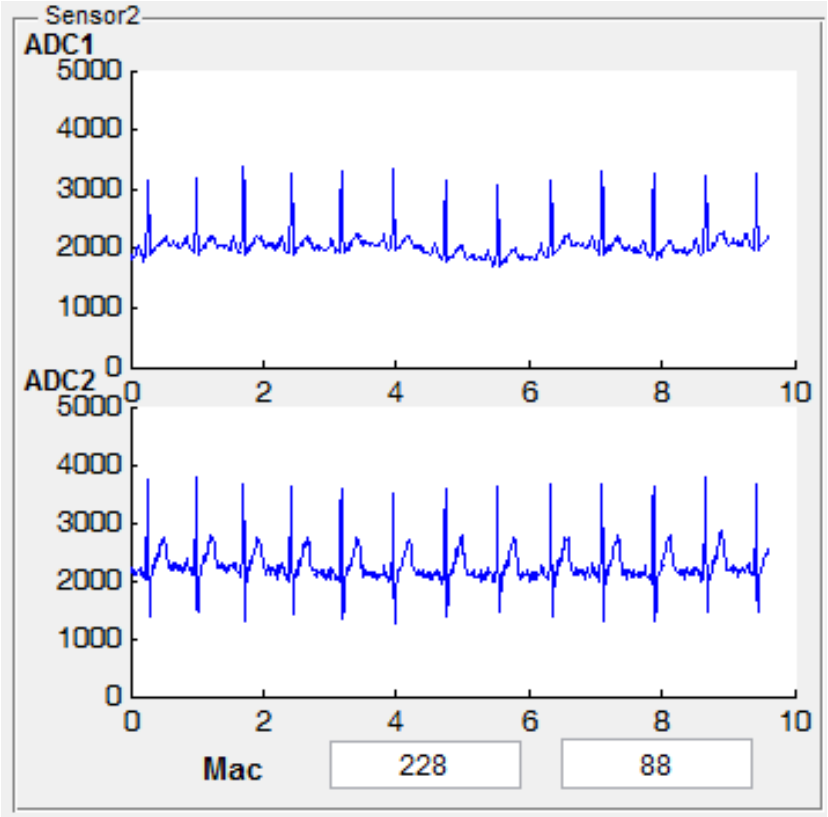

Figure 27. Typical ECG signals.

2.1.3 Accelerometer/Gyrometer

The accelerometer/gyrometer sensor design was initially created by Devon Krenzel, where the application related to a wireless, wearable system for slips and falls prediction [Krenzel2012]. The hardware design was replicated in this study for use with the NASA project, and the device firmware was altered so that the unit could be integrated into the ZigBee wireless network. The accelerometer/gyrometer sensor prototype employs a ZigBee wireless module for wireless communication and data logging, an accelerometer/gyrometer chip for dynamic movement detection, and a mini-USB connection for chargeability and processor programmability. Figure 28 contains a picture of the hardware board.

The CMA3000 MEMS three-axis digital accelerometer and CMR 3000 three-axis digital gyrometer were chosen for their low-power consumption, high precision, and high

sampling rate. This chip can run on voltages from 1.7 V to 3.6 V, and power consumption varies according to sampling rate. For example, the chip consumes 50 µA of current at a sampling rate of 100 Hz. The acceleration range can be set from ±2 g to ±8 g with 8-bit resolution [Murata2004]. Since some activities yield accelerations exceeding ±2 g, an acceleration range of ±8 g was chosen to prevent signal saturation.

The accelerometer communicates with the microcontroller through a serial peripheral interface (SPI) bus which requires four wires (SCLK, MISO, MOSI, SS) between the master (Jennic 5148) and the slave (sensor). The Jennic chip provides a clock for data transmission on SCLK, but actual data transmission occurred through the MOSI (Master Out Slave In) and MISO (Master In and Slave Out) wires. Slave Select (SS) was used for the master device (Jennic 5148 microcontroller) to switch communication from slave devices (accelerometer or gyrometer). The overall board size was 54 x 39 x 19 mm, ideal for placing the sensor in a pocket or a small holder.

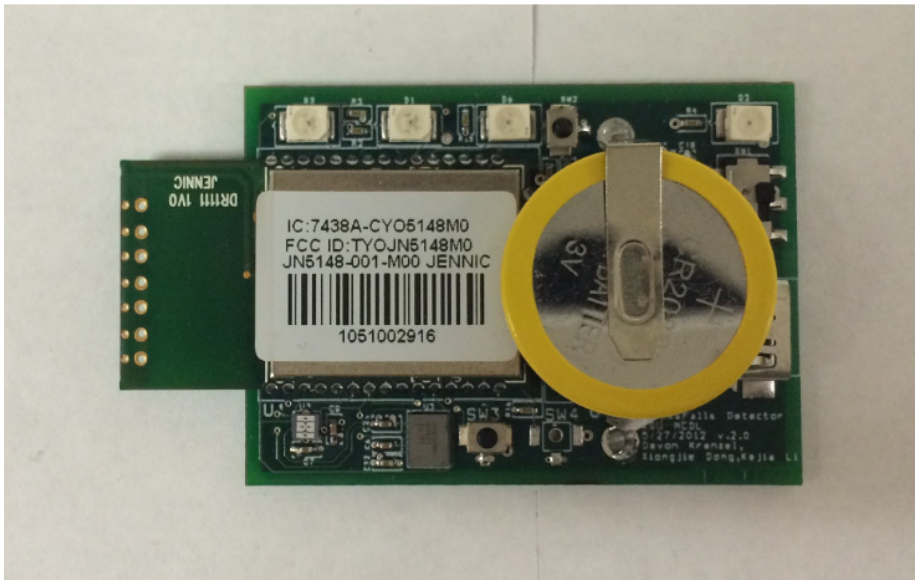

Figure 28. Accelerometer and gyrometer board.

Because nearly all human movement occurs in the frequency range of 0.6 to 50 Hz, the output data rate of the accelerometer chip was configured to 400 Hz. However, the signals were down-sampled to 100 Hz per axis to match the sampling rate of the other wireless sensors so that an identical data package pattern could be adapted.

To test the accelerometer, it was placed in a pocket with the top side of the sensor unit facing various directions. Data were recorded and then transmitted wirelessly during a walking activity. Some of these data are depicted in Figure 29, where the acceleration variations in the *y* direction are larger than the variations in the *x* and *z* directions. To create the data in Figure 30, the sensor unit was placed in such a way that walking highlighted activity along the *x* axis. The *x* axis displayed positive accelerations, while the *y* and *z* axes offered negative accelerations.

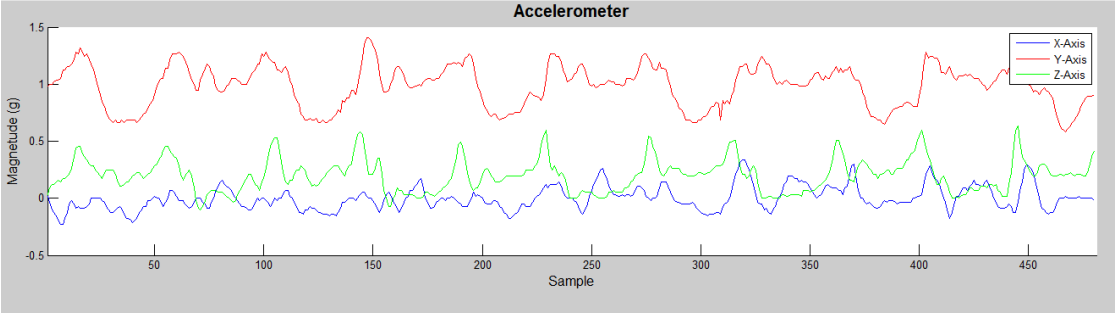

Figure 29. Accelerometer data when walking in the direction of the *y* axis.

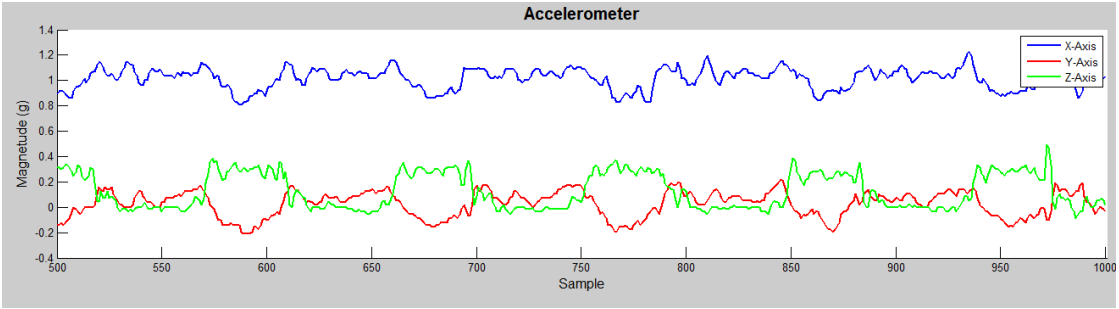

Figure 30. Accelerometer data when walking in the direction of the *x* axis.

2.1.4 ZigBee Receiver

Each sensor device uses a wireless link to communicate with a receiver on a PC, and data are stored on the PC through a MATLAB graphical user interface (GUI). The JN5148-EK010 Evaluation Kit (see Figure 31) includes a ZigBee coordinator receiver which was initially used as a wireless receiver in this study.

Figure 31. JN5148-EK010 evaluation kit components [Jennic2010a].

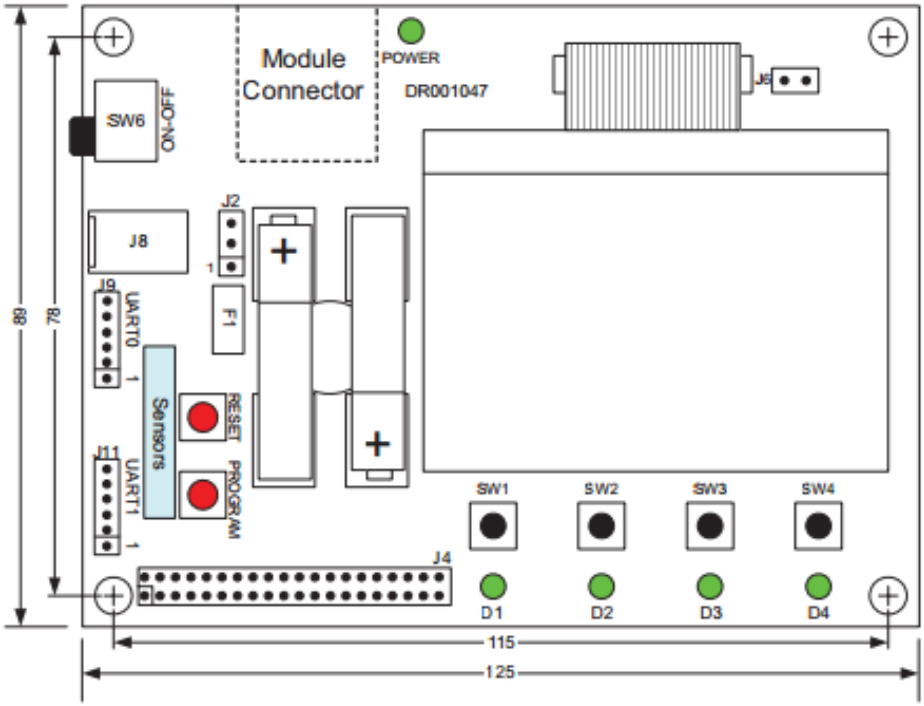

Figure 32. Controller board [Jennic2010a].

As illustrated in Figure 32, the controller board used as a wireless receiver for each sensor unit has several useful features [Jennic2010c]:

- a large 128 × 64 pixel LCD screen with a comprehensive set of driver routines,
- four configurable LED indicators,

- four configurable push-button switches,
- temperature, humidity, and light sensors,
- a serial EEPROM,
- a UART interface for communication and program downloads, and
- an expansion port for additional sensors.

Jennic also offers a pre-installed receiver module mounted on a uFI-to-SMA adaptor board with an SMA connector which can accept one of the supplied screw-on antennas. This module can be removed and replaced with a higher-power module. The three types of modules,are displayed in Figure 33: a standard-power module with a ceramic antenna embedded inside the PCB, a standard-power module with an SMA connector that can hook up to an antenna with a higher gain, and a higher-power module with an SMA connector. The higher-power module is longer than the standard-power modules [Jennic2010a, Jennic2010b].

Figure 33. JN5148-based modules [Jennic2010b].

As can be seen in Figure 32, the controller board is oversized for this application, and it connects to a PC through a USB-to-serial cable. Further, while the controller board contains a few useful components for debugging and broad application use (LCD screen, extension port, serial EEPROM, and temperature, humidity, and light sensors), these components are not required for this wireless biomedical sensor system. The main role of the controller for this biomedical application is to receive data from sensor units and

transfer those data to a PC through a serial port. Additional useful features of the controller may include reset and start buttons as well as LEDs to indicate controller status.

Therefore, the team decided to design a wireless, pluggable, USB-type receiver with an ABS plastic case that could serve the needs of this project. The board, SolidWorks model, and case are depicted in Figure 34. This USB-peripheral receiver provides short-range wireless connectivity to a low-power mesh or multipoint network in an easy-to-carry form factor. It can be plugged directly into the USB port of a laptop or PC, or connected using an extension cable. This receiver is USB-powered, so it does not require batteries or a power adapter.

As illustrated in Figure 35, one side of the receiver board contains power-on and data transmission LED indicators; log-on and permit-joining buttons for user control; a mini-USB connector for debugging; and a type-A USB connector for data streaming. The other side of the receiver board (see Figure 36), comes in two 'flavors.' The configuration in the lower part of Figure 36 is a standard-power module with a ceramic antenna embedded inside the PCB. The configuration in the upper part of Figure 36 includes an SMA connector which connects to an external antenna with higher gain. Table 4 lists the receiver specifications.

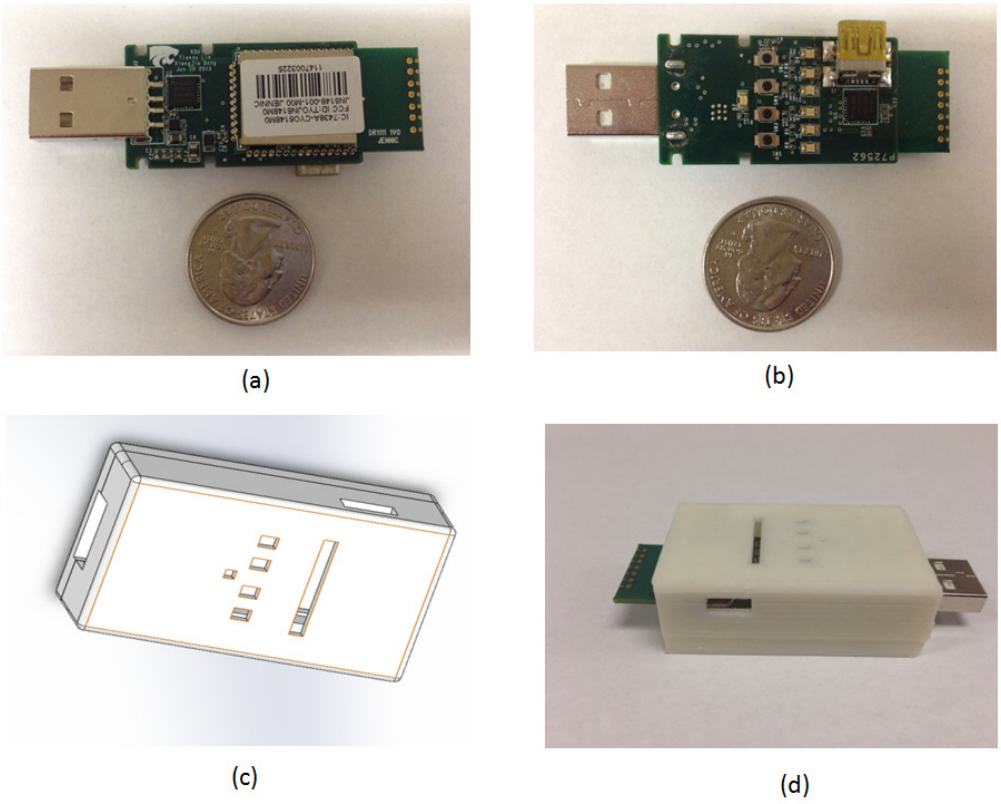

Figure 34. ZigBee receiver and ABS plastic case: (a) top view, (b) bottom view, (c) Solidworks model for the plastic case and (d) complete ZigBee receiver unit.

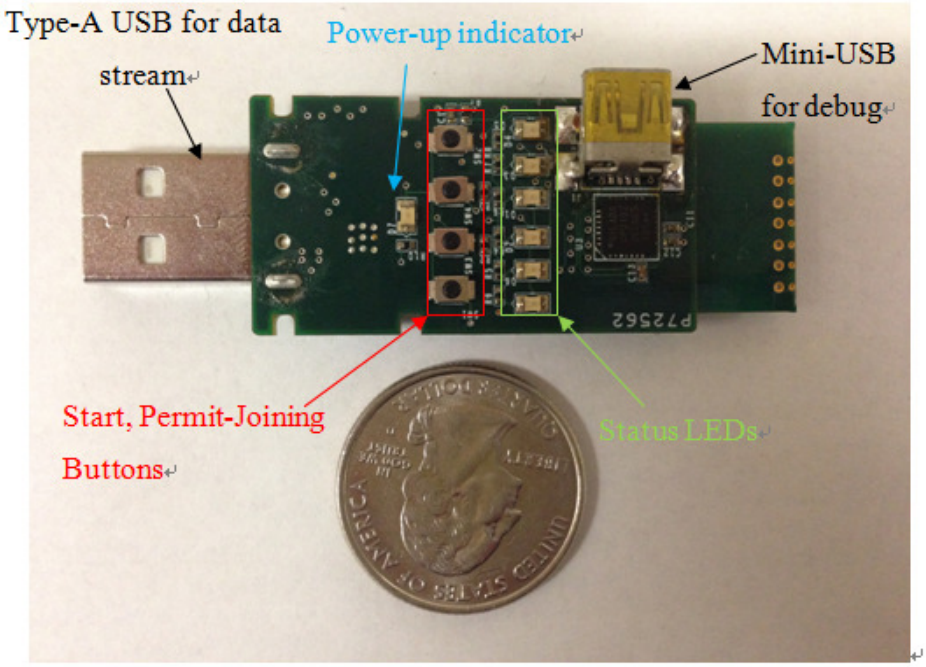

Figure 35. Components of the USB receiver – side 1.

Figure 36. USB receiver (side 2) with two types of Jennic 5148 modules.

Table 4. Specifications of the ZigBee receiver.

Indoor Range	30 m
Outdoor Range	45 m
Receiver Sensitivity	-90 dBm
Supported Network Topologies	Point to Point, Point to Multipoint, Peer-to-Peer, Mesh
RF Data Rate	250 kbps
Serial Interface Data Rate	115200 bits/s
Supply Voltage	5 V
Operating Current	38 mA
Interface Type	USB
Antenna Types	Internal
Connector	USB type A
Number of Channels	16
Dimensions	(L x W x H) 67.5mm x 27mm x 15mm

CHAPTER 3: ZIGBEE WIRELESS SENSOR NETWORK FIRMWARE

The Jennic operating system (JenOS) was designed for use in wireless network applications. JenOS was primarily intended for interaction with the NXP ZigBee Pro stack to develop wireless network applications based on the ZigBee standard. An API library built on IEEE 802.15.4, known as the ZBPro API, provides application layer programming for firmware development. One ZigBee Pro network topology includes a coordinator (topology hub), end device (leaf node in the topology), and router (connects coordinator and end devices) [Jennic2010d, Jennic2012, Jennic2013]. In this sensing network developed here, end devices were set up to communicate directly to the coordinator without a router in order to acquire data in real-time mode.

3.1 ZigBee Pro Application Programming Interface

Code programming was completed in the firmware development environment, Eclipse, which offers a user guide, reference manual, and example code. Eclipse contains the JN5148 ZigBee Pro SDK and tools used to configure JenOS. However, some static configuration was required before the application was built [Jennic2012, Jennic2013]. Configuration tools included the JenOS Configuration Editor, pre-configured JenOS resources, and a ZPS Configuration Editor that allowed ZigBee network parameters to be configured.

The JenOS Configuration Editor, which links setup configurations to application code, can be utilized before, during, or after coding. The Configuration Editor is primarily used to manage JenOS tasks, ISR subroutines, and scheduling. Typical configuration settings include

- priority of individual user-defined tasks and ISRs,
- software timers derived from a particular hardware counter,
- callback functions associated with a particular hardware counter,
- user tasks activated when a software timer expires,
- message types that can be sent and received by a user-defined task, and
- the length of a user task's message queue for message types.

Configuration is accomplished in graphical form. Figure 37 displays the editor's graphical window [Jennic2012].

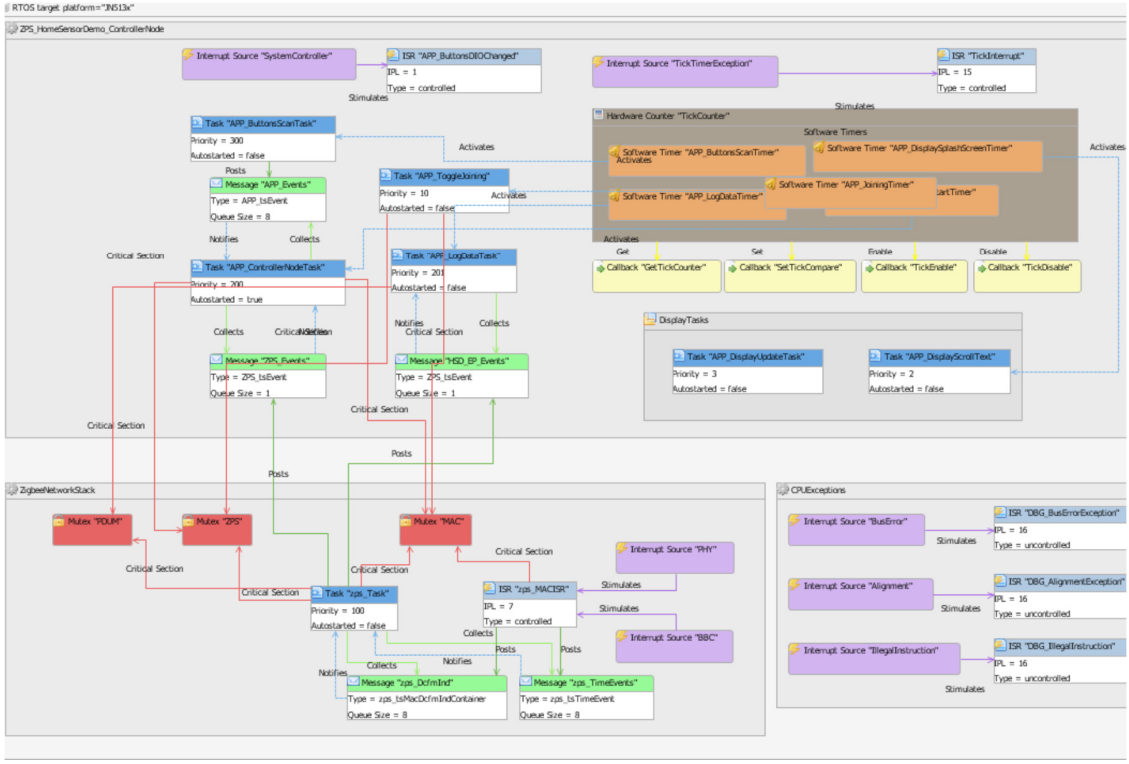

Figure 37. Graphical configuration window.

Colored boxes in the graphical configuration window represent various objects:

- Task (blue)
- ISR (light blue)
- Callback (yellow)
- Message Queue (green)
- Mutex (red)
- Interrupt Source (purple)
- Hardware Counter (brown)
- Software Counter (Orange)

The ZPS Configuration Editor (see Figure 38) configured ZigBee network parameters through a Windows Explorer interface. Parameter values for the entire network were stored in a file with an extension `.zpscfg`.

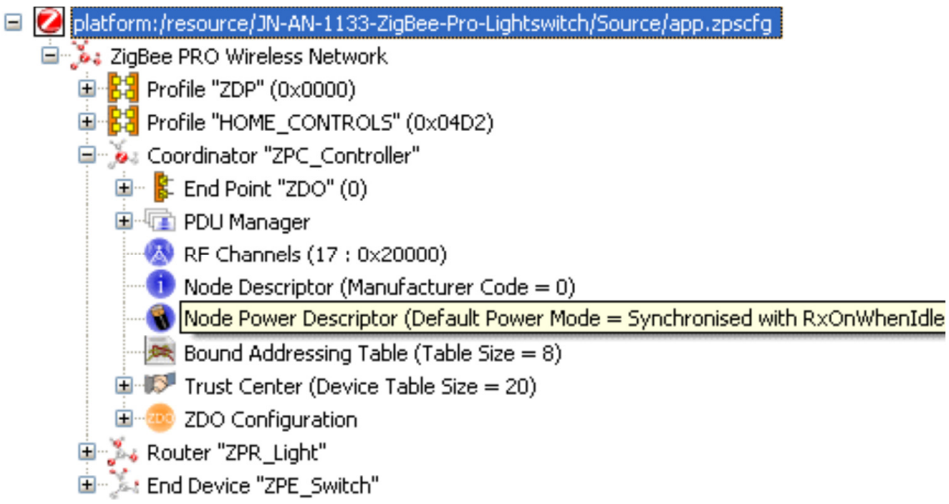

Figure 38. ZPS configuration editor window.

Configurable network parameters configured include the following:

- Extended Pan ID
- Security Enabled
- Maximum Number of Nodes
- Cluster ID
- Profile ID
- Permit Joining Time
- Initial Security Key
- Scan Duration Time
- RF Channels

After setting up the JenOS Configuration Editor and ZPS Configuration Editor for the coordinator and the end device, coding design was initiated, as described in the following sections [Jennic2012, Jennic2013].

Frames were assembled on the application layer of the wireless communication protocol. Wireless communication between biosensors and a receiver utilized a frame structure as illustrated in Figure 39. One data package contains 44 bytes. The first byte is the data length, the next two bytes are a 16-bit MAC address, the next 20 bytes are sensor data, and the last byte is the end byte for the data package. The Data Len byte is used to notify

the coordinator as to how many data will be transmitted. A sensor MAC address is used to identify the various sensor types. The following sections describe the firmware architectures for a sensor (end device) and coordinator.

Frame Structure for Wireless Communication

Position	0	1	3	23	43
Content	Data Len	Sensor MAC Address	First Channel Data	Second Channel Data	End byte

Figure 39. Frame structure for wireless communication.

3.2 Sensor Firmware Architecture

All sensor data (respiration rate, ECG, accelerometer, etc.) were periodically sent to the receiver where they could be displayed in a MATLAB GUI. These transmissions adhered to the same wireless communication data frame structure. Figure 40 contains the flow chart for the sensor node software architecture, and the architecture itself is illustrated in Figure 41. The following sections describe the tasks which implemented this architecture.

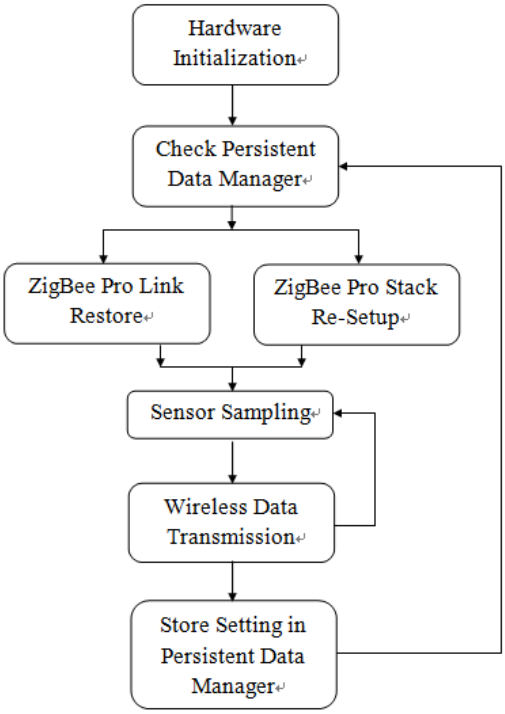

Figure 40. Software flow chart.

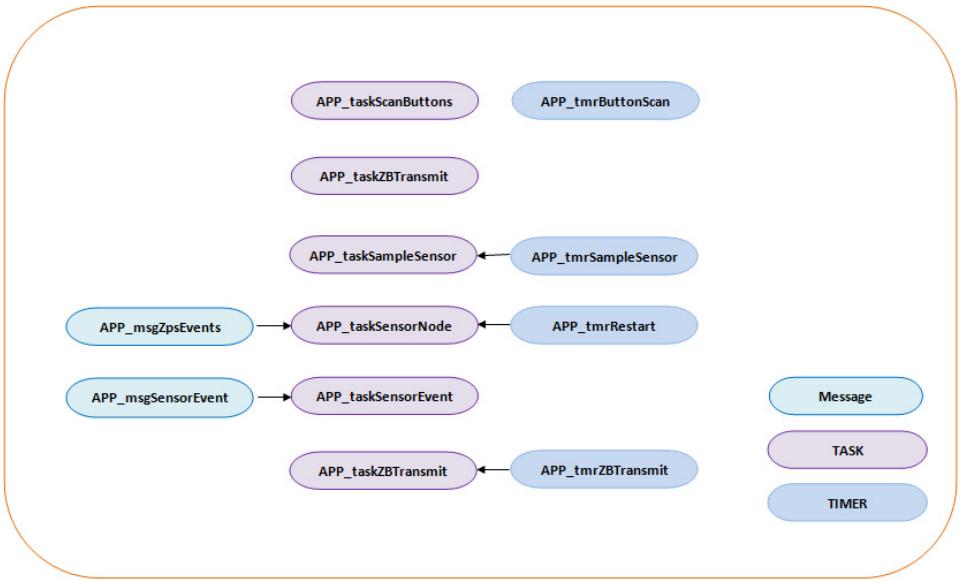

Figure 41. Software architecture of a sensor node.

APP_taskSensorNode

APP_taskSensorNode is the sensor node application's primary task. It is activated by stack events generated by the ZPS after setup of the ZPS Configuration Editor, which posts a message containing details of the stack event to the SensorNode task. The SensorNode task contains the state machine which is necessary to discover and join an appropriate network. The code for the state machine follows:

```
switch (s_sDevice.eState)
  {
case E_STARTUP:
vHandleStartupEvent(sStackEvent);
break;

case E_NETWORK_DISCOVERY:
vHandleNetworkDiscoveryEvent(sStackEvent);
break;

case E_NETWORK_JOIN:
vHandleNetworkJoinEvent(sStackEvent);
break;

case E_MONITOR_SENSORS:
vHandleMonitorSensorsEvent(sStackEvent);
break;
default:
break;
  }
```

APP_taskSampleSensors

APP_taskSampleSensors is the task that implements the primary hardware behavior. The Sample Sensors task acquires measurements from sensors, such as the pulse counter for respiration rate monitoring, the analog-to-digital converter for ECG monitoring, and the SPI communication interface for the accelerometer and gyrometer. Upon completion of a certain number of sensor readings, the task stores these sensor data in predefined buffers for future wireless transmission. This task is periodically activated by a 10 ms software timer, and this task also activates the ZBTransmit task which implements wireless data transmission.

To avoid transmission data loss, a double buffer was employed for sensor data storage in this study. Buffer A is first used to hold sensor data waiting to be sent wirelessly. If Buffer A is full, sampled sensor data are stored in Buffer B, or vice versa. Meanwhile, the full buffer triggers the ZBTransmit task, which transmits sampled sensor data from the full buffer. Results indicated that 100% of the data are successfully transmitted to the controller within close wireless range. The double buffer is depicted in Figure 42.

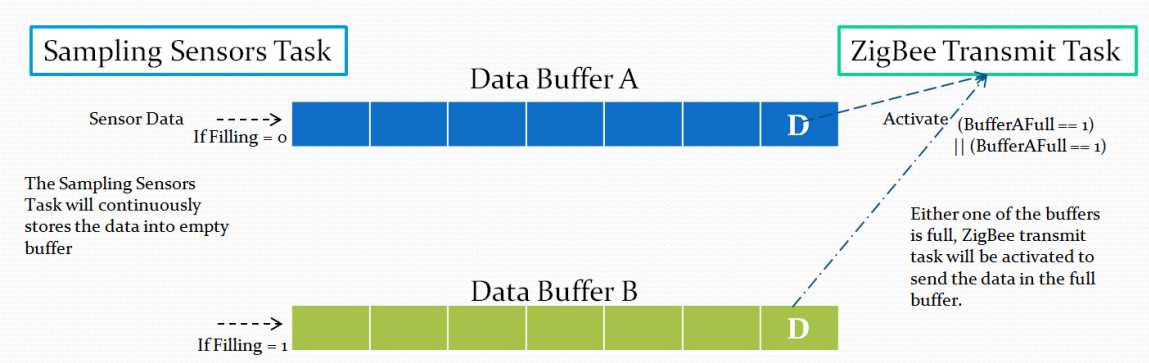

Figure 42. Double buffer for sensor data storage.

The pseudo-code for this task follows:

```
Enable Sensor Reading.
SensorValue1 = u16AHI_Read1();
SensorValue2 = u16AHI_Read2();                  //Sensor data reading, assuming two sensors
If(Filling1 == 0)    //Buffer 1 is empty
{
        U16Sensor_Buffer1[i] = SensorValue1;
        U16Sensor_Buffer1[i+DATA_LEN] = SensorValue2;
```

```
        i++;
        If(i == DATA_LEN )
        {
                Filling1 = 1;
                BUFF1FULL = 1;
                i = 0;
                OS_eActivateTask(APP_taskZBTransmit);     //Activate taskZBTransmit
        }
}
Elseif( Filling1 == 1)          //Buffer 1 is full
{
        U16Sensor_Buffer2[i] = SensorValue1;
        U16Sensor_Buffer2[i+DATA_LEN] = SensorValue2;     //DATA_LEN is number of samples per
        i++;
        If(i == DATA_LEN )
        {
                Filling1 = 0;
                BUFF2FULL = 1;
                i = 0;
                OS_eActivateTask(APP_taskZBTransmit);     //Activate taskZBTransmit
        }
}
```

APP_taskZBTransmit

The APP_taskZBTransmit task implements wireless transmission for sensor data stored in the double buffer. The ZBTransmit task sends buffered data to the controller node using the frame format described above. A message travels through the ZigBee network as a packet that contains application data surrounded by header and footer information relating to the different levels of the protocol stack. A message to be sent is prepared at the application level (at the top of the protocol stack) by creating an Application Protocol Data Unit (APDU) that contains application data to be included in the message. This APDU is then passed down the layers of the stack, with each layer adding unique protocol information to the header and footer. When the 'physical' layer is reached at the bottom of the stack, the message is complete and ready to be transmitted.

The pseudo-code for this task follows:

```
// Allocate an APDU instance
PRIVATE PDUM_thAPduInstances_hAPduInst = PDUM_INVALID_HANDLE;
s_hAPduInst = PDUM_hAPduAllocateAPduInstance(apduSensorData);
if (PDUM_INVALID_HANDLE != s_hAPduInst)
{
        if(BUFF1FULL == 1)
        {
                PDUM_u16APduInstanceWriteNBO(s_hAPduInst, BufferA);
```

```
            BUFF1FULL = 0;
        }
        if(BUFF2FULL == 1)
        {
            PDUM_u16APduInstanceWriteNBO(s_hAPduInst, BufferB);
            BUFF2FULL = 0;
        }


        vSendSensorData(PDUM_thAPduInstancehAPduInst);          //Sending the data
}
```

APP_taskScanButtons

The APP_taskScanButtons task is activated by a software timer which is activated by the System Controller ISR when a button interrupt is generated.

APP_taskSensorEvent

The APP_taskSensorEvent task implements the sensor data endpoint and therefore receives the APS confirm event generated by the ZPS after data in the pre-defined buffer have been sent. The ZPS posts a message containing a confirmation, and the message activates the task. The task then switches an LED on to indicate that the task is complete.

3.3 Coordinator Firmware Architecture

In this study, all signal data yielded by the various sensors are transmitted in real-time to the coordinator via a ZigBee wireless link. The coordinator then streams the sensor data to a serial port for backup, display, and signal processing. The coordinator is fundamentally a ZigBee wireless receiver on the PC side, which communicates with the PC through a serial port.

The primary two tasks implemented in the coordinator software flow are (1) receiving data packages from sensors and extracting sensor data from these packages, and (2) streaming sensor data to a PC using a predefined data frame format for backup, display, and signal processing. The software flow chart is depicted in Figure 43. The two main tasks are divided into subtasks which are explained in the following sections. The software architecture and task relationships are illustrated in Figure 44.

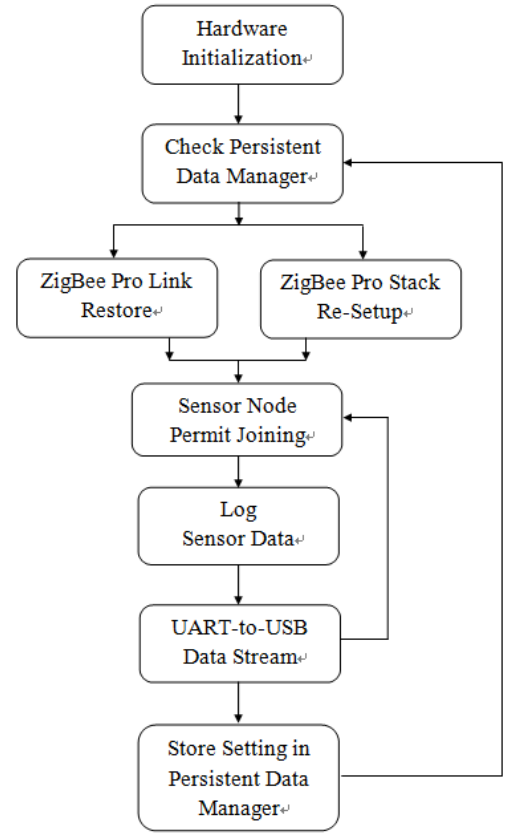

Figure 43. Coordinator software flow chart.

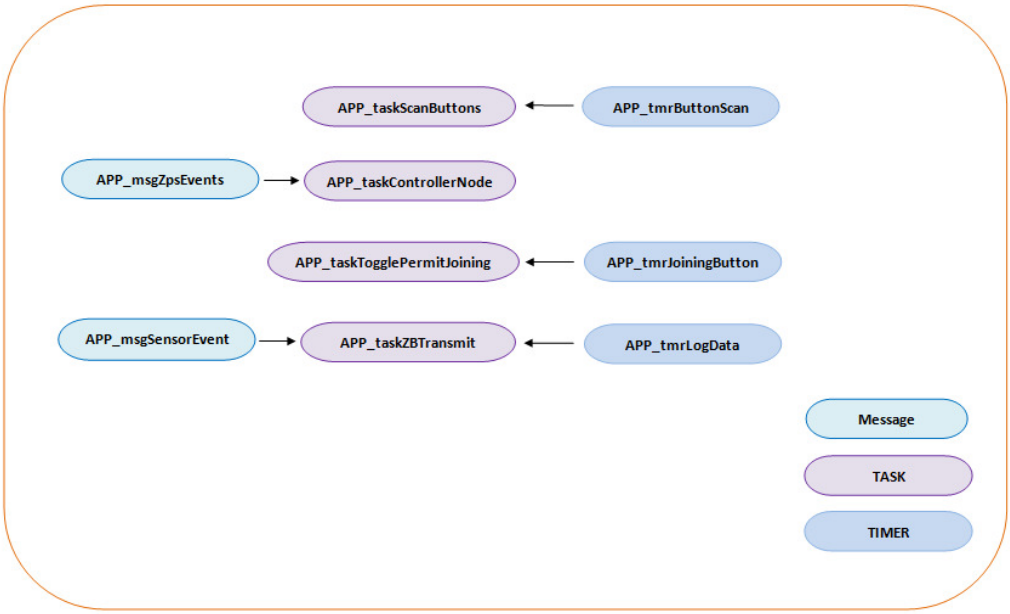

Figure 44. Coordinator firmware architecture.

APP_taskControllerNode

APP_taskControllerNode is the controller node application's primary task. It is activated by stack events generated by the ZigBee Pro Stack (ZPS), which posts messages containing details of the stack event to the ControllerNode task. It is also activated by messages posted from the buttons task. The ControllerNode task contains the state machine necessary to initiate a network and subsequently functions as the application controller.

APP_taskScanButton

The APP_taskScanButton task is activated by a software timer which is subsequently activated by the System Controller ISR when a button interrupt is generated. This task de-bounces the buttons. When a button press is successfully de-bounced, the task generates a BUTTON_UP or BUTTON DOWN event and posts a message to the main controller task to tell the coordinator to initiate the process.

APP_taskLogData

The APP_taskLogData task implements the sensor endpoint which receives data frames containing sensor measurement data from the sensor nodes. When a sensor node initially sends data to the controller, the node's address is registered by the LogData task. The task is activated by the ZPS task, which posts messages containing details of the data frame. The task is also periodically activated by a software timer and also streams sensor data through a serial port to a PC for display and signal processing in the MATLAB user interface.

The pseudo-code for this task follows:

```
if(message from sensor node is collected)
{
        //confirm the received message are from sensor node
        if(sHSDEndPointEv.eType == ZPS_EVENT_APS_DATA_INDICATION)
        {
```

```
                APP_bAppHealthy=  TRUE;
                SensorData = PDUM_u16APduInstanceReadNBO(hAPduInst);
                vWuart_RxData(sSensorData.u16ExtAddr);
                vWuart_RxData(sSensorData.data);
                PDM_vSaveRecord(&s_sLogPDDesc);
                PDUM_eAPduFreeAPduInstance(sHSDEndPointEv.uEvent.sApsDataIndEvent.hAPduInst);
        }
}
else
{       //Continue the  timer for data logging task
        OS_eContinueSWTimer(APP_tmrLogData, LOG_TIME, NULL);
 }
```

As soon as a message arrives in the ZPS data queue, the controller confirms if the message originates from the sensor node. If it does, the coordinator passes in the data package and decomposes it to extract the sensor data. After the process, the coordinator streams the sensor data to the PC serial port. This task also includes a basic check for correct application functionality. If the controller does not regularly receive sensor data frames, then something must be wrong (assuming active sensors are present). APP_bAppHealthy is a flag used in app_start to kick the watchdog so the program can be put back on track.

Finally, the coordinator streams the data package, including the package header, MAC address, and payload data, to the serial port of a PC. The package pattern detail is discussed in the next chapter.

APP_taskTogglePermitJoining

The APP_taskTogglePermitJoining task is activated by a software timer which begins running when the user asks the controller to toggle its Permit-Joining state. Permit-joining is toggled if a user-defined button is pressed for more than two seconds. The button press initiates the software timer. If the button is released before two seconds have passed, the main controller task stops the timer before it expires, preventing this task from being called.

CHAPTER 4: USER INTERFACES AND DATA LOGGING SYSTEM

4.1 MATLAB and LabVIEW Interfaces

Wireless communication (between biomedical sensors and a USB receiver) and serial communication (between the receiver unit and MATLAB interface) both utilize a similar frame structure, as illustrated in Figure 45. The data frame length is N bytes: the first two bytes are headers (0xFF 0xFF) to ensure frame integrity, the next two bytes are assigned to the last two bytes of a unique MAC address, and the next N bytes are assigned to sensor payload data.

Serial Communication Data Frame

1 – 2	3-4	N
Package Header	Last 16 bit MAC Address	Payload Data

Figure 45. Data frame structure used for serial communication.

MATLAB provides a serial port libraries link which tackles serial communication. Many configurable properties can be set up for serial reading and writing. Configurable properties are shown in Table 5. The flow diagram in Figure 46 illustrates the data package decomposition and data display processes.

Table 5. Properties of the MATLAB serial interface

➢ BaudRate	StopBits
➢ ByteOrder	DataBits
➢ ByteAvailable	ByteOrder
➢ FlowControl	RecordName
➢ Parity	RecordMode
➢ Port	Tag
➢ Terminator	DataTerminalReady
➢ Timeout	PinStatusFcn
➢ OutputBufferSize	……

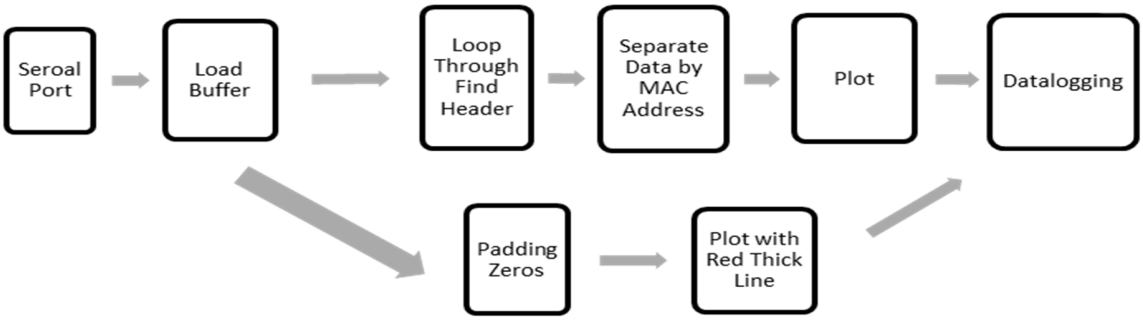

Figure 46. Data decomposition process inside of the MATLAB script.

The MATLAB GUI streams in received data from biomedical sensors and stores these data in the serial port buffer. If no sensor data are coming from the serial port, the GUI plots a red thick line along the *x* axis with padding zeros. If sensor data are stored in the serial buffer, the GUI loops through the stored data to find the header and then decomposes the package to obtain these sampled data. In this study, a MAC address filter was used to sort various sensors and plot sensor data on the MATLAB figures in the user interface.

MATLAB Code

MATLAB code runs behind the graphical interface and includes functions that handle trigger events such as button clicks and text input. The highest priority event is serial communication processing. Once data are received and stored in the buffer, they are extracted into the MATLAB workspace to ensure real-time data acquisition. Meanwhile, the data are stored on the PC hard drive using a predefined file name. The pseudo-code for serial communication processing follows:

```
Serial Port Initialization;
Mac1 = textbox1.value;
……                                          //Get the entered MAC information for sensor partition
MacN = textboxN.value;
While (data received in the buffer)
{
```

```
        Timei = Timei + 1;
        If (BytesAvailable>= Specified data packages)
        {
                Timei = 0;
                Ti = current real time clock;
                Empty the buffer;
        }
        Else
        {
                Pause 0.02 second to prevent program freeze;
                If (timei< Timeout)
                        Continue;
        }
        fori=1:(length(x)/N)
        {
        if x((i-1)*N+1) == 255
            {
                if x((i-1)*N+2) == 255
                {
                        Extract Mac Address;
                        Extract Sensor Data;
                }
             }
        }
}
```

The “specified data package” value is determined by how much delay is tolerable for an interface update. As stated, the length of one data package is N bytes long. For example, if the length of the frame structure is 24 bytes for each sensor and the specified data package is set to 48, then two frames of delay are induced. If the sampling frequency is set to100 Hz, a 20 ms time delay is induced. A small number for “specified data package” would trigger the serial communication event so quickly that MATLAB would be unable to catch up because it slows down the response to other interface functions. Results have shown that a big or small value causes data loss, and

experiments have indicated that a four-frame delay works best for this wireless protocol. No data loss occurs during wireless transmission with this four-frame delay.

Since multiple sensors transmit data to a receiver simultaneously, the sensors need to be separately identified. Therefore, a sensor MAC address was used as a reference for sensor partitioning. The pseudo-code for sensor partitioning follows:

```
for i=1:(length(x)/N)                    //N is the length of frame structure
{
if x((i-1)*N+1) == 255
if x((i-1)*N+2) == 255
sensor = 0;
if x((i-1)*N+3) == Mac1_1 && x((i-1)*N+4) == Mac1_2
sensor = 1;
end
if x((i-1)*N+3) == Mac2_1 && x((i-1)*44+4) == Mac2_2
sensor = 2;
end
        …….
        if x((i-1)*N+3) == Macn_1 && x((i-1)*N+4) == Macn_2
sensor = n;
}
```

The user enters the MAC address for each sensor in the text box (see Figure 47), and then these addresses are used as references to separate the sensors in the manner described above.

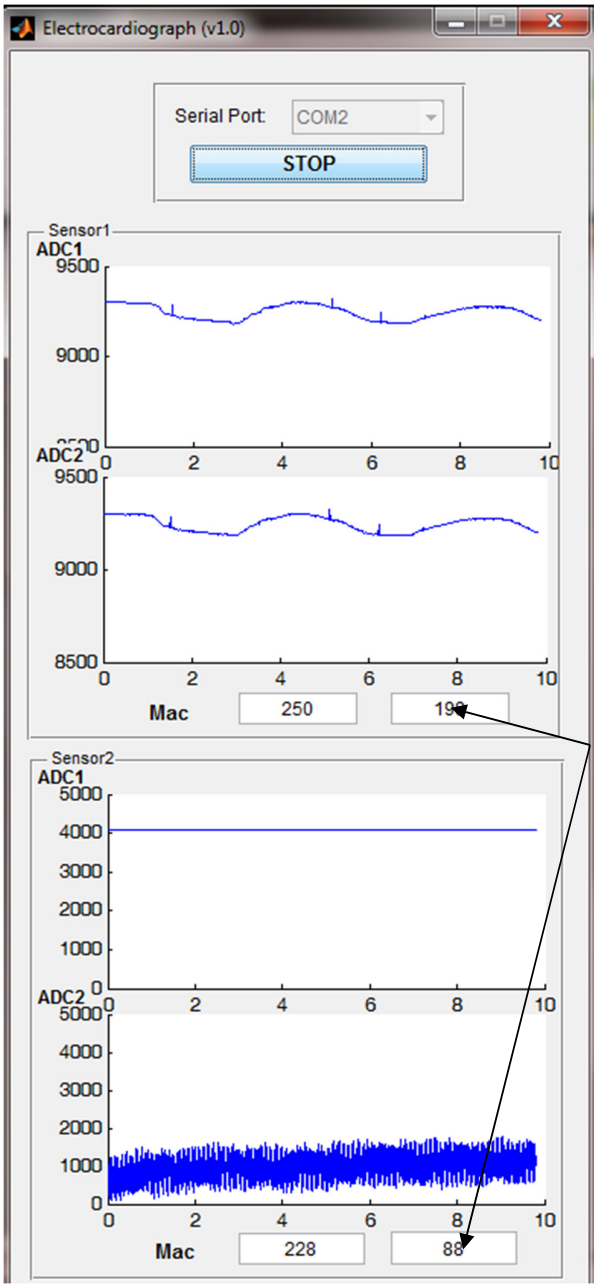

Figure 47. MATLAB user interface with a MAC address filter.

While plotting data on the screen, the user interface saves these data directly to the hard drive with a predefined file name format. The logging system automatically creates a log file every hour and writes real-time sensor data into the file every 10 seconds. The log file name format and log file format are specified below.

Log File Name Format

MAC 1	·····	MAC N	Year	Month	Day	Hour

MAC1: Last 16 bits of the ZigBee device's 64-bit MAC address for the 1st sensor.

.....

MAC N: Last 16 bits of the ZigBee device's 64-bit MAC address for the Nth sensor.

The user interface first checks the number of sensors in the network and defines the file name according to that number. For example, if a serial port streams in received data from two sensors, the file name assigned would be "MAC1_MAC2_Year_Month_Day_Hour," with MAC1 and MAC2 being the last 16 digits of the ZigBee transceivers' IEEE 64-bit MAC addresses. Then the recording time, including year, month, day, and hour, are included. After a file with an associated name is created, the user interface begins writing sensor data into the file every 10 seconds. Data are initially stored in memory before being saved onto the computer hard drive. If the logging time is too short, the responses to other events slow down and the user interface freezes. A long logging time takes up too much memory space, and data temporarily stored in memory are lost if the power shuts down for some reason. A logging time of 10 seconds was sufficient for this system.

Figure 48 illustrates a log file obtained through the user interface. With the file name above as an example, 18 126 and 228 45 are the last 16 bits of two sensors' MAC addresses, and the recording time is at, e.g., 7:00 a.m. on July 26, 2013. If one of the sensors is powered off or placed out of wireless range, the MAC address in the file name is switched to "NaN_NaN,"as shown in Figure 48. One log file contains one hour of sensor data. The size of a log file is approximately 3 MB. The log file frame structure is given in Figure 49.

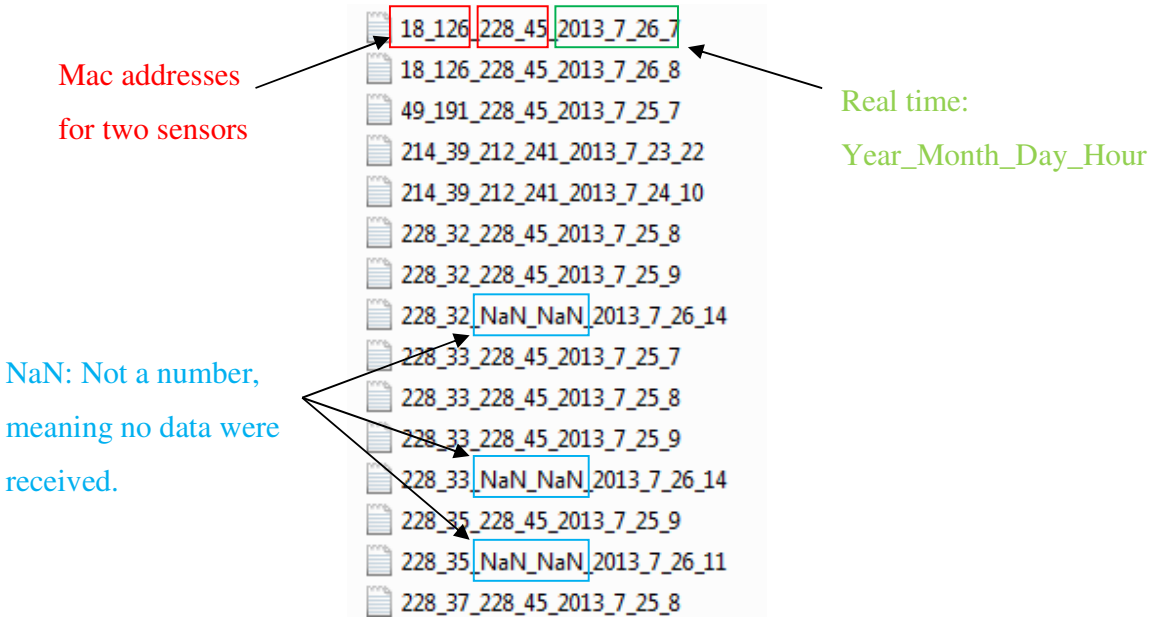

Figure 48. Log data file storage example.

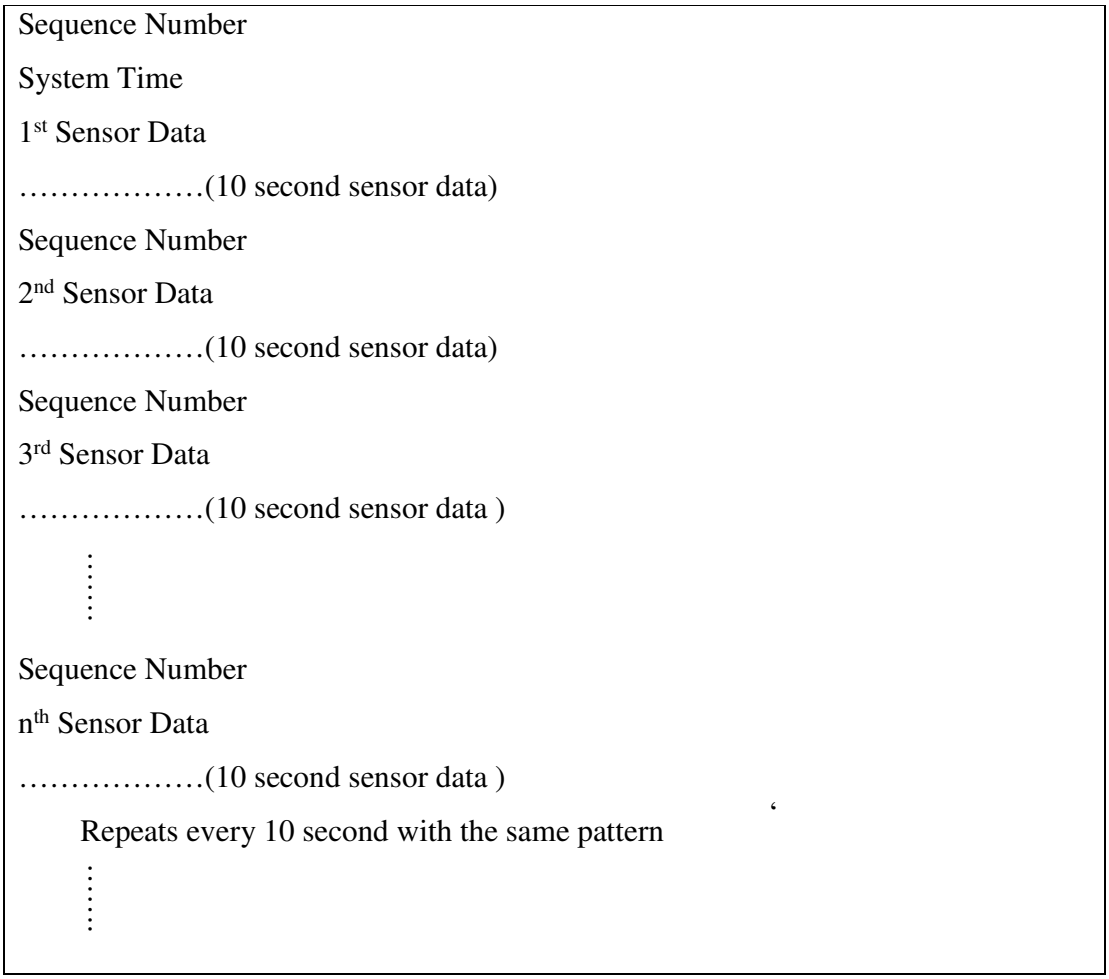

Figure 49. Log file frame structure.

The sequence number is an iterative 5-digit tag for each sensor. E.g., 11111 represents the first sensor and 44444 represents the fourth sensor. Sensor data are followed by the sequence number, and the pattern repeats every 10 seconds. Finally, data plotter software designed in MATLAB extracts and plots the data stored in the file. The pseudo-code for plotting the log data follows:

```
FileName ='file_name';
fileID = fopen(FileName');          //Open the log file
C =  fscanf(fileID, '%f');

fori = 1:length(C)
if C(i) == 11111
if period ~=0
endp(period) = i-1;
```

```
end
period = period + 1;
hour(period) = C(i + 4);
minute(period) = C(i + 5);  // Extract the recording time information
second(period) = C(i + 6);
        ADC1_1p(period) = i + 7;
end

if C(i)== 22222
     ADC1_2p(period) = i+1;
end

if C(i)== 33333
     ADC2_1p(period) = i+1;                    // Find start index for data array
end

if C(i)== 44444
     ADC2_2p(period) = i+1;
end
end
fori = 1 : (period - 1)
   ADC1_1  = [ADC1_1 C(ADC1_1p(i):(ADC1_2p(i)-2))'];
   ADC1_2  = [ADC1_2 C(ADC1_2p(i):(ADC2_1p(i)-2))'];          //Extract the data from the data
   ADC2_1  = [ADC2_1 C(ADC2_1p(i):(ADC2_2p(i)-2))'];          //stream
   ADC2_2  = [ADC2_2 C(ADC2_2p(i):endp(i))'];
end

Plot(ADC1_1);
Plot(ADC1_2);    //Plot the data
Plot(ADC2_1);
Plot(ADC1_2);
```

CHAPTER 5: APPLICATIONS AND OUTREACH

The NASA-funded effort has been beneficial to other domains. The resulting technology has been utilized for other research while providing educational resources to teachers and students interested in science and technology.

5.1 Two-Channel ECG for a Steer Application

The two-channel ECG system, designed for human use, was also applied to a preliminary study to investigate the effect of food supplements on steer cardiac activity. A system that included a two-channel ECG unit, a National Instruments myDAQ unit, and a laptop were set up to measure the ECG of a steer, as shown in Figure 50. Four electrodes were utilized, with electrode A on the left side of the animal near the bottom of the ribs, electrode B at the apex of the heart, electrode C at the base of the heart, and electrode D on the upper back to serve as a reference. Channel 1 was a differential comparison between the voltages at A and B, where each voltage was measured relative to the reference electrode D. Channel 2 was a differential comparison between the voltages at C and B, where each voltage was measured relative to the reference electrode D.

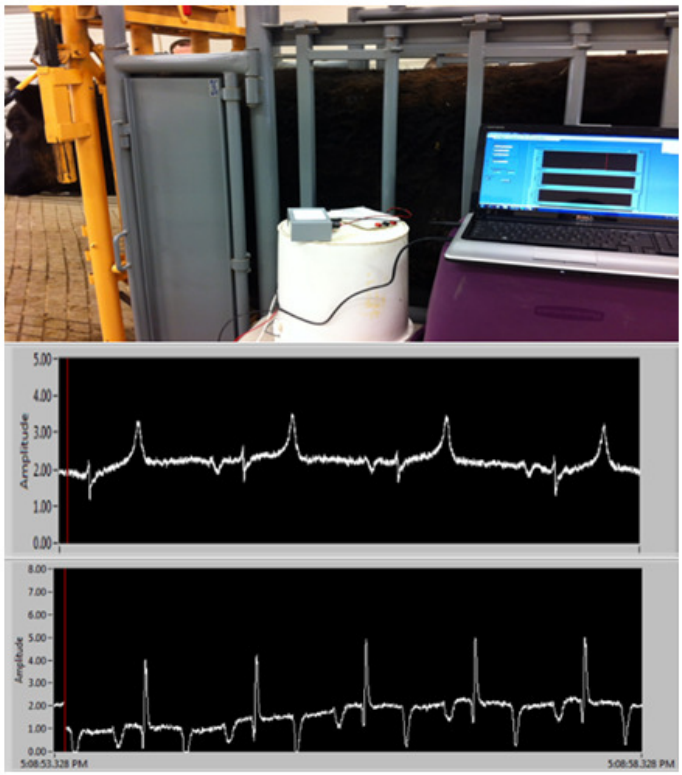

Figure 50. Early setup to acquire a steer ECG along with a typical signal pair.

This study intended to continuously measure and record the cardiac activity of 30 steers before/after food supplements during three-day periods separated by four-day rest intervals. Wireless links were preferred because they would (a) eliminate cabling for the transfer of ECG data, (b) provided the ability to record data from 30 steers simultaneously, (c) relieve steer discomfort so that recorded data could be trusted, and (d) eliminated the on-board data loggers otherwise required for permanent data recording. The wireless two-channel ECG designed for human use was modified to fit this steer application. The overall gain of each system was increased by a factor of ten due to the steers' thick hides, and the MATLAB-based user interface was modified to record real-time ECG data.

These ECG units (see Figure 51) were battery-operated to increase their mobility and decrease their susceptibility to electrical interference (no return path to earth ground). ECG electrodes attached to the steers were pre-treated with conduction jelly that provided good contact and caused minimum irritation to the animals. Finally, a secure harness was used to attach an ECG device to each steer for long-term recording. ECG data sent to a USB receiver connected to a computer via a ZigBee wireless link could be stored directly to the hard drive. Meanwhile, real-time ECG waveforms could be viewed on the computer screen to monitor the health status of these steers and check whether lead attachments were still viable (see Figure 52). To view stored ECG data and analyze cardiac effects from food supplements, a data plotter script was designed for veterinarian use. Representative ECG data are illustrated in Figure 53.

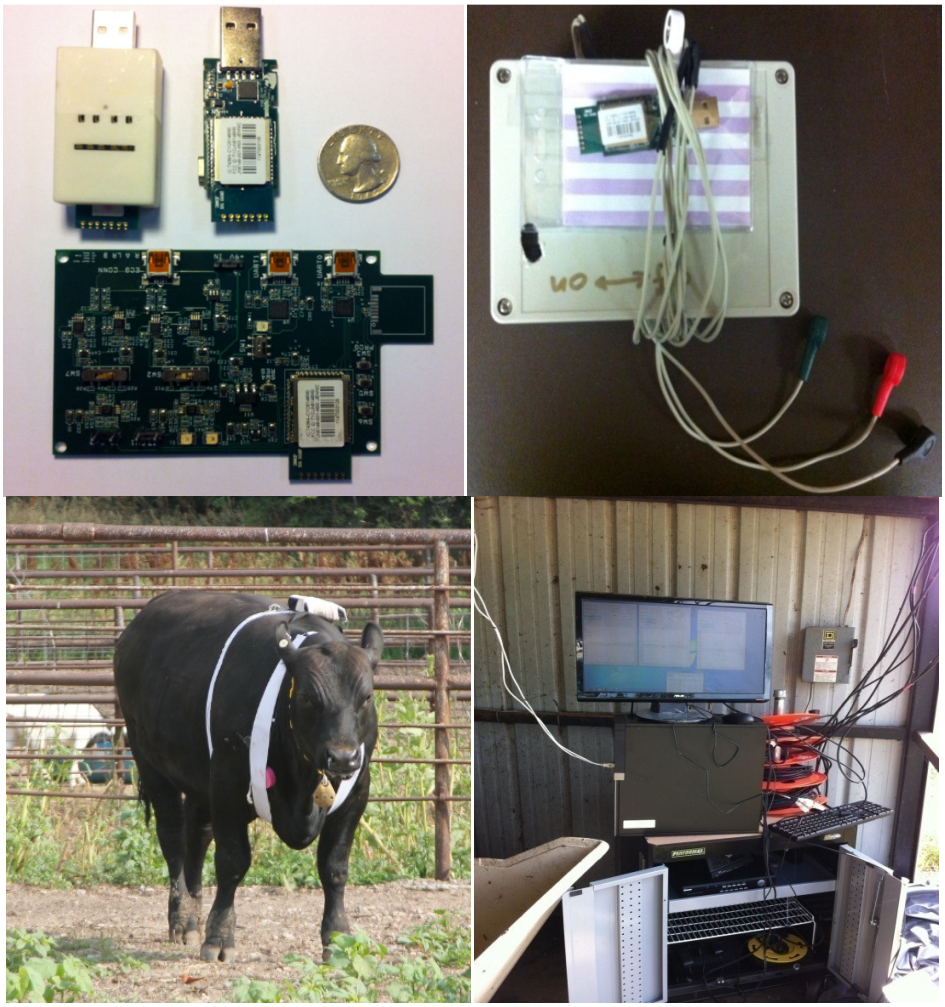

Figure 51. Wireless two-channel ECG system including electronic hardware (upper), harness (lower left), and monitoring/recording computer (lower right).

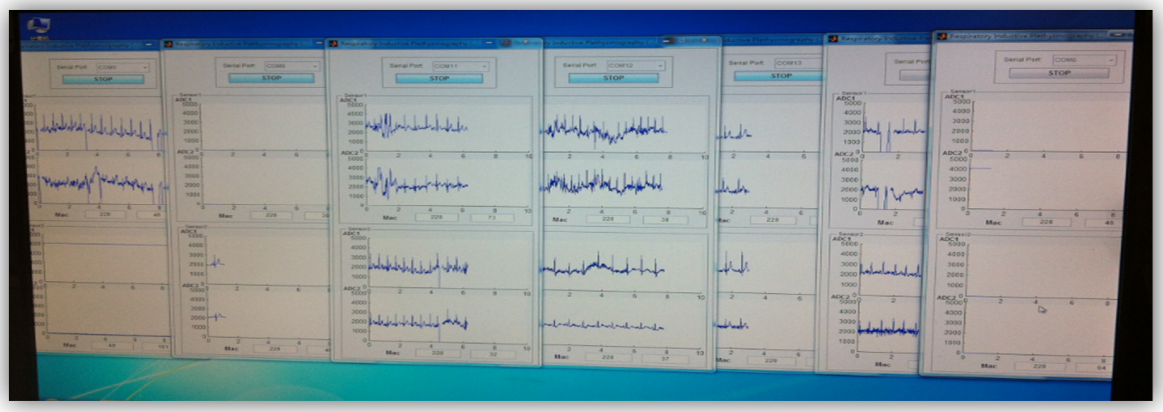

Figure 52. User interface for the steer ECG recording system.

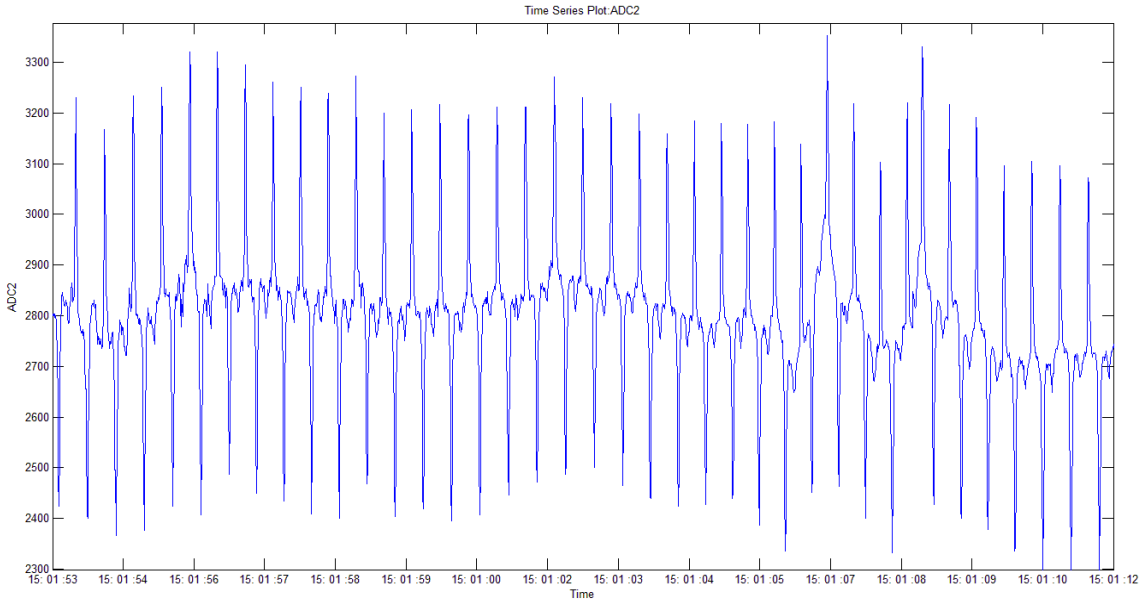

Figure 53. Representative plot of stored data from the computer hard drive.

5.2 E3 Workshop

This NASA project also offers opportunities for STEM education. Members of this NASA project team participated in the “Engineering Education Experience (E3) for Teachers” workshop, in which biomedical sensors and real-time sensor waveforms (respiration and ECG) developed for this project were demonstrated to approximately 40 high school science teachers. The hope is that a new generation of students will be inspired to pursue science, technology, engineering, and mathematics in their college educations and future careers.

Figure 54. NASA team conducting sessions during the KSU-sponsored "Engineering Education Experience (E3) for Teachers" workshop, Summer 2013.

CHAPTER 6: FUTURE WORK

The following sections discuss future efforts that can follow the work described in this thesis.

6.1 Textile Respiratory Inductive Plethysmography Sensor

Comfort and signal quality are important for all body-worn sensors [Dong2013]. Although inductive plethysmography has existed for many years, the challenge in this context is to design a textile belt that can be sewn into a comfortable garment or be defined by part of that garment and still provide data fidelity required for accurate respiration-rate measurements. The respiration sensor developed for this effort demonstrated good accuracy and signal-to-noise ratios, but further work must be done to address belt comfort, which raises issues of (a) belt tension versus belt comfort, (b) the effect of motion on the respiration signal, and (c) options for sensor placement and configuration.

At least three types of interference affect signal quality during respiration monitoring: motion artifact, RF interference, and hysteresis of the wearable sensor. Tests must be conducted to evaluate respiration signal quality in varied usage environments. These respiration sensors have only been tested on a handful of subjects to date, so additional experiments must be conducted to assess wearability and reliability. A commercial respiration belt should be used for performance comparisons.

Improvements could also be made to the hardware design. As depicted in Figures 18 and 19, the respiration belt was wrapped snugly around the chest so the sensor unit was in contact with a skin/clothing interface while acquiring respiration data. Rigid FR4 PCB material held against a wearer's chest would become uncomfortable over time. In addition to integrating an inductive wire into a space suit, the sensing module (Colpitts oscillator) and processing module (microprocessor, transmitter, and other peripheral circuits) could also be mounted separately in less conspicuous places. Furthermore, flexible PCB material may help to reduce the board size, profile, and weight.

6.2 Accelerometer and Gyrometer

The motion module originally designed for slip and fall detection/prediction included a CMA3000 MEMS 3-axis digital accelerometer and a CMR 3000 3-axis digital gyrometer. A 3-axis accelerometer was also chosen to be the sensor for activity recognition. The accelerometer sensor measures acceleration in three directions: vertical, sagittal, and lateral.

As stated in the introduction, accelerometer data may be, in the long term, a sensible supplement or alternative to electromyographic data when assessing and predicting fatigue, since an accelerometer does not require skin contact. While these data would be surrogate data for EMGs that are more closely tied to physiology, accelerometer data require a lower sampling rate (e.g., 100 Hz as opposed to 1 kHz for an EMG), making these data more appealing for resource-constrained wireless sensor networks.

For fatigue prediction, body orientation or angular velocity information may help improve prediction accuracy. This type of information can be acquired from a 3-axis gyrometer, which is already bundled with the accelerometer on the prototype sensor board. Driver code for the on-board gyrometer would be straightforward to integrate into the current firmware design.

6.3 Integration of a Pulse Oximeter into the Current Wireless Network

The pulse oximeter is an optical, noninvasive medical device that monitors cardiopulmonary parameters. The device is typically placed on the fingertip to acquire and display heart rate and arterial blood oxygen saturation. A pulse oximeter reports heart rate and SpO_2 while offering other potential clinical parameters, such as blood pressure (systolic BP, diastolic BP, mean BP, SV, and CO), respiratory rate, and metabolic rate. All of these clinical parameters are valuable for monitoring astronauts' state of health [Li2012a].

An existing pulse oximeter, designed by Kejia Li, should be modified for integration into the current sensor network. The design employs a wireless-integrated JN5139 microprocessor module based on the ZigBee wireless protocol. The JN5139 is an earlier version of the JN5148 which is currently marketed by Jennic. The JN5139 includes a 32-bit RISC processor with a 2.4 GHz IEEE 802.15.4 transceiver, 192 kB of ROM, 96 kB of RAM, and a mixture of analog and digital peripherals which are similar to those provided by the JN5148 [Jennic2008,Jennic2010a].

The good news is that the JN5139 and JN5148 share the same pin-out configuration, as depicted in Figure 55, with only slight differences in function on some pins. I.e., some I/O pins are special-use pins, but those pins were not used in the pulse oximeter design. Therefore, the JN5139 can be replaced with the newer JN5148 microprocessor, imposing minimal disruption to the data acquisition hardware design. Unfortunately, the JN5148 that employs a ZigBee Pro wireless protocol is not backward compatible with the JN5139 ZigBee implementation because they have different SDKs and IDEs. Also, the JN5148 is developed under Eclipse, while the JN5139 is supported by CodeBlocks and, of course, different SDK libraries and development platforms. The JN5139 is designed on the AT-Jennic platform, while the JN5148 is designed on a ZigBee Pro template which runs an operating system. As a result, solutions must be developed which merge the pulse oximeter with the current system [Jennic2008, Jennic2010d, Jennic2013].

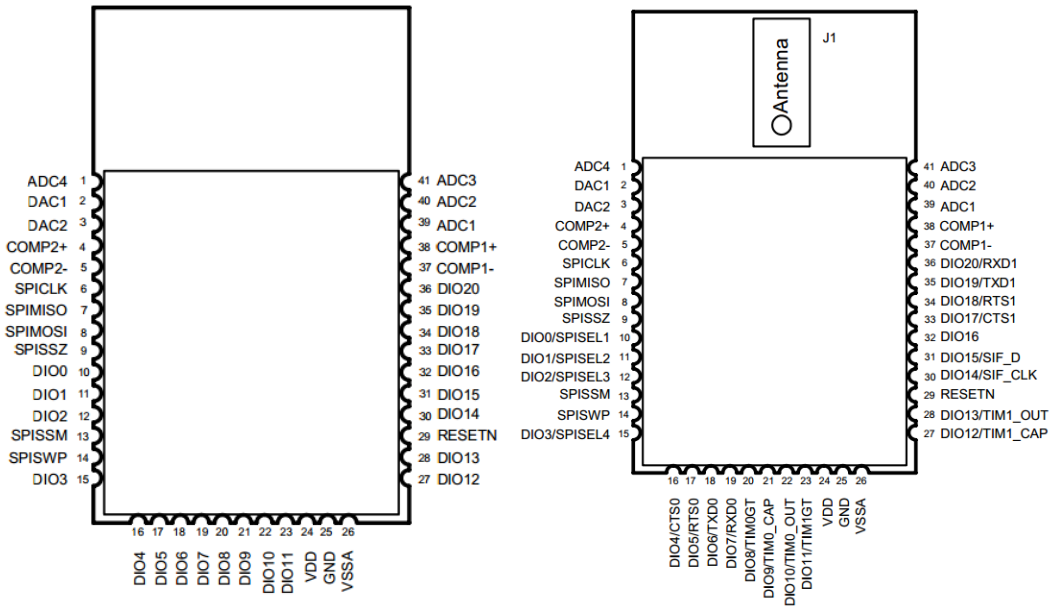

Figure 55. Pinout configuration for Jennic microprocessors: JN5148 (left) and JN5139(right) [Jennic2008, Jennic2010d].

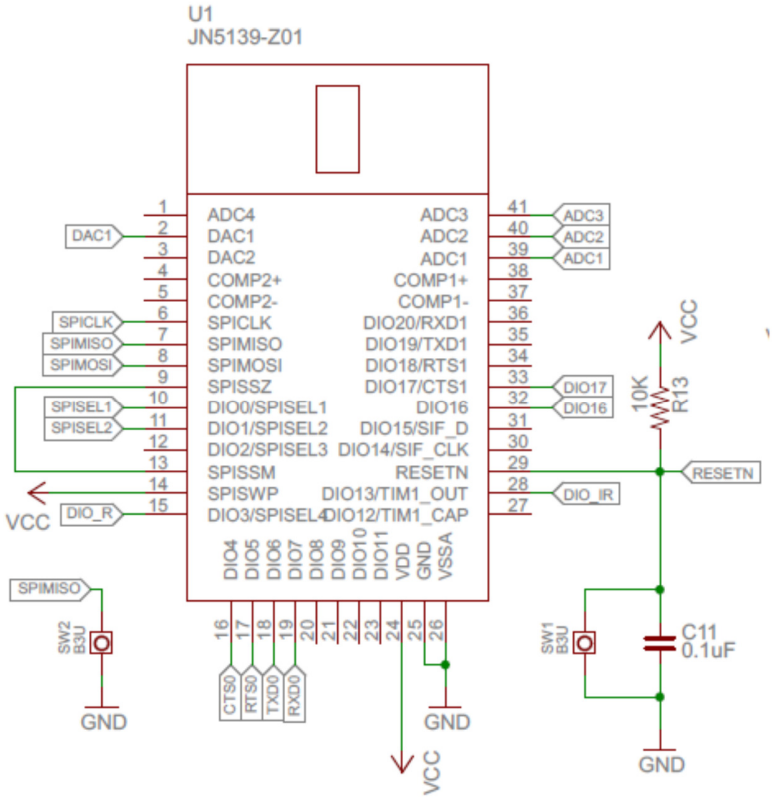

Figure 56. JN5139 I/O connections for the pulse oximeter [Li2012a].

One solution is to replace the JN5139 microprocessor with the JN5148, maintain the rest of the hardware, and translate the firmware code on the JN5139 to be compatible with the JN5148. Because development environments are completely different, and Kejia Li's firmware code for the pulse oximeter must be fully understood in order to re-program it, this approach could be time-consuming. The hardware may be arguably easier to modify than the software, especially when sensors are developed by other designers. In addition, the ZigBee wireless biosensor network serves only as a baseline for the biomedical sensor network that should eventually incorporate low-power FPGA transceivers. The time and effort to redesign the entire pulse oximeter may not be justifiable.

Another solution would be to add a JN5139 receiver and USB hub to the current USB receiver design, as depicted in Figure 57, in which case the receiver would be able to receive data from all sensors. Received sensor data would be streamed to downstream ports of the USB hub and transferred to the upstream port of the PC to be processed. If the serial communication data frame structure is known, data can be plotted on the user interface and stored to disk. This data pattern was obtained from Kejia Li's Master's thesis [Li2012b] and is shown in Figure 58. The data package was 18 bytes long, including 8 bytes of a unique 64-bit MAC address of a specific pulse oximeter and 8 bytes of four channels of signal data: DC value of the red channel, AC value of the red channel, DC value of the near-infrared channel, and AC value of near-infrared channel. The last two bytes were end-indicators [Li2012a]. The firmware code for the pulse oximeter would not need to be modified, but the serial communication data acquisition code would need to be changed in MATLAB.

Advantages of an additional hub include the idea that sensors which employ other wireless protocols (e.g., Bluetooth, Bluetooth LE, and Wi-Fi) could also be embedded into the sensor network and data acquisition system. USB2517-JZX is a USB 2.0 compatible Hi-Speed USB hub controller that supports seven downstream ports. It would be a good fit for this application.

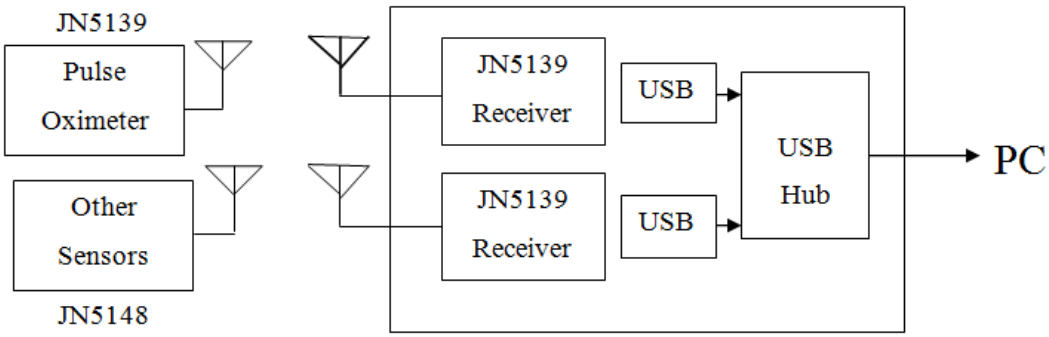

Figure 57. Add-ons to the current receiver design.

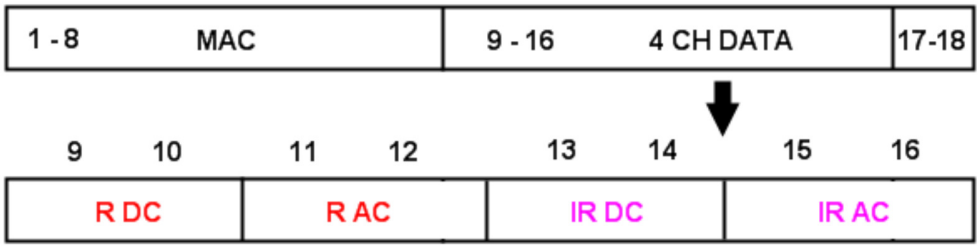

Figure 58. Serial communication data frame structure for pulse oximeter [Li2012b].

Either route can be taken to integrate the pulse oximeter into the current wireless biomedical sensor network, and each route has pros and cons. Replacing the JN5139 with a JN5148 module and modifying the firmware code could require more time, but it may save space on the receiver board and maintain system development consistency. Adapting the USB hub decreases development time for the firmware design and potentially improves system compatibility with other wireless protocols.

CHAPTER 7: CONCLUSION

Networks of low-power, in-suit, wired and wireless health sensors offer the potential to track and predict the health of astronauts engaged in extra-vehicular and in-station activities in zero- or reduced-gravity environments. The effort addressed in this report includes the design of compact, low-power biomedical sensors and the creation of a ZigBee Pro wireless network that can be used to test new sensor prototypes and serve as a comparison baseline for low-power custom networks that will be built into spacesuits.

The six-axis accelerometer/gyrometer can assess acceleration, tilt angle, or angular velocity at various body locations/joints, and the accelerometer/gyrometer can be placed in meaningful spots, such as the chest, leg, or wrist, as an alternative means to potentially track or predict fatigue. The respiration inductance plethysmograph uses a belt to obtain respiration rate, where the belt (typically worn around the chest) may be sewn into the upper portion of the cooling garment worn under the spacesuit. The two-channel ECG was used to monitor cardiac activity. Finally, a previously designed reflectance pulse oximeter design could be integrated into this system and perhaps customized to function effectively in a helmet (e.g., for forehead measurements) or a glove (e.g., for wrist and finger measurements). All of these sensors are useful for monitoring an astronaut's state of health during EVA missions.

Sensor prototypes and the ZigBee wireless sensor network discussed in this report were developed and tested. MATLAB and LabVIEW GUIs were developed for real-time signal monitoring and recording. Data were saved on the hard drive while displaying the signal waveform for signal interpretation and processing. Sensor measurements need to be conducted on additional subjects to validate these sensors' usability, durability, and capability. Future work should be considered for hardware improvement, signal interpretation, and processing, as detailed in Chapter 6.

REFERENCES

[Abreu2011] Abreu, C.; Mendes, P., "Wireless sensor networks for biomedical applications," *2013 IEEE 3rd Portuguese Meeting* in *Bioengineering (ENBENG)*, Feb. 2013, pp. 1, 4, 20-23.

[Ade2011] Ade, C.J., R.M. Broxterman, S. Warren, R.D. Taylor, T.J. Barstow. "Development of standardized exercise tests for predicting planetary task performance," *The International Academy of Astronautics Humans in Space Symposium*, Houston, 2011.

[Ade2012] Ade, C.J., R.M. Broxterman, G. L. Gadbury, D. Schinstock, S. Warren, and T.J. Barstow. "Physiological responses during simulated planetary field test," *American College of Sports Medicine*, San Francisco, 2012.

[Akbulut2011] Akbulut, A.; Patlar, F.; Zaim, A.H.; Yilmaz, G., "Wireless sensor networks for space and Solar-system missions," *5th International Conference on Recent Advances in Space Technologies* (RAST), June 9-11, 2011, pp. 616-618.

[Analog1999] Analog Devices. "Low Cost, Low Power Instrumentation Amplifier," AD620 Data Sheet, ©1999, Analog Devices, Inc. http://www.analog.com.

[Ansa2011] Ansari, S.; Belle, A.; Najarian, K.; Ward, K., "Impedance plethysmography on the arms: Respiration monitoring," *Bioinformatics and Biomedicine Workshops (BIBMW), 2010 IEEE International Conference*, Dec. 18, 2011, pp. 471-472.

[Baldi2012] Baldi, M.; Appignani, F.; Zanaj, B.; Chiaraluce, F., "Body movement compensation in UWB radars for respiration monitoring," *2012 IEEE 1st AESS European Conference on Satellite Telecommunications (ESTEL),* Oct. 2-5, 2012, pp. 1-6.

[Bu2007] Nan Bu; Ueno, N.; Fukuda, O., "Monitoring of Respiration and Heartbeat during Sleep using a Flexible Piezoelectric Film Sensor and Empirical Mode Decomposition," *29th Annual International Conference of the IEEE Engineering in Medicine and Biology Society, EMBS 2007*, Aug. 22-26, 2007, pp. 1362-1366.

[Broxterman2012] Broxterman, R.M., C.J. Ade, G.L. Gadbury, D. Schinstock, S. Warren, and T.J. Barstow. "10-km Walkback Performance Predicted From Standardized Exercise Tests," *NASA Human Research Program Workshop*, Houston, 2012.

[Broxterman2013] Broxterman, R.M., C. J Ade, S.L. Wilcox and T.J. Barstow. "Gender differences in laboratory assessment and simulated EVA performance," *NASA Human Research Program Workshop*, Galveston, 2013.

[Camilo2009] Camilo, T.; Oscar, R.; Carlos, L., "Biomedical signal monitoring using wireless sensor networks," *IEEE Latin-American Conference on Communications, LATINCOM '09*, Sept. 10-11, 2009, pp. 1-6.

[Canina2006] Canina, M.; Newman, D.J.; Trotti, G.L., "Preliminary considerations for wearable sensors for astronauts in exploration scenarios," *3rd IEEE/EMBS International Summer School on Medical Devices and Biosensors*, Sept. 4-6, 2006, pp. 16-19.

[Cao2010] Zhe Cao; Rong Zhu; RuiYiQue, "Low-cost portable respiration monitor based on micro hot-film flow sensor," *2010 IEEE 4th International Conference on Nano/Molecular Medicine and Engineering (NANOMED)*, Dec. 5-9, 2010.

[Chen2006] Chen Xijun; Meng, M.Q.-H.; Ren Hongliang, "Design of Sensor Node Platform for Wireless Biomedical Sensor Networks," *27th Annual International Conference of the IEEE EMBS,* Jan. 17-18, 2006, pp. 4662-4665.

[Delsys] DelsysTrigno (Natick, MA).

[Dhamdhere 2008] Dhamdhere, A.; Sivaraman, V.; Mathur, V.; Shuo Xiao, "Algorithms for Transmission Power Control in Biomedical Wireless Sensor Networks," *Asia-Pacific Services Computing Conference*, *APSCC 2008,* Dec. 9-12, 2008, pp. 1114-1119.

[Dong2013] Dong, Xiongjie, Timothy Sobering, Thomas Barstow, and Steve Warren. "A Wireless Inductance Plethysmograph as a Precursor to a Networked Suite of Low-Power Sensors for In-Spacesuit Health Monitoring," *HRP 2013, NASA Human Research Program Investigators' Workshop*, February 11–14, 2013, Moody Gardens Hotel, Galveston, TX.

[Dong2014] Dong, Xiongjie, Tianyu Lin, Timothy Sobering, Thomas Barstow, and Steve Warren. "A ZigBee-Wireless Biomedical Sensor Network as a Predecessor to an In-Suit Collection of Low-Power Health Sensors," HRP 2014, NASA Human Research Program Investigators' Workshop, February 12–13, 2014, Moody Gardens Hotel, Galveston, TX.

[Gama2007] Gama, O.; Figueiredo, C.; Carvalho, P.; Mendes, P.M., "Towards a Reconfigurable Wireless Sensor Network for Biomedical Applications," *International Conference on Sensor Technologies and Applications , SensorComm 2007,* Oct. 14-20, 2007, pp. 490-495.

[Gao 2012] Zeli Gao; Jie Wu; Jianli Zhou; Wei Jiang; Lihui Feng, "Design of ECG Signal Acquisition and Processing System," *2012 International Conference on Biomedical Engineering and Biotechnology (iCBEB)*, May 28-30, 2012, pp. 762-764.

[Gude2013a] Gude, Dana, Ryan Broxterman, Carl Ade, Thomas Barstow, Thomas Nelson, Wen Song, and Steve Warren. "Automated Hand-Forearm Ergometer Data Collection System," *HRP 2013, NASA Human Research Program Investigators' Workshop*, February 11–14, 2013, Moody Gardens Hotel, Galveston, TX.

[Gude2013b] Gude, Dana. Automated Hand-Forearm Ergometer Data Acquisition and Analysis System, Master's thesis, Kansas State University, August 2013. Available at http://krex.k-state.edu/.

[Hodges2013] Hodges, Amelia L. Investigation of Antennas and Harvesting Methods for Use with a UHF Microtranscriver in a Biosensor Network, Master's Thesis, Kansas State University, Manhattan, KS, 2013. Available at http://krex.k-state.edu/.

[Honeine2011] Honeine, P.; Mourad, F.; Kallas, M.; Snoussi, H.; Amoud, H.; Francis, C., "Wireless sensor networks in biomedical: Body area networks," *7th International Workshop on Systems, Signal Processing and their Applications (WOSSPA)*, May 9-11, 2011, pp. 388-391.

[Jennic2008] Jennic Ltd., "Data Sheet: JN5139-001 and JN5139-EK10," 2008, http://www.jennic.com.

[Jennic2010a] Jennic Ltd., "Data Sheet: JN5148-001 and JN5148-EK10," 2010, http://www.jennic.com.

[Jennic2010b] Jennic Ltd., "Preliminary Data Sheet – JN5148-xxx-Myy," 2010, http://www.jennic.com.

[Jennic2010c] Jennic Ltd., "DR1080 Starter Kit Board Reference Manual," 2010, http://www.jennic.com.

[Jennic2010d] Jennic Ltd., "Jenie API Reference Manual (JN-RM-5148)," 2010,http://www.jennic.com.

[Jennic2012] Jennic Ltd., "JenOS User Guide," 2012,http://www.jennic.com.

[Jennic2013] Jennic Ltd., "ZigBee PRO User Guide (JN-UG-3048)," 2013, http://www.jennic.com.

[Jia2014] Jia, Chen, Phillip Kuehl, Dana Gude, Ryan Broxterman, Thomas Barstow, and Steve Warren. "Improved Algorithms for EMG Burst Identification and Processing," *HRP 2014*, *NASA Human Research Program Investigators' Workshop*, February 12–13, 2014, Moody Gardens Hotel, Galveston, TX.

[Kuehl2014] Kuehl, Phillip, Chen Jia, Dana Gude, Ryan Broxterman, Thomas Barstow, and Steve Warren. "Real-Time Processing of Electromyograms in an Automated Hand-Forearm Ergometer Data Collection and Analysis System," *HRP 2014*, *NASA Human Research Program Investigators' Workshop*, February 12–13, 2014, Moody Gardens Hotel, Galveston, TX.

[Krenzel2012] Krenzel, Devon, Steve Warren, Kejia Li, Bala Natarajan, and Gurdip Singh. "Wireless Slips and Falls Prediction System," *34th Annual International Conference of the IEEE Engineering in Medicine and Biology Society*, Hilton Bayfront Hotel, San Diego, CA, USA, Aug. 28 – Sept. 1, 2012, pp. 4042–4045.

[Lee2008] Lee, G. S.; Park, K.S., "Resonant plethysmography for unconstrained monitoring of respiration," *Electronics Letters*, Vol. 44, No. 2, January 17, 2008, pp. 89-90.

[Li2012a] Li, Kejia and Steve Warren. "A Wireless Reflectance Pulse Oximeter Suitable for Wearable and Surface-Integratable Designs that Produces High-Quality Unfiltered Photoplethysmograms," *IEEE Transactions on Biomedical Circuits and Systems*, Vol. 6, No. 3, June 2012, pp. 269–278.

[Li2012b] Li, Kejia, Steve Warren, and Balasubramaniam Natarajan. "Onboard Tagging for Real-Time Quality Assessment of Photoplethysmograms Acquired by a Wireless Reflectance Pulse Oximeter," *IEEE Transactions on Biomedical Circuits and Systems*, Vol. 6, No. 1, February 2012, pp. 54–63.

[Liu2009] Liu Yanfei; Wang Cheng; QiaoXiaojun; Zhang Yunhe; Yu Chengbo, "An improved design of ZigBee Wireless Sensor Network," *ICCSIT 2009, 2nd IEEE International Conference on Computer Science and Information Technology*, Aug. 8-11, 2009, pp. 515-518.

[Liu2013] Yao-Hong Liu; Xiongchuan Huang; Vidojkovic, M.; Ba, A.; Harpe, P.; Dolmans, G.; de Groot, H., "A 1.9nJ/b 2.4GHz multistandard (Bluetooth Low Energy/Zigbee/IEEE802.15.6) transceiver for personal/body-area networks," *2013 IEEE International Solid-State Circuits Conference Digest of Technical Papers (ISSCC)*, Feb. 17-21, 2013, pp. 446-447.

[Merritt2009] Merritt, C.R.; Nagle, H.T.; Grant, E., "Textile-Based Capacitive Sensors for Respiration Monitoring," *IEEE Sensors Journal*, Vol.9, No.1, Jan. 2009, pp. 71-78.

[Murata2002] Murata Electronics Oy. "3-Axis Ultra Low Power Gyro with Digital SPI and I2C Interface," CMR3000-D01 Data Sheet, ©2002, Murata Electronics Oy, Inc. http://www.muratamems.fi/en.

[Murata2004] Murata Electronics Oy. "3-Axis Ultra Low Power Accelerometer with Digital SPI and I2C Interface," CMA3000-D01 Data Sheet, ©2004, Murata Electronics Oy, Inc. http://www.muratamems.fi/en.

[Nan2007] Nan Bu; Ueno, N.; Fukuda, O., "Monitoring of Respiration and Heartbeat during Sleep using a Flexible Piezoelectric Film Sensor and Empirical Mode Decomposition," *29th Annual International Conference of the IEEE Engineering in Medicine and Biology Society, EMBS 2007*, Aug. 22-26, 2007, pp. 1362-1366.

[Ko2012] Sung-Yuan Ko; Kang-Min Wang; Wei-Cheng Lian; Chun-Heng Kao, "A portable ECG recorder," *2nd International Conference on Consumer Electronics, Communications and Networks (CECNet)*, April 21-23, 2012, pp. 3063-3067.

[Kim2013] Kim, JaYeong; Song, Nah-Oak; Jung, ByoungHoon; Leem, Hansung; Sung, Dan Keun, "Placement of WiFi access points for efficient WiFi offloading in an overlay network," *24th International Symposium of the IEEE*, Sept. 8-11, 2013, pp. 3066-3070.

[KSU-NASA1] "Task 1- Medical Sensor Development," Department of Electrical and Computer Engineering, Kansas State University, [Online]. Available at http://nasa.ece.ksu.edu/task1.htmlhttp://nasa.ece.ksu.edu/task1.html [Accessed 22 Oct. 2013].

[Rashid2008] Rashid, R.A.; Rahim, M.R.A.; Sarijari, M.A.; Mahalin, N., "Design and implementation of Wireless Biomedical Sensor Networks for ECG home health monitoring," *ICED 2008, International Conference on Electronic Design*, Dec. 1-3, 2008, pp. 1-4.

[Poo2010] Poo, T. S.; Sundaraj, K., "Design and development of a low cost EMG signal acquisition system using surface EMG electrode," *2010 IEEE Asia Pacific Conference on Circuits and Systems (APCCAS)*, Dec. 6-9, 2010, pp. 24-27.

[Ren2005a] Hongliang Ren; Meng, M.Q.-H.; Xijun Chen, "Physiological information acquisition through wireless biomedical sensor networks," *2005 IEEE International Conference on Information Acquisition*, June 27 - July 3, 2005, pp. 6.

[Ren2005b] Hongliang Ren; Meng, M.Q.-H., "Bioeffects Control in Wireless Biomedical Sensor Networks," *3rd Annual IEEE Communications Society on Sensor and Ad Hoc Communications and Networks,* Vol.3, Sept. 28, 2006, pp. 896-904.

[Sakurai2010] Sakurai, T.; Toda, M.; Sakurazawa, S.; Akita, J.; Kondo, K.; Nakamura, Y., "Detection of Muscle Fatigue by the Surface Electromyogram and Its Application," *IEEE/ACIS 9th International Conference on Computer and Information Science (ICIS)*, Aug. 18-20, 2010, pp. 43-47.

[Song2013a] Song, Wen, Carl Ade, Ryan Broxterman, Thomas Nelson, Dana Gude, Thomas Barstow, and Steve Warren. "Classification Algorithms Applied to Accelerometer Data as a Means to Identify Subject Activities Related to Planetary Navigation Tasks," *HRP 2013*, *NASA Human Research Program Investigators' Workshop*, February 11–14, 2013, Moody Gardens Hotel, Galveston, TX.

[Song2013b] Song, Wen. Planetary Navigation Activity Recognition Using Wearable Accelerometer Data, Master's thesis, Kansas State University, May 2013.

[Taj-Eldin2013] M. Taj-Eldin, W. Kuhn and B. Natarajan, "Study of Radio Channel for Biomedical Sensors in Spacesuits," *8th International Conference on Body Area Networks*, Boston, Sept. 30 – Oct. 2, 2013.

[Trasvina2014] Trasvina-Moreno, C.A.; Asensio, A.; Casas, R.; Blasco, R.; Marco, A., "WiFi Sensor Networks: A study of energy consumption," *11th International Multi-Conference on Systems, Signals & Devices (SSD)*, Feb. 11-14, 2014, pp. 1-6.

[Tseng2009] Shao-Yen Tseng; Chung-Han Tsai; Yu-Sheng Lai; Wai-Chi Fang, "A wireless biomedical sensor network using IEEE802.15.4," *LiSSA 2009, IEEE/NIH Life Science Systems and Applications Workshop*, April 9-10, 2009, pp. 183-186.

[Wang2010] Lei Wang; Guang-Zhong Yang; Jin Huang; Jinyong Zhang; Li Yu; Zedong Nie; Cumming, D.R.S., "A Wireless Biomedical Signal Interface System-on-Chip for Body Sensor Networks," *IEEE Transactions on Biomedical Circuits and Systems*, Vol.4, No.2, April 2010, pp. 112-117.

[Wagner2012] Wagner, R.S.; Barton, R.J., "Performance comparison of wireless sensor network standard protocols in an aerospace environment: ISA100.11a and ZigBee Pro," *2012 IEEE Aerospace Conference,* March 3-10, 2012, pp. 1-14.

[Warren2011] Warren, Steve, Xiongjie Dong, Timothy Sobering, and Jianchu Yao, "A Rapid Analysis and Signal Conditioning Laboratory (RASCL) Design Compatible with the National Instruments myDAQ®Platform," *2011 Annual Conference and Exposition, American Society for Engineering Education*, Vancouver, British Columbia, Canada, June 26-29, 2011.

[Wu2009] Dan Wu; Lei Wang; Yuan-Ting Zhang; Bang-Yu Huang; Bo Wang; Shao-Jie Lin; Xiao-Wen Xu, "A wearable respiration monitoring system based on digital respiratory inductive plethysmography," *EMBC 2009. Annual International Conference of the IEEE EMBS*, Sept. 3-6, 2009, pp. 4844-4847.

[Xiao2007] Yanming Xiao; Changzhi Li; Jenshan Lin, "A Portable Noncontact Heartbeat and Respiration Monitoring System Using 5-GHz Radar," *Sensors Journal, IEEE*, Vol.7, No.7, July 2007, pp. 1042-1043.

[Zhang2009] Lili Zhang; Xiaoming Wu, "Recent Progress in Challenges of Wireless Biomedical Sensor Network," *ICBBE 2009. 3rd International Conference on Bioinformatics and Biomedical Engineering*, June 11-13, 2009, pp. 1-4.

[Zhou2013] Bing Zhou; Xianxiang Chen; Xinyu Hu; Ren Ren; Xiao Tan; Zhen Fang; Shanhong Xia, "A Bluetooth low energy approach for monitoring electrocardiography and respiration," *2013 IEEE 15th International Conference on e-Health Networking, Applications & Services (Healthcom)*, Oct. 9-12, 2013, pp. 130-134.

APPENDIX A: INDUCTIVE PLETHYSMOGRAPH CIRCUIT SCHEMATICS AND PCB LAYOUT

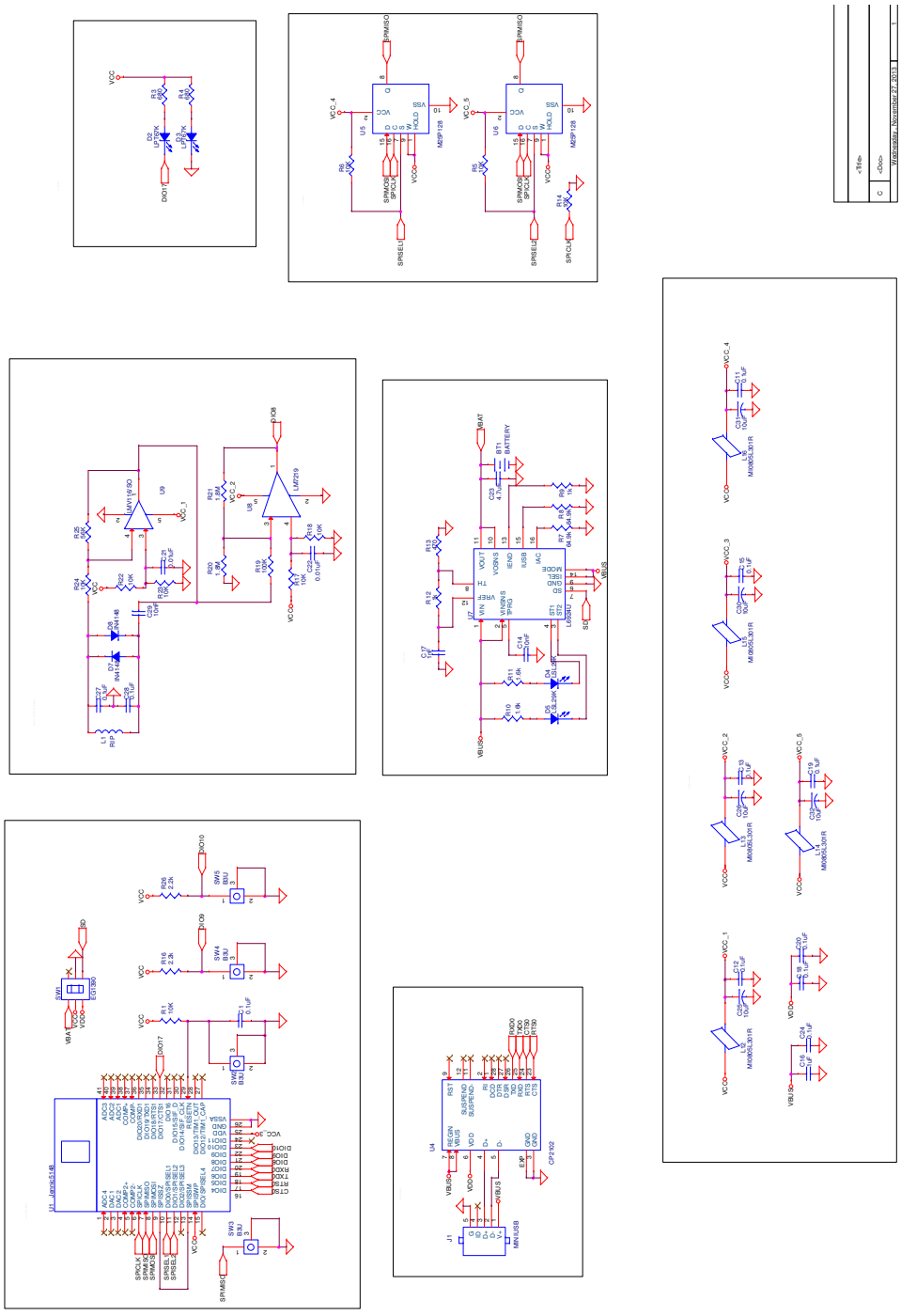

Figure 59. Respiration belt circuit schematics.

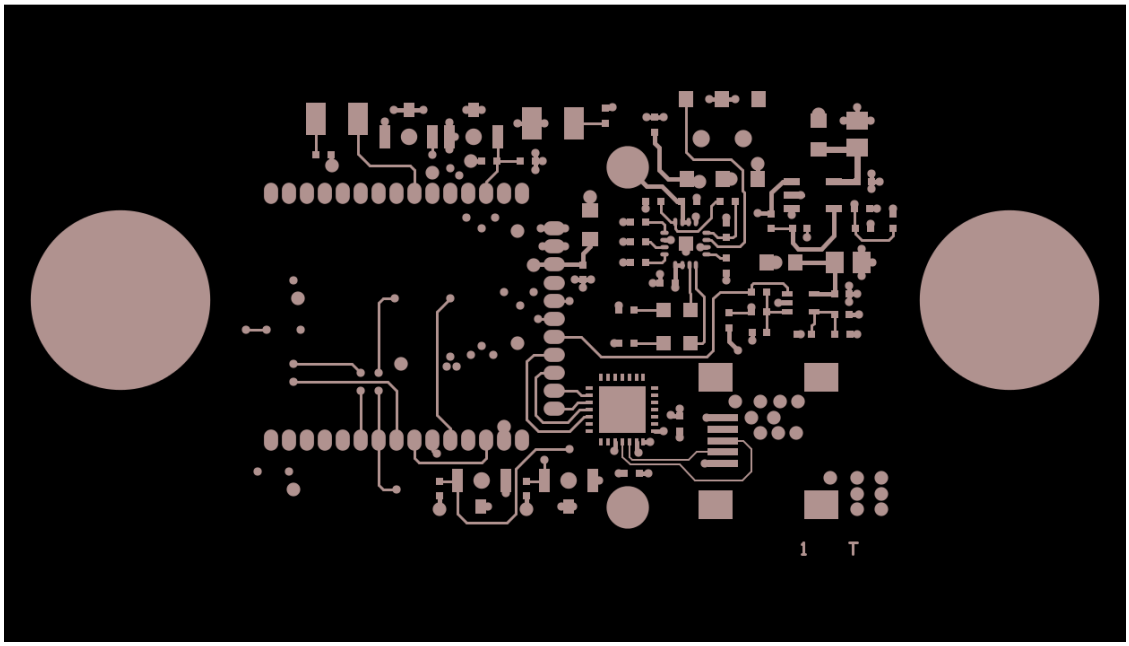

Figure 60. Respiration sensor PCB top layer.

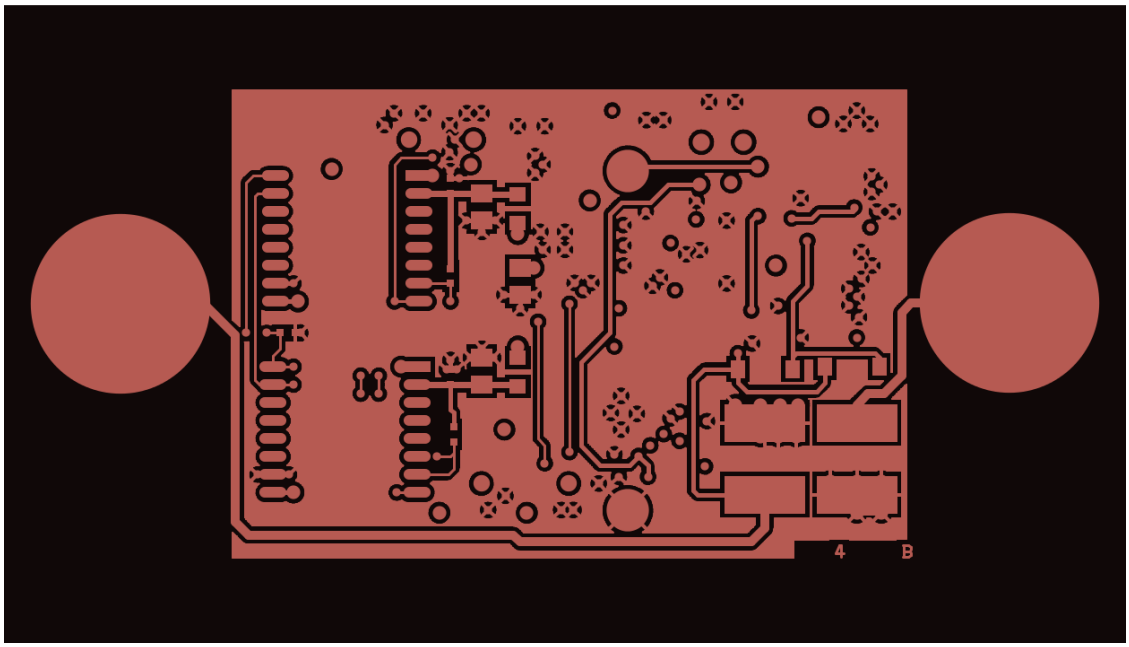

Figure 61. Respiration sensor PCB bottom layer

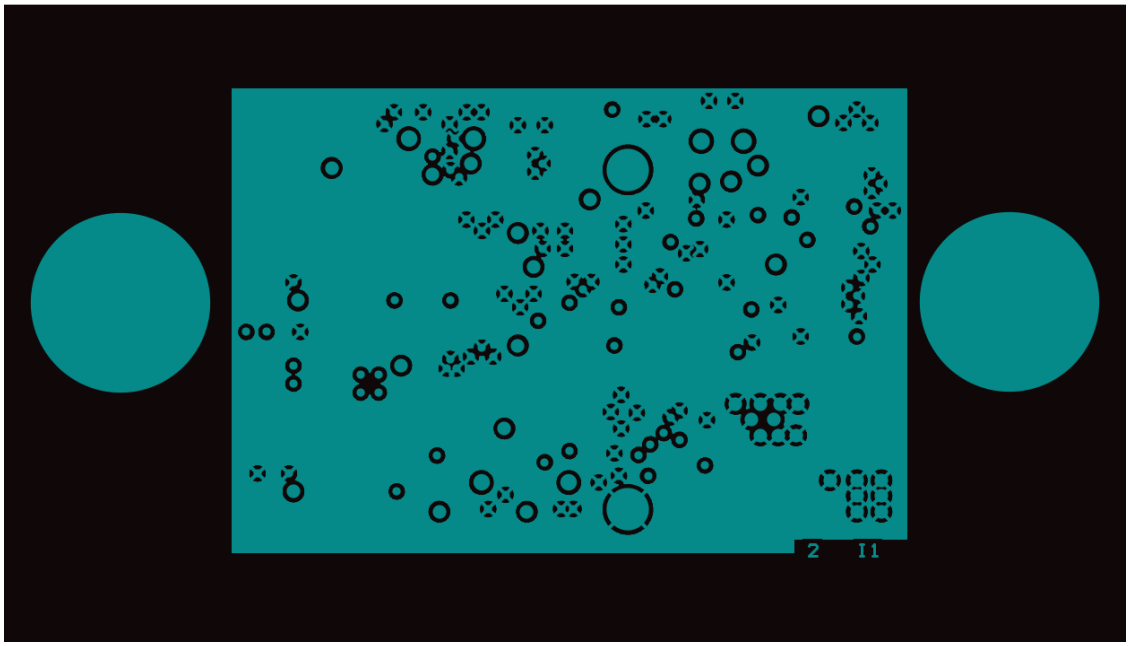

Figure 62. Respiration sensor Inner1 solid GND plane.

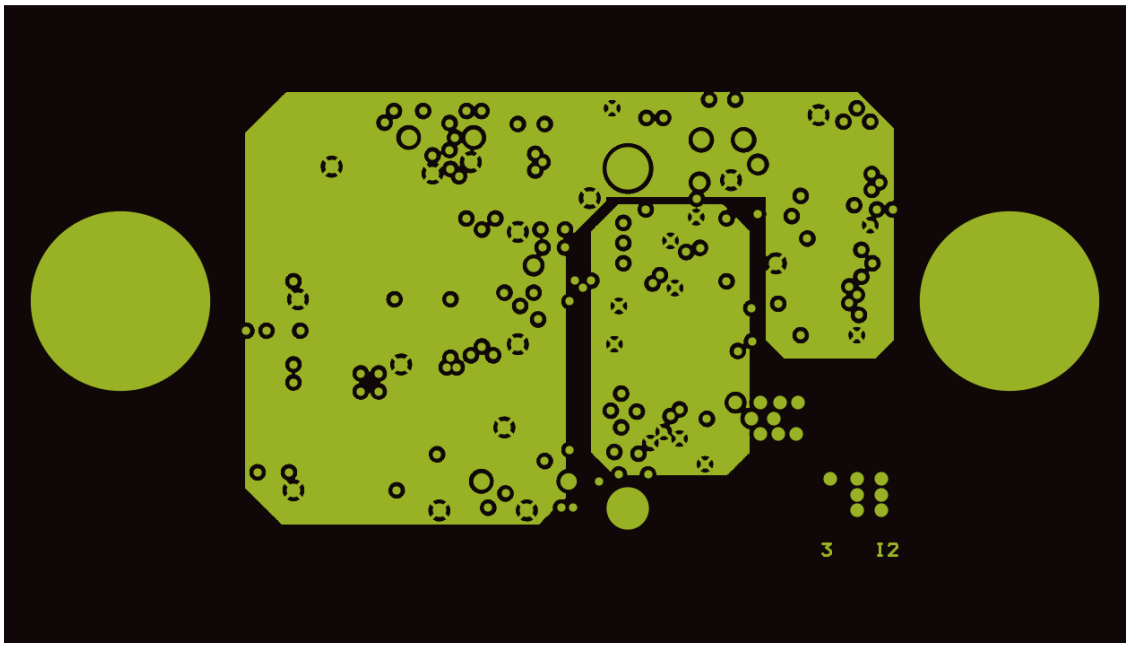

Figure 63. Respiration sensor Inner2 power plane.

APPENDIX B: TWO-CHANNEL ELECTROCARDIOGRAPH SCHEMATICS AND PCB LAYOUT

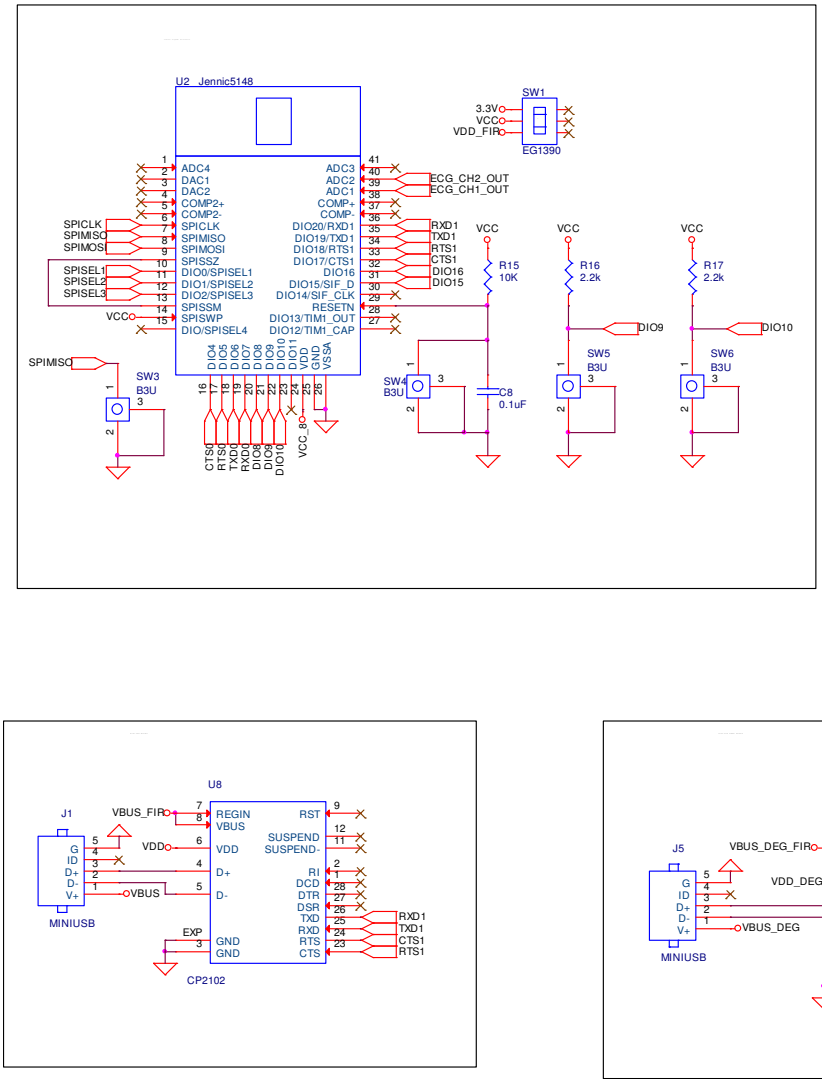

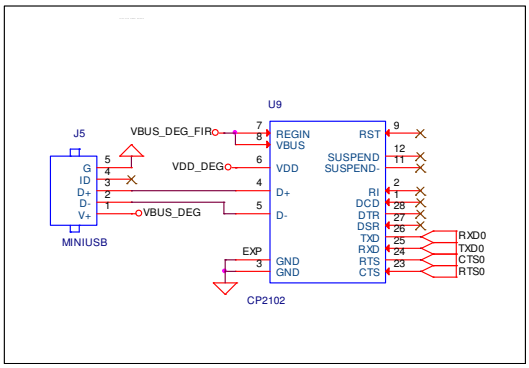

Figure 64. Two-channel ECG : microprocessor and USB bridge.

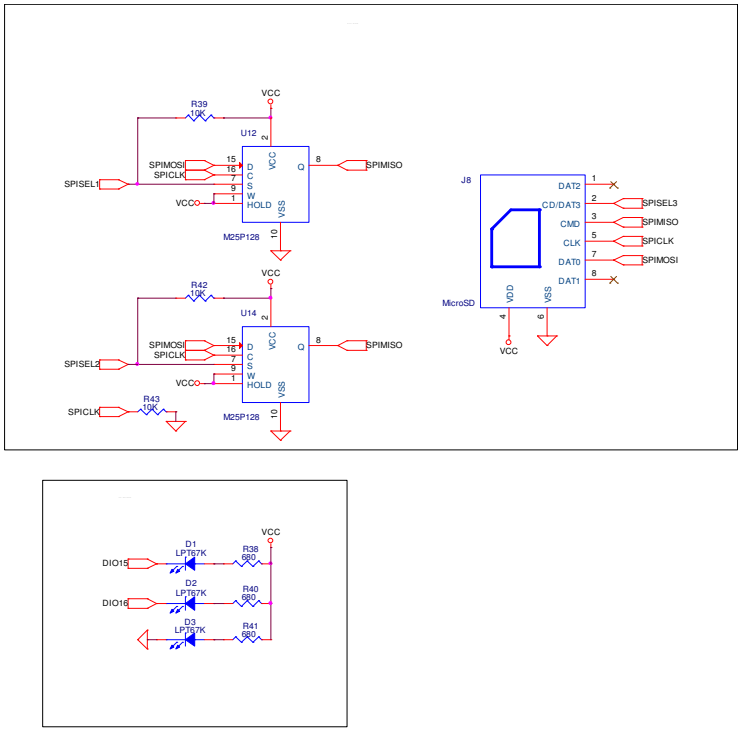

Figure 65. Two-channel ECG: flash and SD card memory storage.

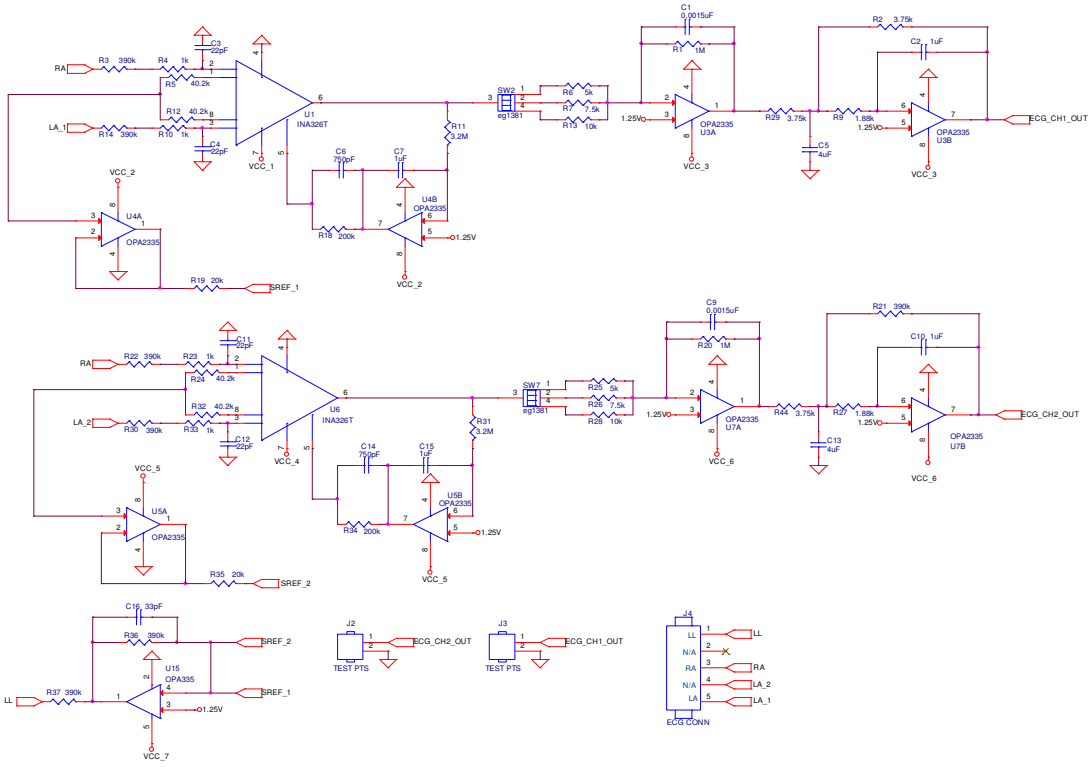

Figure 66. Two-channel ECG : sensing circuit.

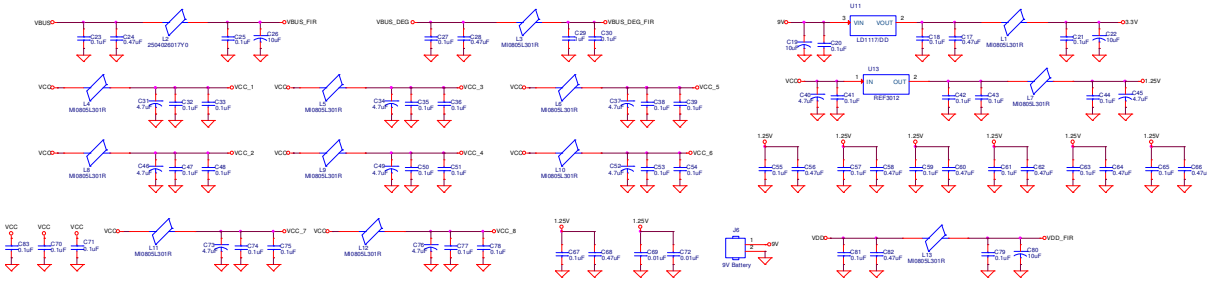

Figure 67. Two-channel ECG : main power and decoupling network.

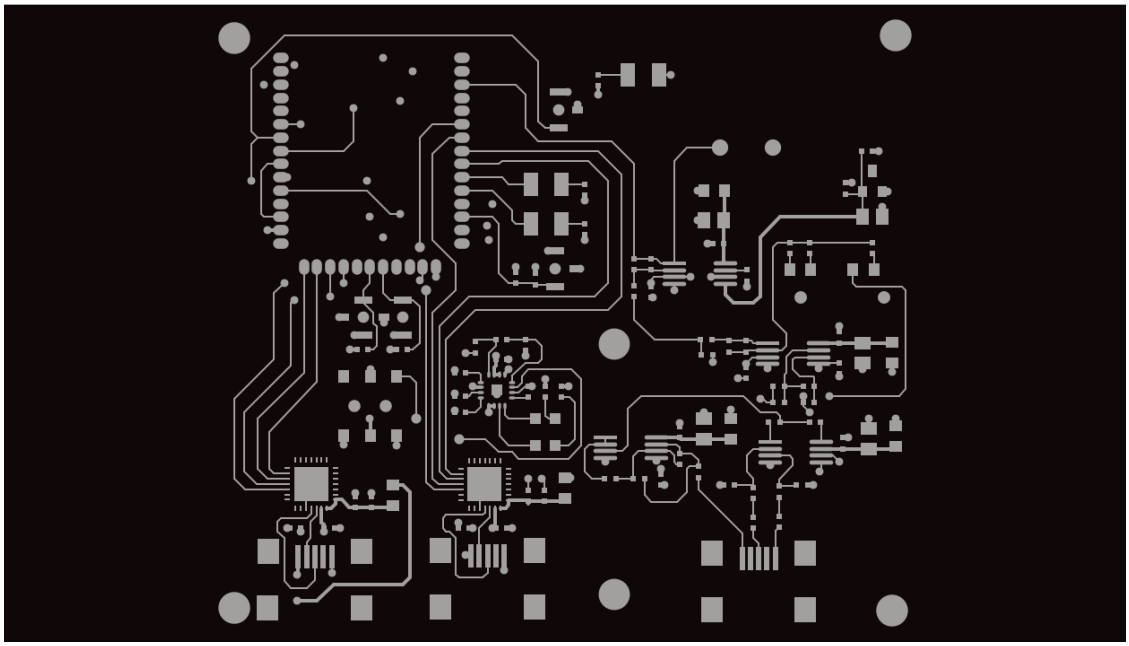

Figure 68. Two-channel ECG: PCB top layer.

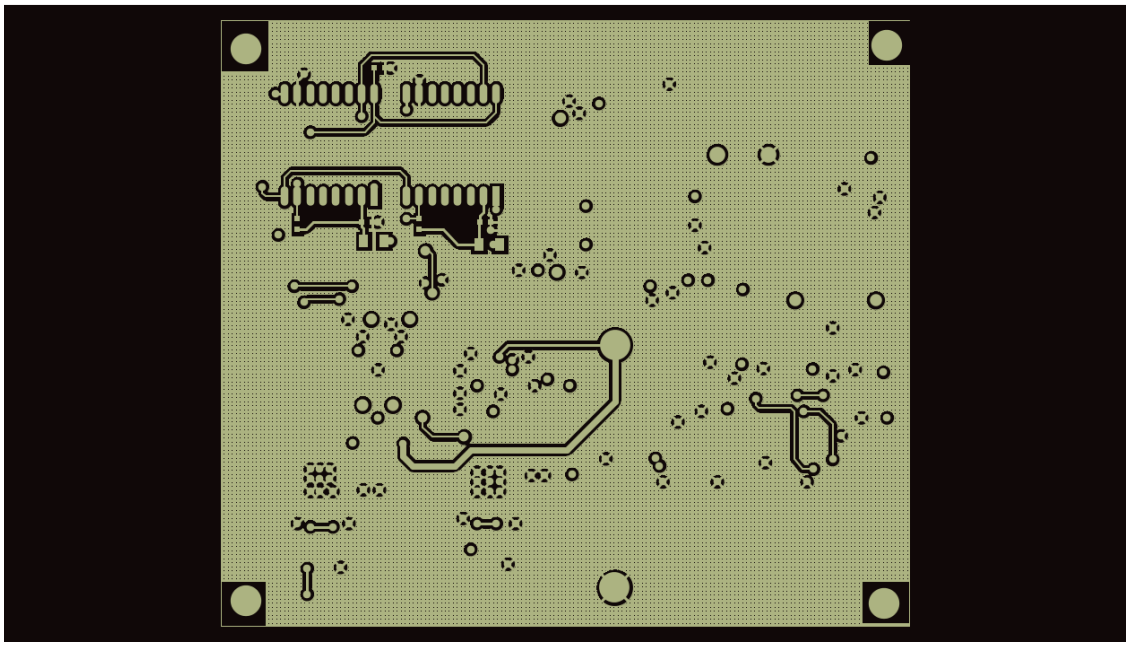

Figure 69. Two-channel ECG: PCB bottom layer.

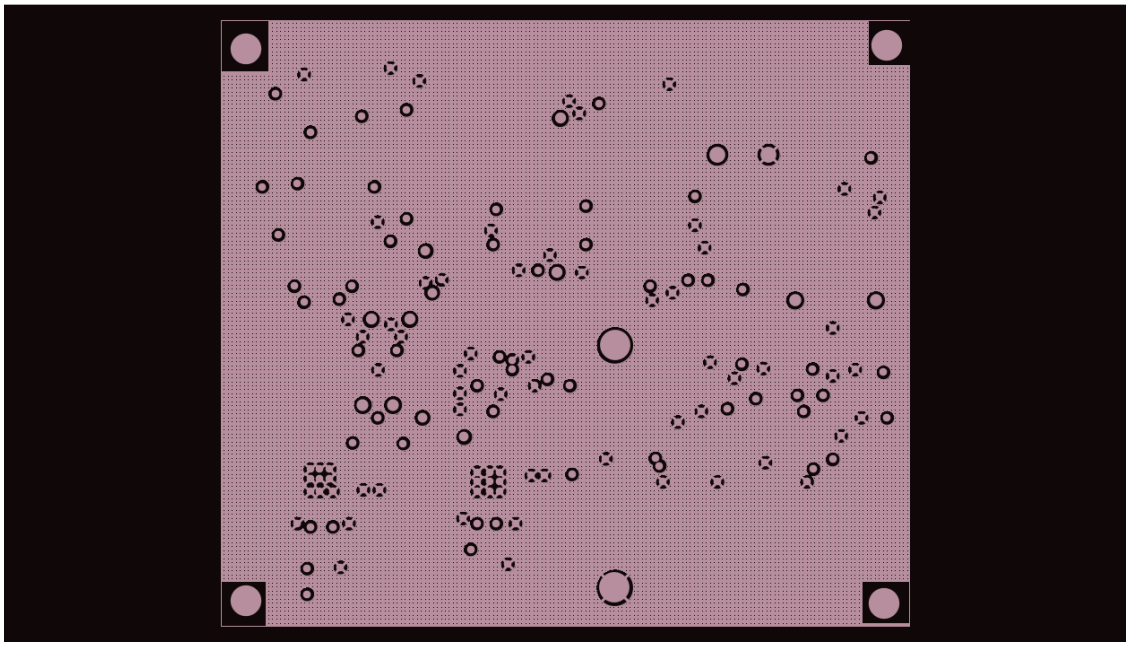

Figure 70. Two-channel ECG : PCB Inner1 solid ground plane.

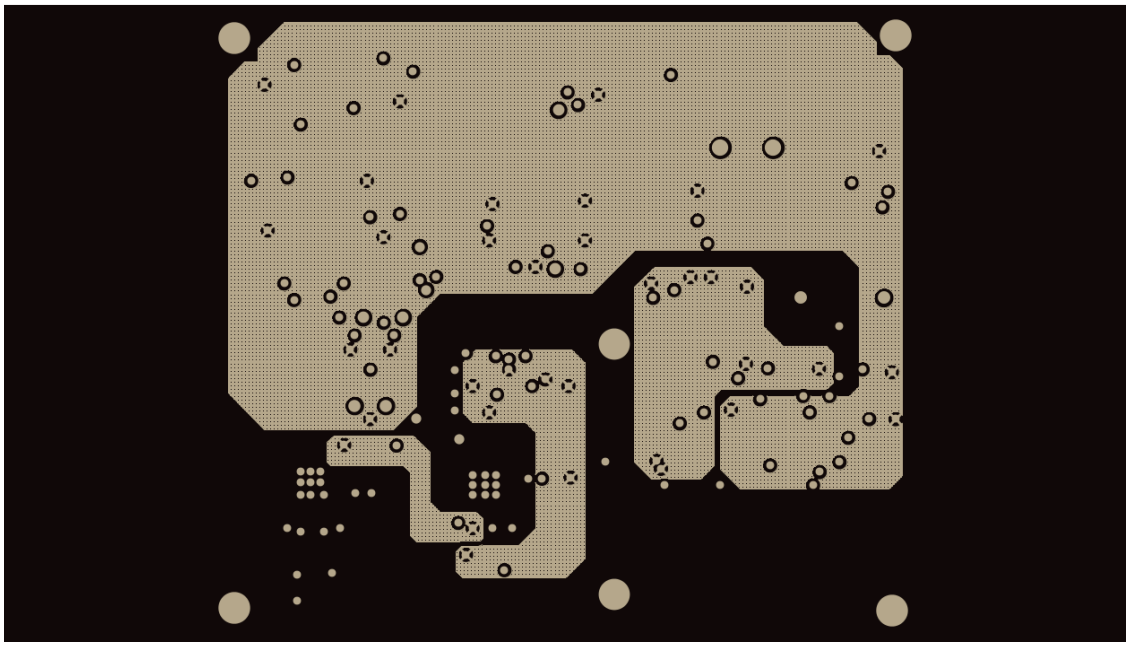

Figure 71. Two-channel ECG : PCB Inner2 split power plane.

APPENDIX C: ACCELEROMETER/GYROMETER SCHEMATICS AND PCB LAYOUT

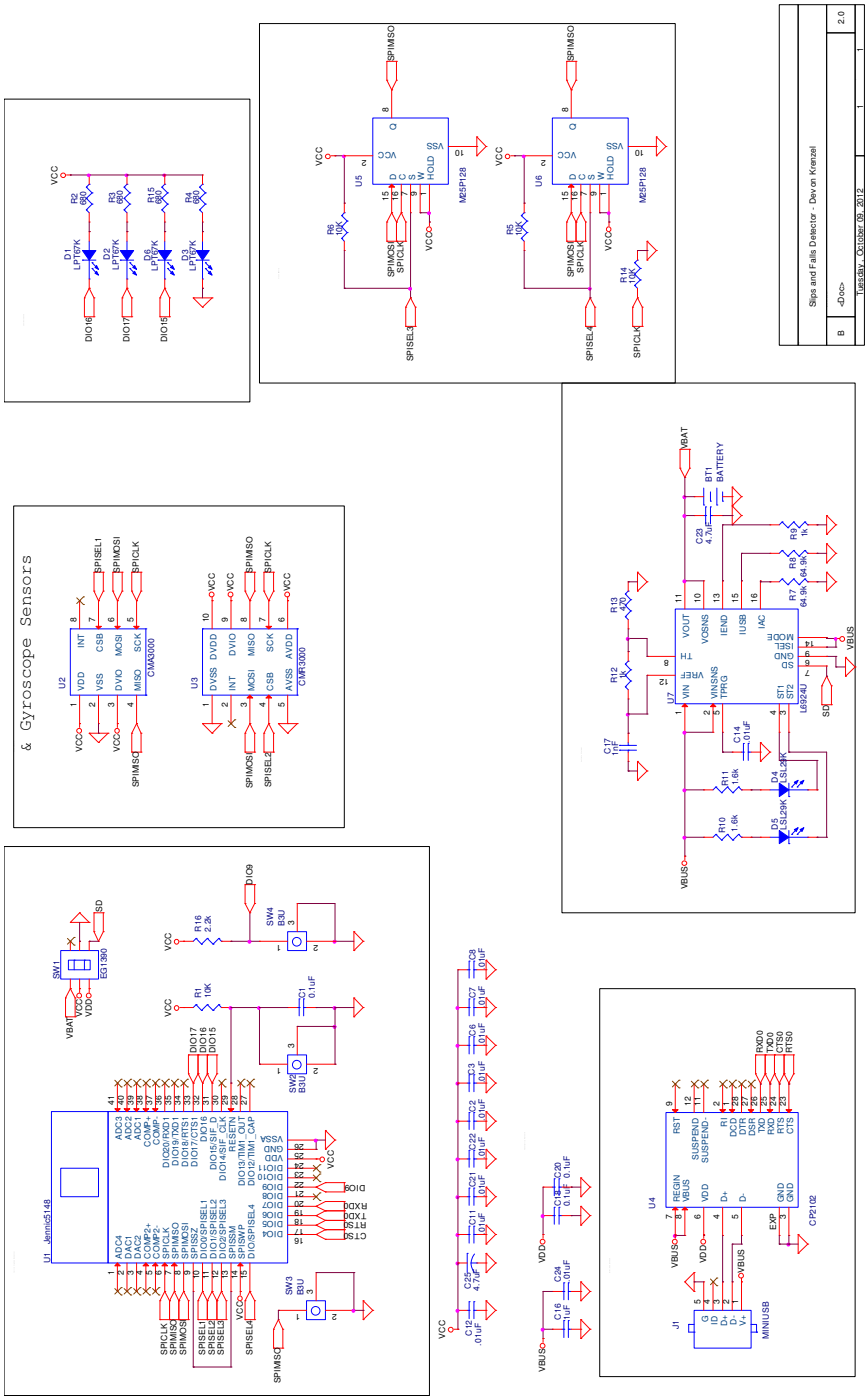

Figure 72. Accelerometer/gyrometer circuit schematics

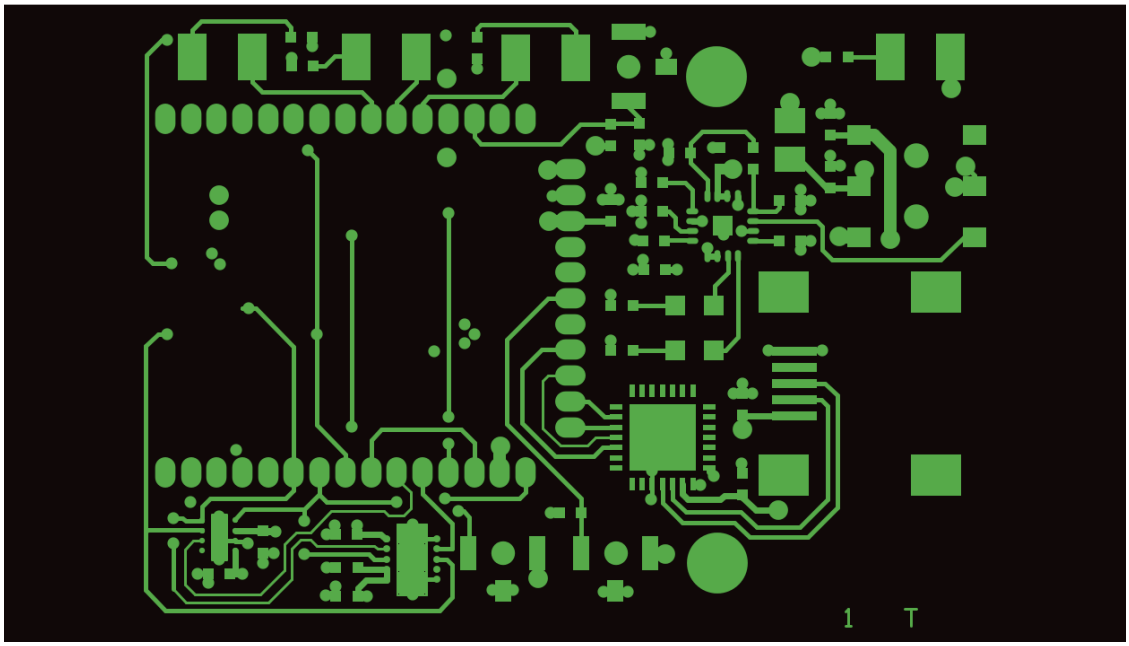

Figure 73. Accelerometer/gyrometer: PCB top layer.

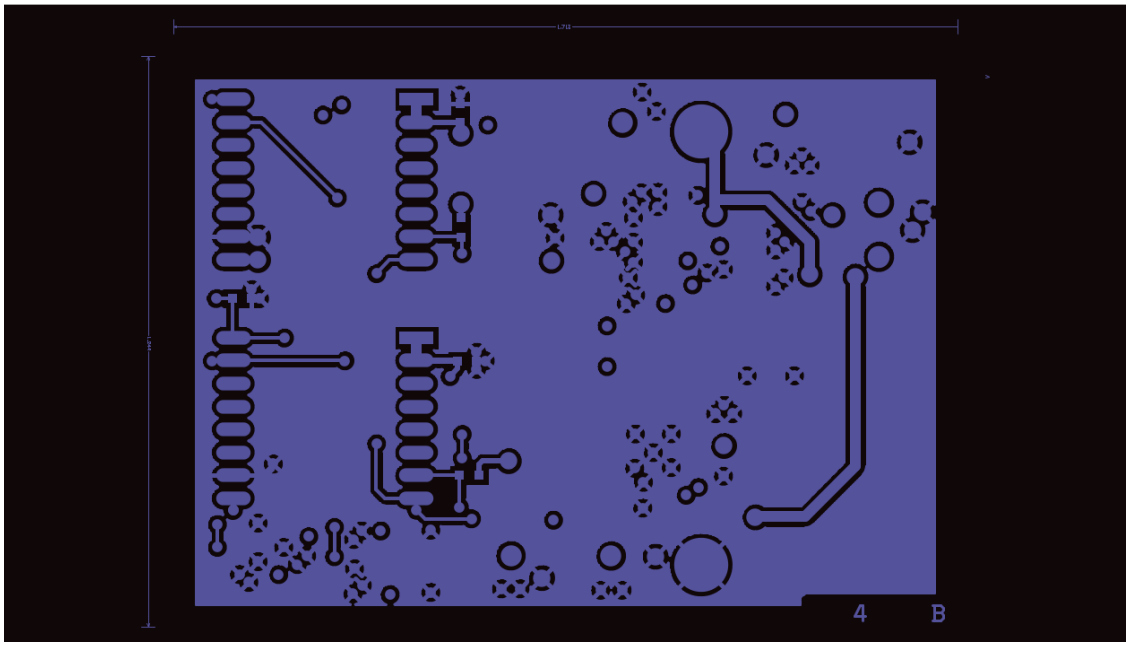

Figure 74. Accelerometer/gyrometer: PCB bottom layer.

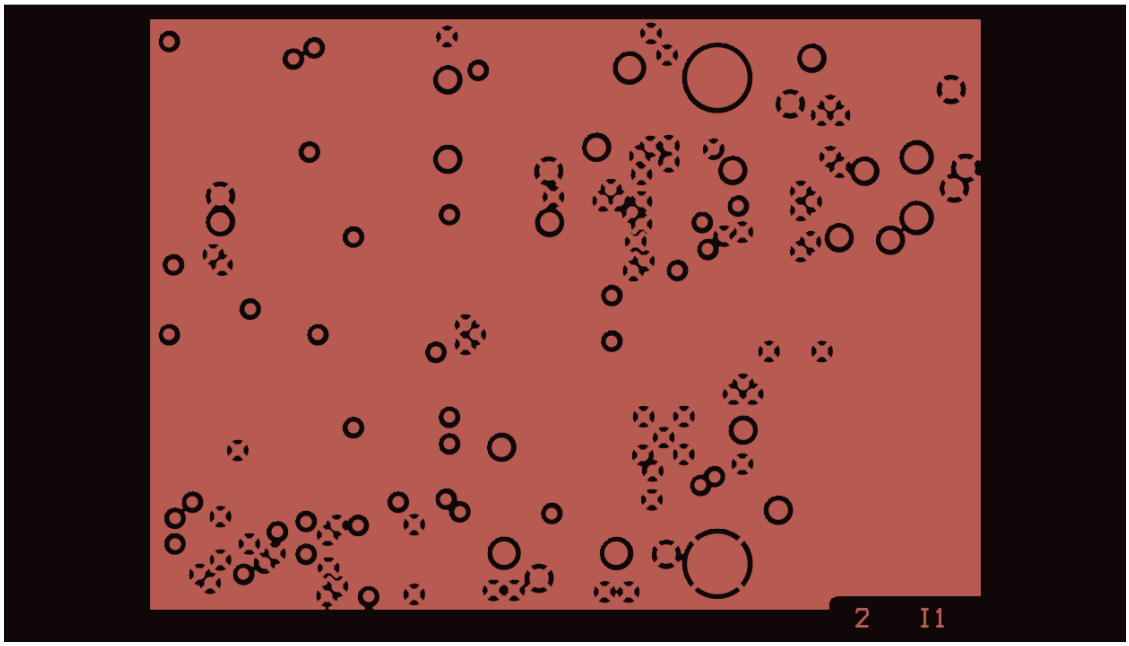

Figure 75. Accelerometer/gyrometer: Inner1 solid ground layer.

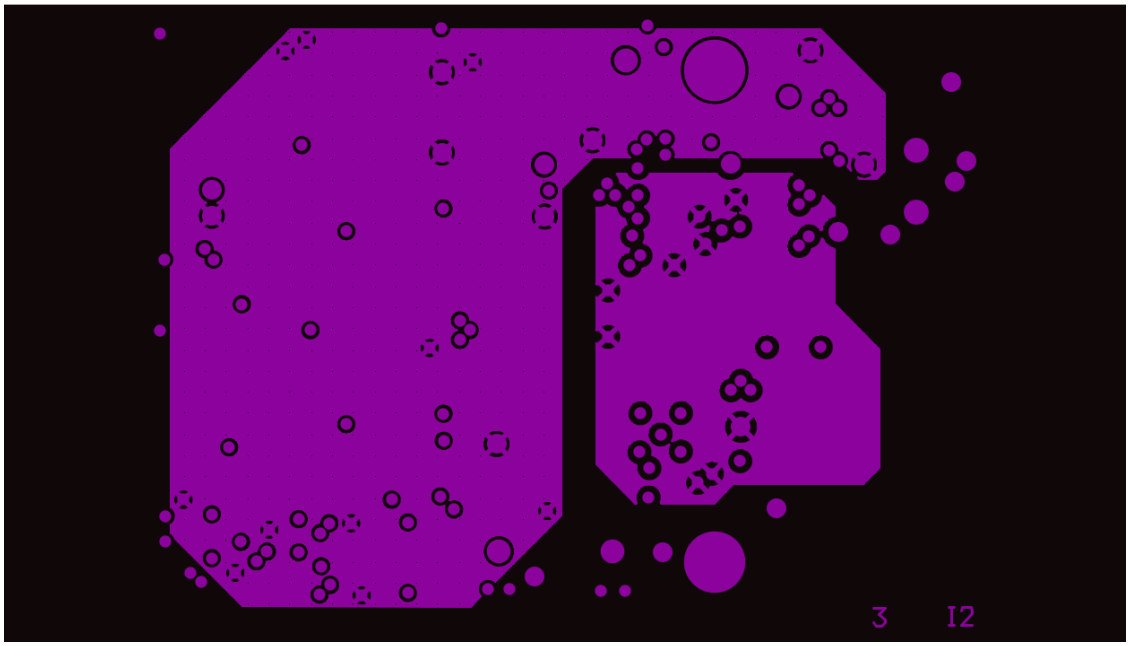

Figure 76. Accelerometer/gyrometer: Inner2 split power layer.

APPENDIX D: COORDINATOR/RECEIVER SCHEMATICS AND PCB LAYOUT

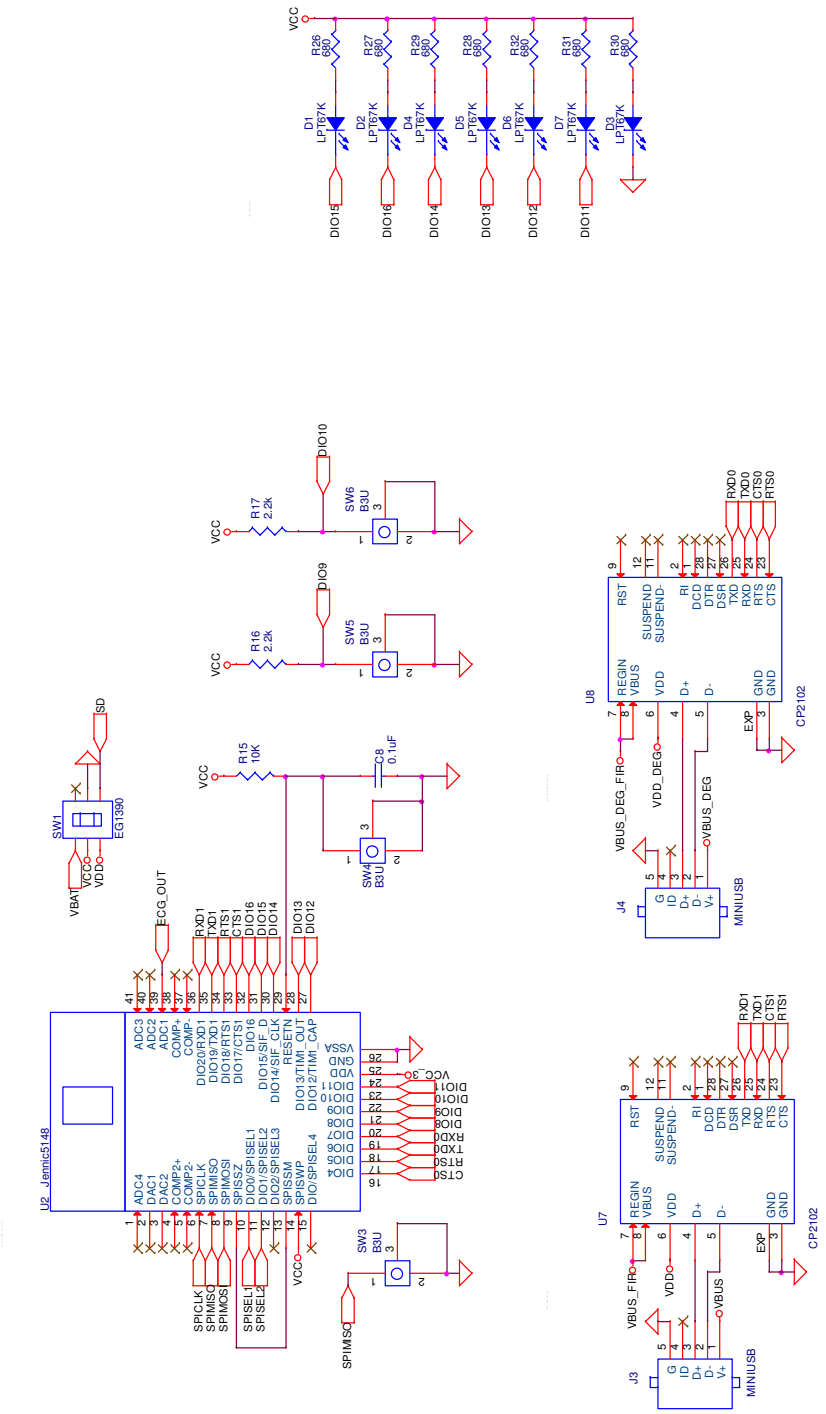

Figure 77. Coordinator/receiver circuit schematics.

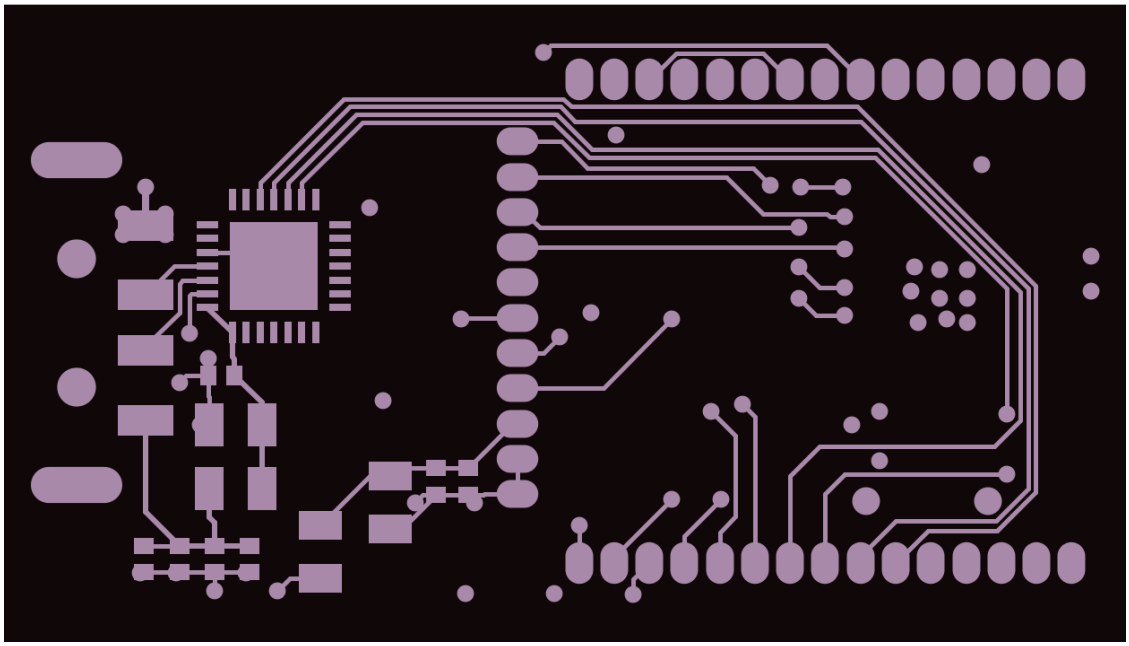

Figure 78. Coordinator/receiver: PCB top layer.

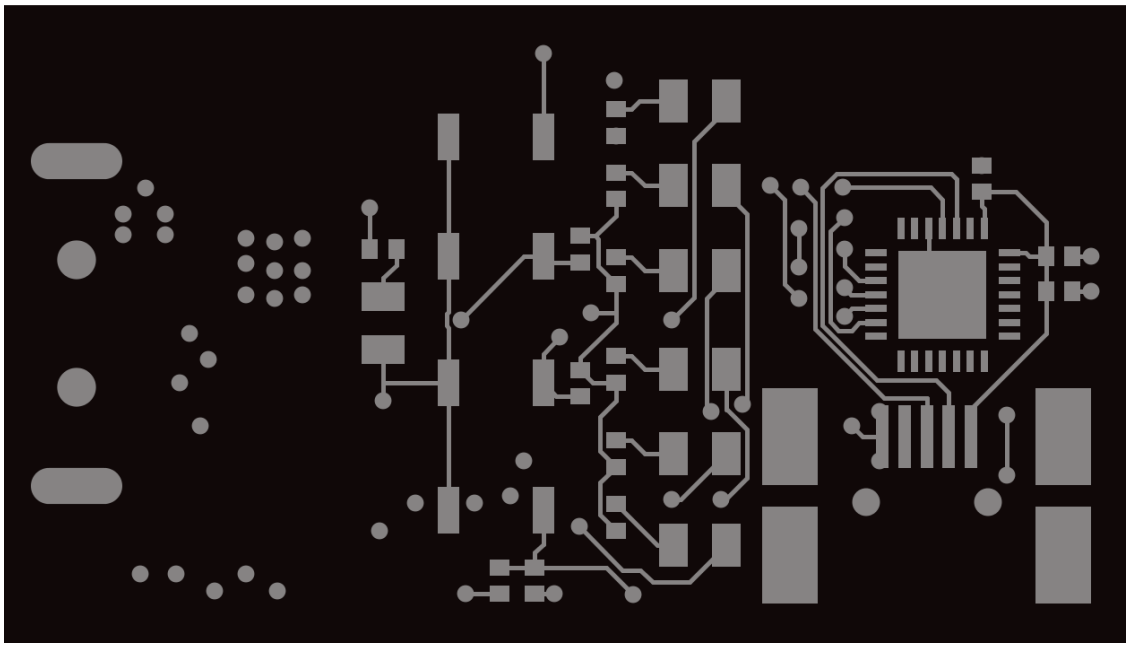

Figure 79. Coordinator/receiver: PCB bottom layer.

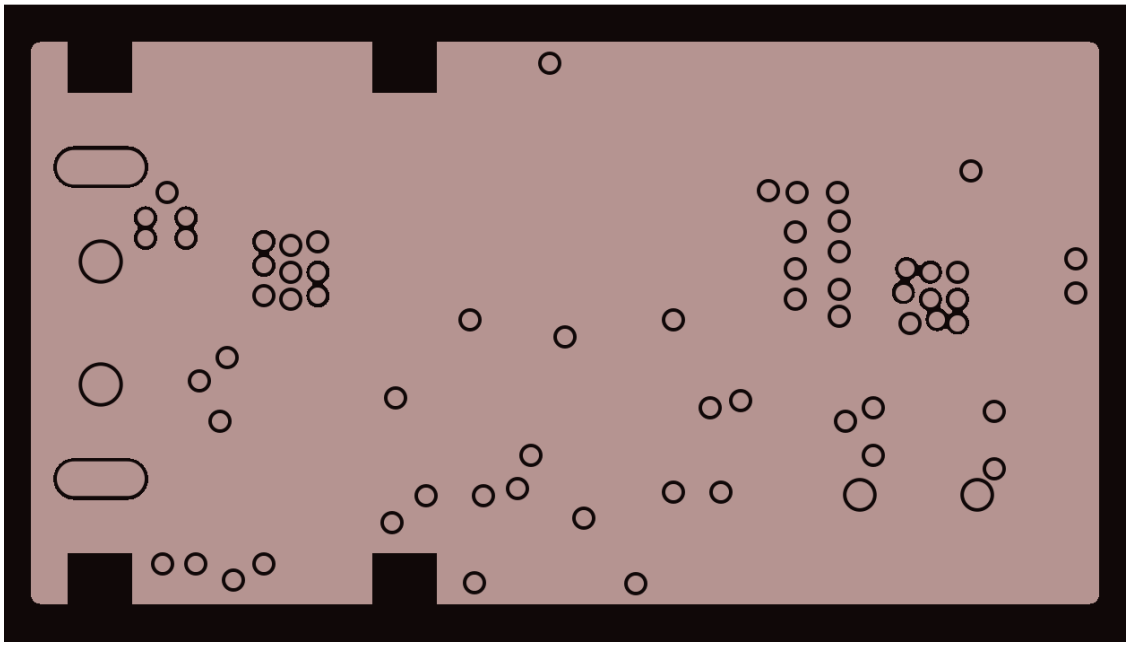

Figure 80. Coordinator/receiver: Inner1 solid power plane.

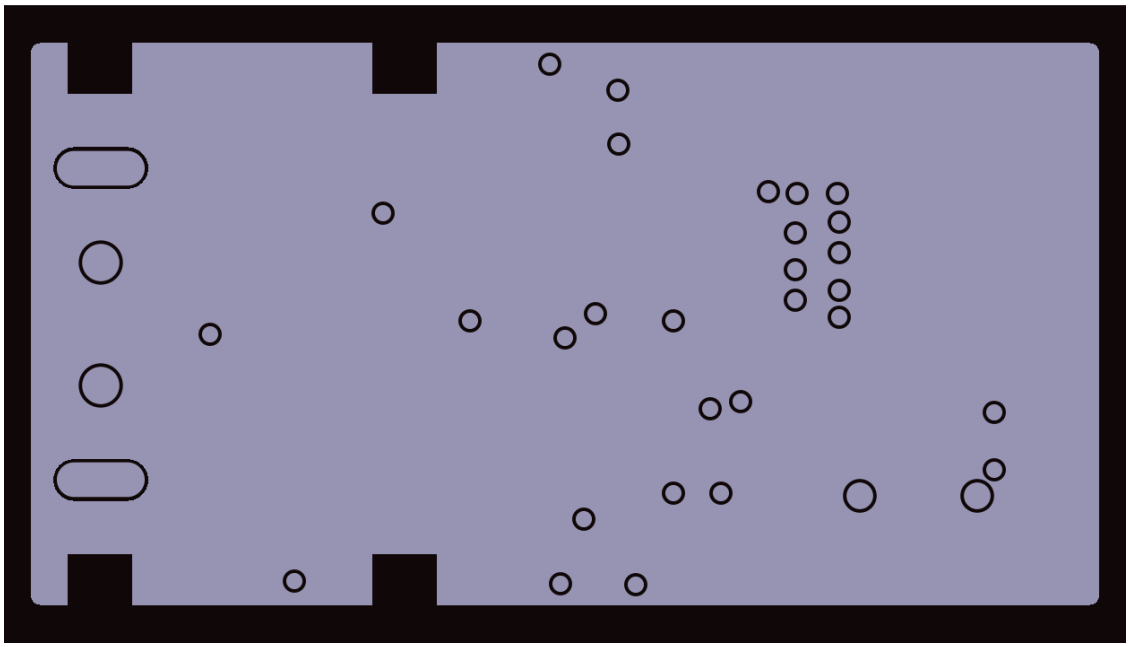

Figure 81. Coordinator/receiver: Inner2 solid power plane.

APPENDIX E: SENSOR NODE REAL-TIME SYSTEM CONFIGURATION

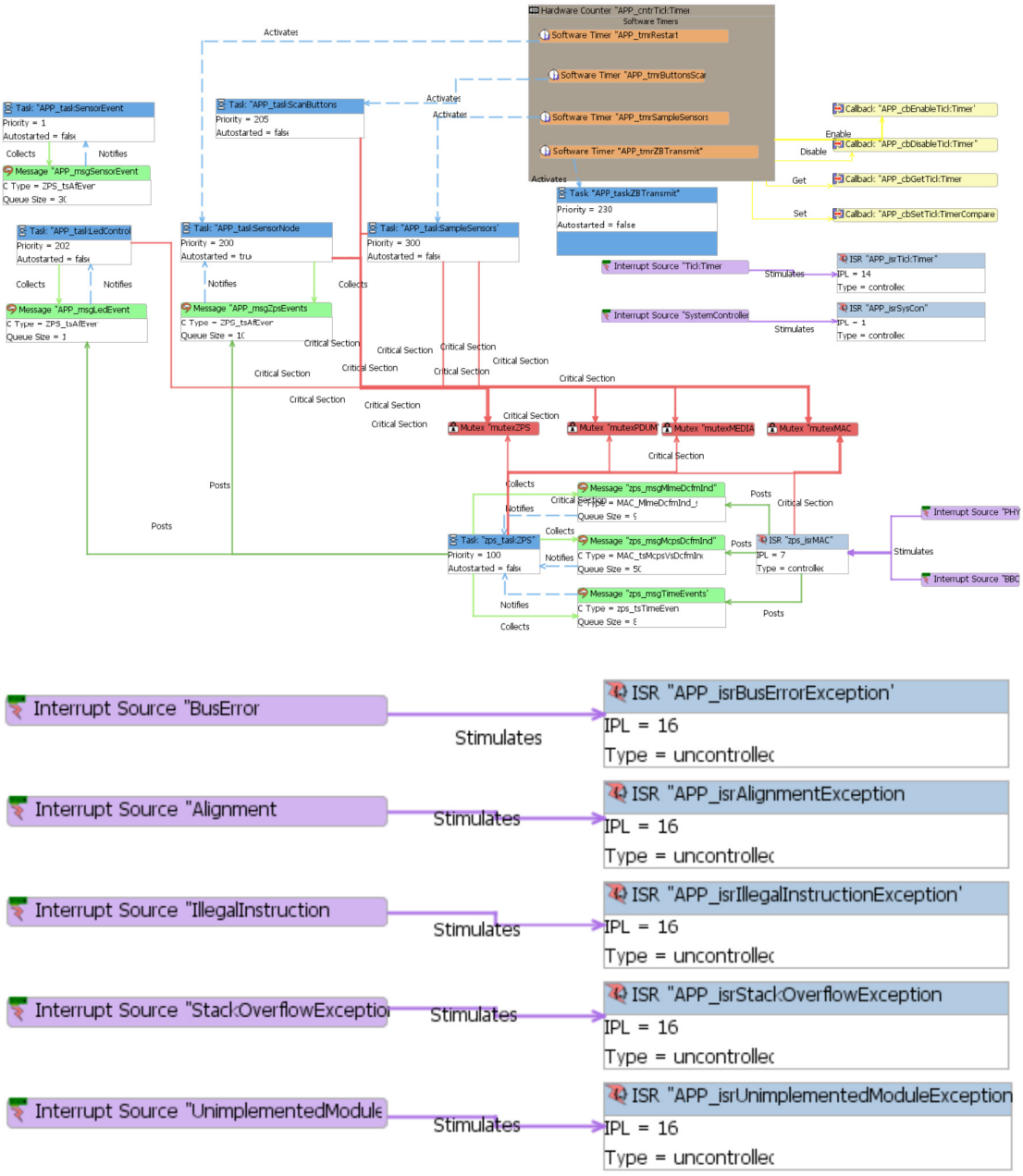

Figure 82. Sensor node real-time system configuration.

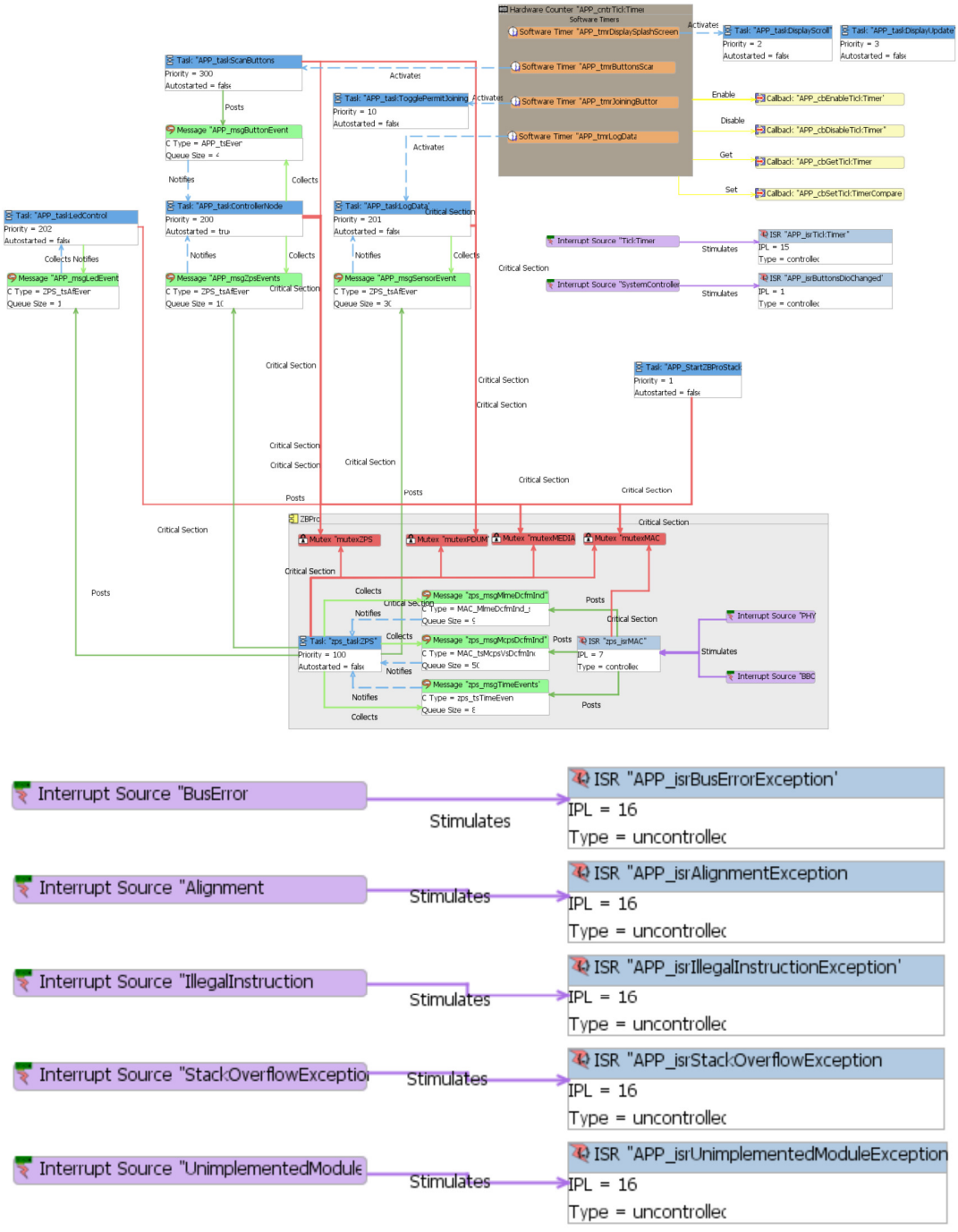

Figure 83. Coordinator real-time system configuration.